ELECTRONIC STRUCTURES OF METALLOCENE COMPLEXES

I. ELECTRONIC STRUCTURE OF METALLOCENES. OPTICAL SPECTROSCOPIC STUDY OF METALLOCENE COMPLEXES

II. MAGNETIC SUSCEPTIBILITY STUDY OF THE FERRICENIUM ION

III. SYNTHESIS AND CHARACTERIZATION OF SEVERAL OXIDATION PRODUCTS OF RUTHENOCENE

Thesis by

Youn Soo Sohn

In Partial Fulfillment of the Requirements

For the Degree of

Doctor of Philosophy

California Institute of Technology

Pasadena, California

1970

(Submitted August 7, 1970)

To my wife and mother

ACKNOWLEDGMENTS

I express my sincere appreciation to my research advisor, H. B. Gray, for his enthusiasm, inspiration and encouraging advice throughout the course of this research. He gave me insight and confidence in addition to his excellent guidance in chemistry. He also greatly contributed to improving my English.

My special thanks are due to Dr. D. N. Hendrickson with whom I have been working, enjoying and breathing together in ferrocene chemistry. Thanks are expressed to Dr. A. W. Schlueter for his interest and valuable X-ray data on some metallocenes. Many discussions and cooperation with Drs. Hendrickson and Schlueter have been a great factor in the accomplishment of this work.

I would like to express my gratitude to Mr. G. R. Rossman and all other members of the Gray's porkers. Particularly, Rossman's assitance during my experimental work is greatly appreciated.

I also acknowledge Dr. F. C. Anson and G. W. Robinson for the use of their equipment and helpful suggestions.

I am most grateful to my wife, You Kyung, for her patience, continuing encouragement and deep understanding in my academic career. I wish to express my heartfelt thanks to my mother and brother who made all of my education possible.

Finally, the California Institute of Technology and the National Science Foundation are gratefully acknowledged for their financial support for the whole period of time of this work.

ABSTRACTS

I. ELECTRONIC STRUCTURE OF METALLOCENES

The electronic absorption spectra of various low-spin d^5 and d^6 metallocene complexes have been studied in different environments (glasses, KBr pellets, and single crystals) and as a function of temperature. Ferrocene, phenylferrocene, ruthenocene, and cobalticenium ion were selected in the d^6 study and several ferricenium, n-butylferricenium, and 1,1′-di-n-butylferricenium salts were examined in the d^5 case. The electronic spectra of ferrocene and phenylferrocene single crystals at 4.2°K clearly indicate that the bands at 22,700 cm^{-1} and 22,400 cm^{-1}, respectively, consist of two electronic transitions each. The corresponding band systems in ruthenocene and cobalticenium ion also exhibit asymmetry at 77°K. Ligand field theory has been successfully applied to the above d^6 metallocenes, utilizing the three observed spin-allowed d-d absorption band positions. Emission of ruthenocene has been observed at 23,300 cm^{-1} and discussed in conjunction with the reported ferrocene emission. The visible absorption spectra of the various ferricenium complexes show a low-energy charge transfer transition (16,200 cm^{-1} in the unsubstituted ion). Ring substitution and temperature effects have been used to assign this band to the ligand-to-metal $^2E_{2g} \rightarrow {}^2E_{1u}$ transition. The vibrational structure observed for this band at 77°K appears as a doubled progression of the lowest energy a_{1g} vibration. The doubling has been attributed to

splitting of the $^2E_{1u}$ excited state. Detailed assignments of this vibrational structure are given for $[Fe(cp)_2]PF_6$ and $[Fe(cp)_2](CCl_3CO_2H)_3$. The intense charge transfer band of ferrocene ($\sim$ 50,000 cm^{-1}), as well as the corresponding bands in the other d^6 metallocenes, have been assigned as ligand-to-metal transitions. A similar assignment has been proposed for the three strong ($f \approx 0.1$) bands observed in the ferricenium ultraviolet absorption spectrum.

II. MAGNETIC SUSCEPTIBILITY STUDY OF THE FERRICENIUM ION

The ground electronic state $[^2E_{2g}(a_{1g})^2(e_{2g})^3]$ of the ferricenium ion has been further characterized by a variable-temperature (40-300°K) magnetic susceptibility study of nine ferricenium and two analogous Fe(III) dicarbollide ($1,2\text{-}B_9C_2H_{11}^{2-}$) compounds. The observed temperature independence of the effective magnetic moments for these ferricenium compounds is explicable in terms of either a temperature-dependent, low-symmetry crystal field distortion or thermal population of the $^2A_{1g}(a_{1g})^1(e_{2g})^4$ state. Solvent and counter ion effects on the magnetic properties of the ferricenium ion are appreciable.

III. SYNTHESIS AND CHARACTERIZATION OF SEVERAL OXIDATION PRODUCTS OF RUTHENOCENE

Attempts to prepare ruthenicenium salts have resulted in the synthesis and characterization of several interesting ruthenocene

derivatives. Contrary to a previous report, electrochemical oxidation of ruthenocene employing a mercury anode yields the mercury-bridged dimer $[(cp)_2Ru—Hg—Ru(cp)_2](ClO_4)_2$. Analytical, infrared, Raman, and electronic absorption spectral data were utilized in assigning the molecular structure. In particular, a Raman band at 110 cm^{-1} was assigned to the symmetrical Ru—Hg—Ru stretching mode. Preliminary X-ray crystallographic data for the hexafluorophosphate salt, which was obtained by anion exchange, are in agreement with the above dimeric formulation. Chemical oxidation of ruthenocene by iodine and bromine gives $[Ru(cp)_2I]I_3$ and $[Ru(cp)_2Br]Br_3$, respectively, as indicated by analytical and spectral data.

TABLE OF CONTENTS

	Page
ACKNOWLEDGMENTS	iii
ABSTRACTS	v
PART I.	
Introduction	3
Experimental	6
Preparation and Purification of Compounds	6
Solvents and Liquid Glasses	7
Absorption Spectral Measurements	8
Emission Measurements	10
Theory	11
Electronic Spectra of d^6 Metallocenes	15
Spin-Allowed d-d Transitions	15
Emission and Spin-Forbidden d-d Transitions	27
Charge Transfer Bands	30
Electronic Spectra of d^5 Metallocenes	32
Band System I	32
Spin-Allowed d-d Transitions	49
Charge Transfer Bands	51
Acknowledgments	54
References	56
PART II.	
Introduction	62
Experimental Section	64

Page

Compound Preparations 64
Magnetic Measurements 66

Theory 67

Results and Discussion 72

Room Temperature Measurements 72
Variable Temperature Measurements 77

Acknowledgments 84

References 85

PART III.

Introduction 89

Experimental 90

Compound Preparation 90
Physical Measurements 92

Results and Discussion 93

Electrochemical Oxidation 93
Halides 103

Acknowledgments 105

References 106

PART IV.

PROPOSITIONS 107

PART I. ELECTRONIC STRUCTURE OF METALLOCENES. OPTICAL SPECTROSCOPIC STUDY OF METALLOCENE COMPLEXES

Part I is to partly appear in Vol. VI, "Chemical Physics Letters." The whole manuscript has been submitted for publication in J. Am. Chem. Soc.

Electronic Structure of Metallocenes

Y. S. Sohn, David N. Hendrickson, and Harry B. Gray

Contribution No. 4104 from the Arthur Amos Noyes Laboratory of Chemical Physics, California Institute of Technology, Pasadena, California 91109.

Received .

Abstract: The electronic absorption spectra of various low-spin d^5 and d^6 metallocene complexes have been studied in different environments (glasses, KBr pellets, and single crystals) and as a function of temperature. Ferrocene, phenylferrocene, ruthenocene, and cobalticenium ion were selected in the d^6 study and several ferricenium, n-butylferricenium, and 1,1′-di-n-butylferricenium salts were examined in the d^5 case. The electronic spectra of ferrocene and phenylferrocene single crystals at 4.2°K clearly indicate that the bands at 22,700 cm^{-1} and 22,400 cm^{-1}, respectively, consist of two electronic transitions each. The corresponding band systems in ruthenocene and cobalticenium ion also exhibit asymmetry at 77°K. Ligand field theory has been successfully applied to the above d^6 metallocenes, utilizing the three observed spin-allowed d-d absorption band positions. Emission of ruthenocene has been observed at 23,300 cm^{-1} and discussed in conjunction with the reported ferrocene emission. The visible absorption spectra of the various ferricenium

complexes show a low-energy charge transfer transition (16, 200 cm^{-1} in the unsubstituted ion). Ring substitution and temperature effects have been used to assign this band to the ligand-to-metal $^2E_{2g} \rightarrow {}^2E_{1u}$ transition. The vibrational structure observed for this band at 77°K appears as a doubled progression of the lowest energy a_{1g} vibration. The doubling has been attributed to splitting of the $^2E_{1u}$ excited state. Detailed assignments of this vibrational structure are given for $[Fe(cp)_2]PF_6$ and $[Fe(cp)_2](CCl_3CO_2H)_3$. The intense charge transfer band of ferrocene ($\sim 50,000$ cm^{-1}), as well as the corresponding bands in the other d^6 metallocenes, have been assigned as ligand-to-metal transitions. A similar assignment has been proposed for the three strong ($f \approx 0.1$) bands observed in the ferricenium ultraviolet absorption spectrum.

Since its discovery in 1951,[1,2] ferrocene has played an important role, both theoretically and experimentally, in developing an understanding of the electronic structures of organometallic compounds. On the theoretical side the studies have included numerous MO calculations[3-12] as well as some qualitative crystal field approaches.[13-16] From the reviews of these works by Rosenblum,[17] Brown,[18] and Ballhausen and Gray,[19] it is evident that none of the calculations is successful in explaining the totality of experimental facts.

The theoretical studies do give, however, a useful qualitative framework for the interpretation of various physical properties. For instance, the MO calculations in general indicate that the highest occupied orbitals are a_{1g} and e_{2g}, with the lowest unoccupied level being e_{1g}. ESR and magnetic susceptibility studies on the ferricenium ion,[20, 21] its carborane analogs,[22] vanadocene, and nickelocene,[23] are in agreement with a level ordering of $e_{2g} \sim a_{1g} < e_{1g}$.

The most powerful tool for locating the excited states and checking various features of the bonding theories of ferrocene is optical spectroscopy. Consequently, the ferrocene ultraviolet and visible spectrum has been extensively studied by Scott and Becker,[24] and more recently by Armstrong et al ,[25] Smith and Meyer,[26] and Stephenson and Winterrowd.[27] Very recently we communicated[28] the results of a 4.2°K visible absorption spectroscopic study of ferrocene and proposed assignments for the three spin-allowed d-d transitions. Improved resolution of the lowest energy (4400 Å) ferrocene band provided the key to this assignment scheme.

In this paper the results of a detailed absorption spectral study of several d^5 and d^6 metallocenes are given. In the case of the d^6 metallocenes, ferrocene will be used as a model compound. The resolution into two bands of the lowest energy visible peak observed for ferrocene[28] will be shown to be general. We have analyzed these two bands and a slightly higher energy band (3250Å in ferrocene) as d-d transitions and obtained ligand field parameters

which are used to predict the positions of the spin-forbidden d-d bands. Previous emission spectroscopic results for ferrocene as well as new results for ruthenocene are discussed in light of these predictions.

In another recent communication[21] the lowest energy electronic band in the ferricenium ion was shown to be a $^2E_{2g} \rightarrow {}^2E_{1u}$ transition, in disagreement with previous reports.[29, 30] Low temperature spectral data for various ferricenium salts, unsubstituted as well as substituted, are shown to support the $^2E_{2g} \rightarrow {}^2E_{1u}$ assignment and a detailed interpretation of the observed vibrational structure is given. A ligand field treatment of the d-d transitions for the ferricenium ion also is developed and compared with experimental results. Finally, the ultraviolet bands of both d^6 and d^5 metallocene complexes have been assigned.

Experimental

Preparation and Purification of Compounds. Ferrocene from two different sources (Alfa and Eastman-Kodak) was used after purification. No spectral difference was noted between the purified materials. Purification was carried out by recrystallization in ethanol, followed by repeated sublimation in vacuum and finally zone-refining. Transparent single crystal plates of ferrocene were grown in reagent grade absolute ethanol by slow evaporation.

Ruthenocene, $Ru(C_5H_5)_2$, (Research Inorg.) was recrystallized in ethanol and sublimed twice in vacuum. Light yellow single crystals with well developed faces were obtained.

$[Co(C_5H_5)_2]ClO_4$. To an aqueous solution of cobalticenium picrate[31] was added a slight excess of perchloric acid and the resultant picric acid was extracted with ether. The perchlorate solution was concentrated and cooled in ice. Light orange needles were obtained. Anal. (Galbraith) Calcd for $[Co(C_5H_5)_2]ClO_4$: Co, 20.42%; C, 41.62%; H, 3.49%; Cl, 12.28%. Found: Co, 20.25%; C, 41.83%; H, 3.62%; Cl, 12.21%.

$Fe(C_6H_5-C_5H_4)(C_5H_5)$. Phenylation of ferrocene was accomplished by the method of Broadhead and Pauson.[32] Monophenylferrocene was isolated using an alumina column; reddish orange needles (mp 111°, lit.[33] 109-110°) were obtained by repeated recrystallization in acetone. Further identification was obtained by a n.m.r spectrum.

Transparent single crystal plates of phenylferrocene were grown in reagent grade acetone by slow evaporation.

$[Fe(C_5H_5)_2](CCl_3CO_2H)_3$.[34] Ferrocene (10 mmol) and trichloroacetic acid (60 mmol) were allowed to react in 30 ml benzene at room temperature for a day. The benzene was then slowly evaporated giving crystals of the desired compound (mp 129-130°, lit.[34] 126-128°). Anal. Calcd for $[Fe(C_5H_5)_2](CCl_3CO_2H)_3$: Fe, 8.26%; Cl, 47.19%; C, 28.42%; H, 1.94%. Found: Fe, 8.54%; Cl, 47.44%; C, 28.55%; H, 2.11.

$[Fe(C_5H_5)_2]BF_4$, $[Fe(C_5H_5)_2]PF_6$, $[Fe(n\text{-}C_4H_9\text{—}C_5H_4)(C_5H_5)]PF_6$ and $[Fe(n\text{-}C_4H_9\text{—}C_5H_4)_2]PF_6$. See Part II of this thesis.[35]

Solvents and Liquid Glasses. The following solvents for room temperature spectral measurements or for low temperature glass preparation were used without further purification: spectroquality acetonitrile, methanol, and EPA (ethyl ether, isopentane, and ethanol in volume ratio of 5:5:2), and anhydrous U.S.P.-N.F. grade ethanol.

Propionitrile (Eastman-Kodak) was further purified by repeated fractional distillation. Chromatoquality (MC&B) 2-methyltetrahydrofuran (2-MTHF) was distilled from $LiAlH_4$ to remove peroxides and residual water. Pure grade 3-methylpentane used in the emission study was further purified by stirring with concentrated sulfuric acid for three days, washing several times with sodium bicarbonate solution and water, and finally fractionally distilling over P_2O_5. No phosphorescence from solvent impurities was detectable after this

purification procedure.

When EPA was not a suitable solvent the following solvent mixtures were used for low temperature glasses: 2-Me-THF and ethanol (1:2); ethyl ether, propionitrile, and ethanol (3:1:1); ethanol and methanol (5:1); and 10M aqueous LiCl solution. IR spectrograde KBr powder (MC&B) was used in the preparation of KBr pellets.

Absorption Spectral Measurements. Visible and near ultraviolet absorption spectra were usually recorded on a Cary Model 14 CMRI spectrophotometer equipped with both a Cary low temperature dewar modified to hold a standard 1.00 cm cell and with another quartz dewar designed for direct immersion of the sample cell into the liquid nitrogen. With this latter dewar a sample can be cooled down to liquid nitrogen temperature in a few minutes.

The following procedure was used in obtaining the relative intensity spectra of various species (using the Cary spectrophotometer) at room and liquid nitrogen temperatures. Solutions of $Fe(C_5H_5)_2$, $Ru(C_5H_5)_2$, $Fe(C_6H_5-C_5H_4)(C_5H_5)$, and $[Co(C_5H_5)_2]ClO_4$, were prepared by dissolution in an appropriate organic solvent mixture. The room temperature spectrum was recorded with the solution in the dewar and then liquid nitrogen was added for the low temperature (77°K) measurement. This procedure gave relative intensity measurements after correction for solvent contraction at the lower temperature. Bubbling of the liquid nitrogen was prevented by cooling under reduced pressure. Window fogging was eliminated by continuous flushing of the sample

compartment with dry nitrogen gas. Room temperature and 77°K absorption spectra for various ferricenium compounds in KBr pellets were also obtained using the above technique employing the quartz dewar in the Cary instrument. The ferricenium ion is very unstable in most organic solvents, even acetonitrile and nitromethane. It is well known, however, that the ferricenium ion is fairly stable in acidic aqueous solution. We carefully checked spectroscopically the stability of various ferricenium salts in the neutral LiCl solution used for the low temperature glass and no evidence for decomposition was detected for at least one hour.

Exact solution absorption band intensity measurements at room temperature were completed on the Cary instrument (without dewar) using the following solvents: ethanol, isopentane, and EPA for ferrocene, ruthenocene and phenylferrocene; acetonitrile and water for $[Co(C_5H_5)_2]ClO_4$; 0.01 M $HClO_4$ solution for the ferricenium salts.

The single crystal visible spectra of ferrocene and phenylferrocene were measured photographically on a Jarrell-Ash 0.75 meter instrument equipped with a grating blazed at 10,000 Å. Well formed crystals of ferrocene and phenylferrocene were mounted between two quartz plates and lowered slowly into liquid nitrogen. After a short annealing period, the crystals were cooled rapidly in liquid helium. Approximately one half of the crystals powdered during such treatment, in agreement with previous observations.[27] Band II of ferrocene and phenylferrocene was recorded in second

order using a tungsten lamp source, Kodak 103a-F plates, and Corning filters 3-74 and 4-97, which pass light between 3800-6000 Å. Band III of ferrocene was recorded in third order using a 150-watt xenon lamp source, Kodak 103a-O plates, a water filter, and a Corning filter 7-54 which passes only ultraviolet light below 3900 Å.

Emission Measurements. Phosphorescence emission was measured using an Aminco-Bowman Spectrofluorometer connected to a X-Y recorder. Solutions of ferrocene and ruthenocene (10^{-2} - 10^{-3} M) in purified 3-methylpentane were used. The sample solutions were degassed, sealed in quartz tubes, and then cooled to 77°K for the emission measurements.

Theory

In the solid state the molecular symmetry of ferrocene is D_{5d}. The cyclopentadienyl π basis orbitals can be classified in this symmetry and ordered in energy as shown in Figure 1. The iron valence orbitals (see Figure 1) transform as $a_{1g}(3d)$, $e_{1g}(3d)$, $e_{2g}(3d)$, $a_{1g}(4s)$, $a_{2u}(4p)$, and $e_{1u}(4p)$.

A useful molecular orbital energy level diagram for ferrocene may be constructed from the above symmetry considerations and from the values of overlap integrals between the ring and the metal orbitals. The best available iron and carbon π orbitals give:[9]

$S(a_{1g})_d$	$S(e_{1g})$	$S(e_{2g})$	$S(a_{1g})_s$	$S(a_{2u})$	$S(e_{1u})$
0.030	0.148	0.079	0.527	0.236	0.468

Strong bonds between the metal orbitals $a_{1g}(4s)$, $a_{2u}(4p)$, and $e_{1u}(4p)$ and the carbon π orbitals result in placing their corresponding anti-bonding levels high in energy. Of the 3d orbitals of the metal, the e_{1g} set has the greatest overlap with the ring orbitals and thus should form relatively strong bonds. These considerations were put forward in a recent review[19] as the basis of the estimated energy level diagram for ferrocene which is reproduced in Figure 1. The ground state of d^6 ferrocene is $^1A_{1g}(1e_{2g})^4(2a_{1g})^2$. The one-electron transition $2a_{1g} \rightarrow 2e_{1g}$ results in excited states of $^1E_{1g}$ and $^3E_{1g}$ symmetries, whereas $1e_{2g} \rightarrow 2e_{1g}$ gives excited states of $^1E_{1g}$, $^3E_{1g}$, $^1E_{2g}$, and $^3E_{2g}$ symmetries. Theoretical expressions for the

Fig. 1. Estimated relative ϵ^{core} energies for the molecular orbitals in metallocene complexes.

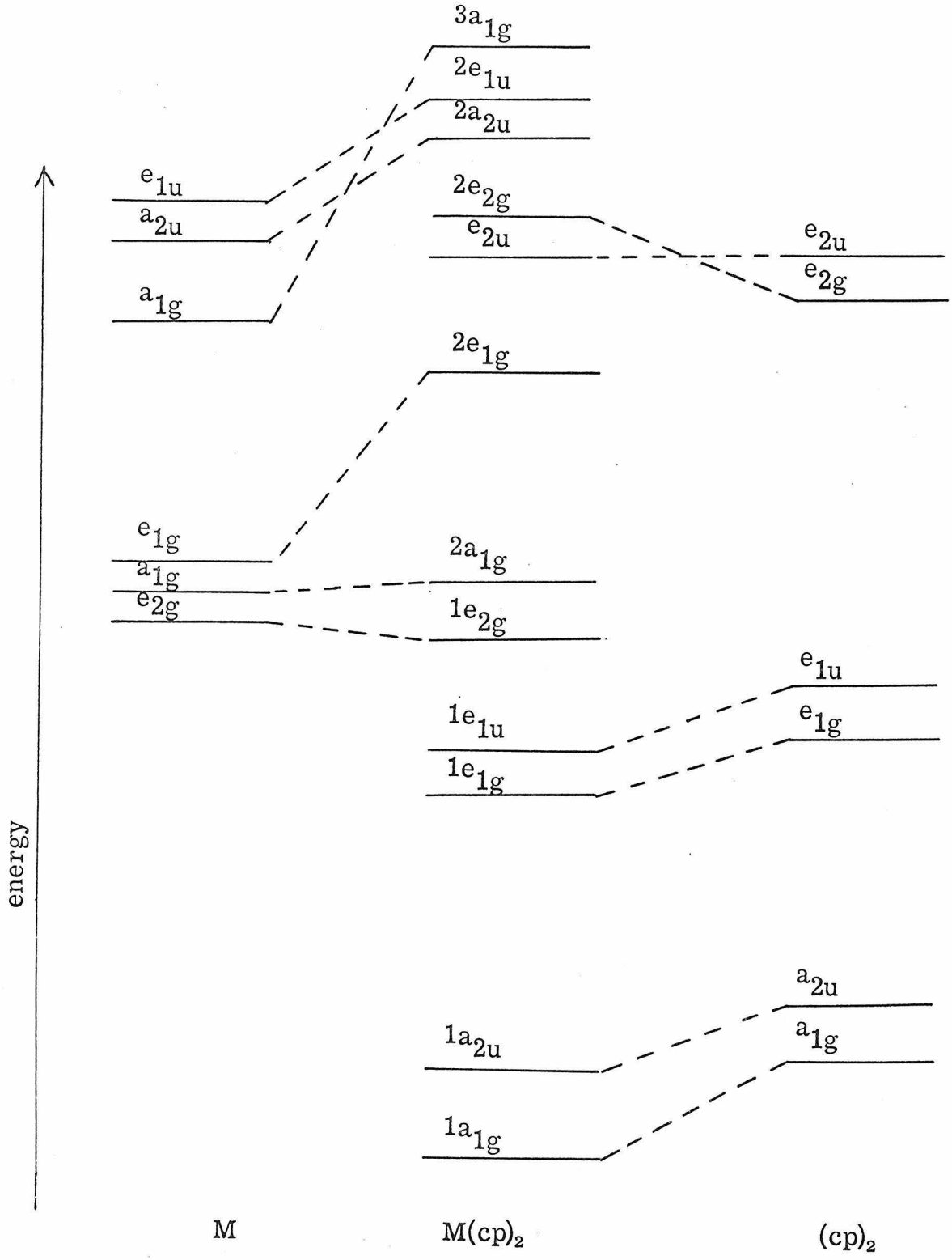
energy
M
M(cp)2
(cp)2
e1u
a2u
a1g
3a1g
2e1u
2a2u
2e2g
e2u
e2u
e2g
2e1g
e1g
a1g
e2g
2a1g
1e2g
e1u
e1g
1e1u
1e1g
a2u
a1g
1a2u
1a1g

spin-allowed transitions, including configurational interaction between the two $^1E_{1g}$ states, were given in our recent communication.[28] These expressions as well as those for the singlet-triplet transitions, are set out in Table I. All the expressions were derived by standard procedures[36] using a strong field approach.

The ground electronic state of the ferricenium ion has been shown by esr[20, 22] and magnetic susceptibility studies[35] to be $^2E_{2g}\ (1e_{2g})^3\ (2a_{1g})^2$. This state is split into two Kramers doublets by spin-orbit coupling and crystal fields of symmetry lower than D_5. Similarly, the degenerate excited states (E_{1g} or E_{2g} symmetry) resulting from d-d transitions are expected to split into two Kramers doublets. However, the splitting of the two Kramers doublets will be small and as such will not be included in our treatment of the d-d transitions in the ferricenium ion. Eight spin-allowed d-d transitions are predicted (spin-forbidden transitions will not be discussed) from three one-electron transitions: $^2E_{2g} \rightarrow {}^2A_{1g}$ for the $2a_{1g} \rightarrow 1e_{2g}$ one-electron transition; $^2E_{2g} \rightarrow {}^2E_{1g}$ and $^2E_{2g}$ for $2a_{1g} \rightarrow 2e_{1g}$; $^2E_{2g} \rightarrow 2\,{}^2E_{1g}$, $^2E_{2g}$, $^2A_{1g}$, and $^2A_{2g}$ for $1e_{2g} \rightarrow 2e_{1g}$. The theoretical transition energy expressions are given in Table I. There is no configurational interaction between the two $^2A_{1g}$ states and likewise the ground state $^2E_{2g}$ does not mix with the two $^2E_{2g}$ excited states. In the theoretical expressions for the three $^2E_{1g}$ transitions configurational interaction was not included, but in the numerical treatment it was incorporated by matrix diagonalization using the following non-zero off-diagonal elements: $H_{ab} = -4\sqrt{3}B$, $H_{ac} = 2\sqrt{6}B$ and $H_{bc} = 3\sqrt{2}B$.

TABLE I[a]. Ligand Field Transitions of d^6 and d^5 Metallocenes

	Transitions	Transition Energy Expressions
d^6	$^1A_{1g} \rightarrow a^1E_{1g}$	$\epsilon^c(e_{1g}) - \frac{1}{2}[\epsilon^c(e_{2g}) + \epsilon^c(a_{1g})] + 6B - C - \frac{1}{2}X$
	$\rightarrow b^1E_{1g}$	$\epsilon^c(e_{1g}) - \frac{1}{2}[\epsilon^c(e_{2g}) + \epsilon^c(a_{1g})] + 6B - C + \frac{1}{2}X$
	$\rightarrow {}^1E_{2g}$	$\epsilon^c(e_{1g}) - \epsilon^c(e_{2g}) - 9B - C$
	$^1A_{1g} \rightarrow a^3E_{1g}$	$\epsilon^c(e_{1g}) - \frac{1}{2}[\epsilon^c(e_{2g}) + \epsilon^c(a_{1g})] - B - 3C - \frac{1}{2}Y$
	$\rightarrow b^3E_{1g}$	$\epsilon^c(e_{1g}) - \frac{1}{2}[\epsilon^c(e_{2g}) + \epsilon^c(a_{1g})] - B - 3C + \frac{1}{2}Y$
	$\rightarrow {}^3E_{2g}$	$\epsilon^c(e_{1g}) - \epsilon^c(e_{2g}) - 9B - 3C$
d^5	$^2E_{2g} \rightarrow a^2A_{1g}$	$\epsilon^c(e_{2g}) - \epsilon^c(a_{1g}) + 20B$
	$\rightarrow b^2A_{1g}$	$\epsilon^c(e_{1g}) - \epsilon^c(e_{2g}) - 3B - C$
	$\rightarrow {}^2A_{2g}$	$\epsilon^c(e_{1g}) - \epsilon^c(e_{2g}) - 3B - C$
	$\rightarrow a^2E_{2g}$	$\epsilon^c(e_{1g}) - \frac{1}{2}[\epsilon^c(e_{2g}) + \epsilon^c(a_{1g})] + 5B - C - \frac{1}{2}Z$
	$\rightarrow b^2E_{2g}$	$\epsilon^c(e_{1g}) - \frac{1}{2}[\epsilon^c(e_{2g}) + \epsilon^c(a_{1g})] + 5B - C + \frac{1}{2}Z$
	$\rightarrow a,b,c^2E_{1g}$	$\begin{bmatrix} \epsilon^c(e_{1g}) - \epsilon^c(a_{1g}) + 7B - C \\ \epsilon^c(e_{1g}) - \epsilon^c(e_{2g}) + 3B - 2C \\ \epsilon^c(e_{1g}) - \epsilon^c(e_{2g}) - 3B - 3C \end{bmatrix}$[b]

$$X = \{[\epsilon^c(e_{2g}) - \epsilon^c(a_{1g}) + 6B]^2 + 384B^2\}^{\frac{1}{2}}$$

$$Y = \{[\epsilon^c(e_{2g}) - \epsilon^c(a_{1g}) + 16B]^2 + 96B^2\}^{\frac{1}{2}}$$

$$Z = \{[\epsilon^c(e_{2g}) - \epsilon^c(a_{1g}) + 4B]^2 + 192B^2\}^{\frac{1}{2}}$$

[a]Here the ϵ^c are one-electron core energies and B and C are Racah electron repulsion parameters.

[b]These expressions as given do not include configurational interaction; see Theory section.

Electronic Spectra of d^6 Metallocenes.

The room temperature absorption spectra of three d^6 metallocenes (ferrocene, ruthenocene, and cobalticenium) are displayed in Fig. 2; band positions and intensities are given in Table II for these three complexes as well as for phenylferrocene. Similarities in band shapes and intensities are apparent in these spectra. We have elected to use ferrocene as the model molecule in the following discussion; absorption spectral data for the other ferrocene-like molecules will be discussed when providing insight or support for the ferrocene assignments. As a matter of convenience, the bands in the intensity range $10 < \epsilon \leq 1000$ will be considered first.

Spin-Allowed d-d Transitions. The d^6 metallocenes exhibit two low intensity bands in the visible range (see Figure 2 and Table II). The two ferrocene bands at 22,700 and 30,800 cm^{-1} (i.e., band systems II and III, respectively, in Figure 2) have generally been assigned as d-d transitions.[24, 25, 28] Using strong-field theory three spin-allowed d-d transitions (two $^1A_{1g} \rightarrow {}^1E_{1g}$ and one $^1A_{1g} \rightarrow {}^1E_{2g}$) are expected for ferrocene (see Theory). There has been considerable controversy as to the location of these three transitions. Initial reports[23, 37] of the resolution of band system II into two bands have not been accepted by other workers. The ferrocene single crystal low-temperature absorption spectra recently reported by Stephenson and Winterrowd[27] (at 77°K) and by Sohn et al.[28] (at 4.2°K) have conclusively shown that the ferrocene 22,700 cm^{-1} system consists of two bands (see Figure 3). In this section we will expand on

Fig. 2. Electronic spectra of d^6 metallocenes in solution at 300°K: $Fe(cp)_2$ in isopentane (——); $Ru(cp)_2$ in isopentane (----); $[Co(cp)_2]ClO_4$ in aqueous solution (—•—•—•—).

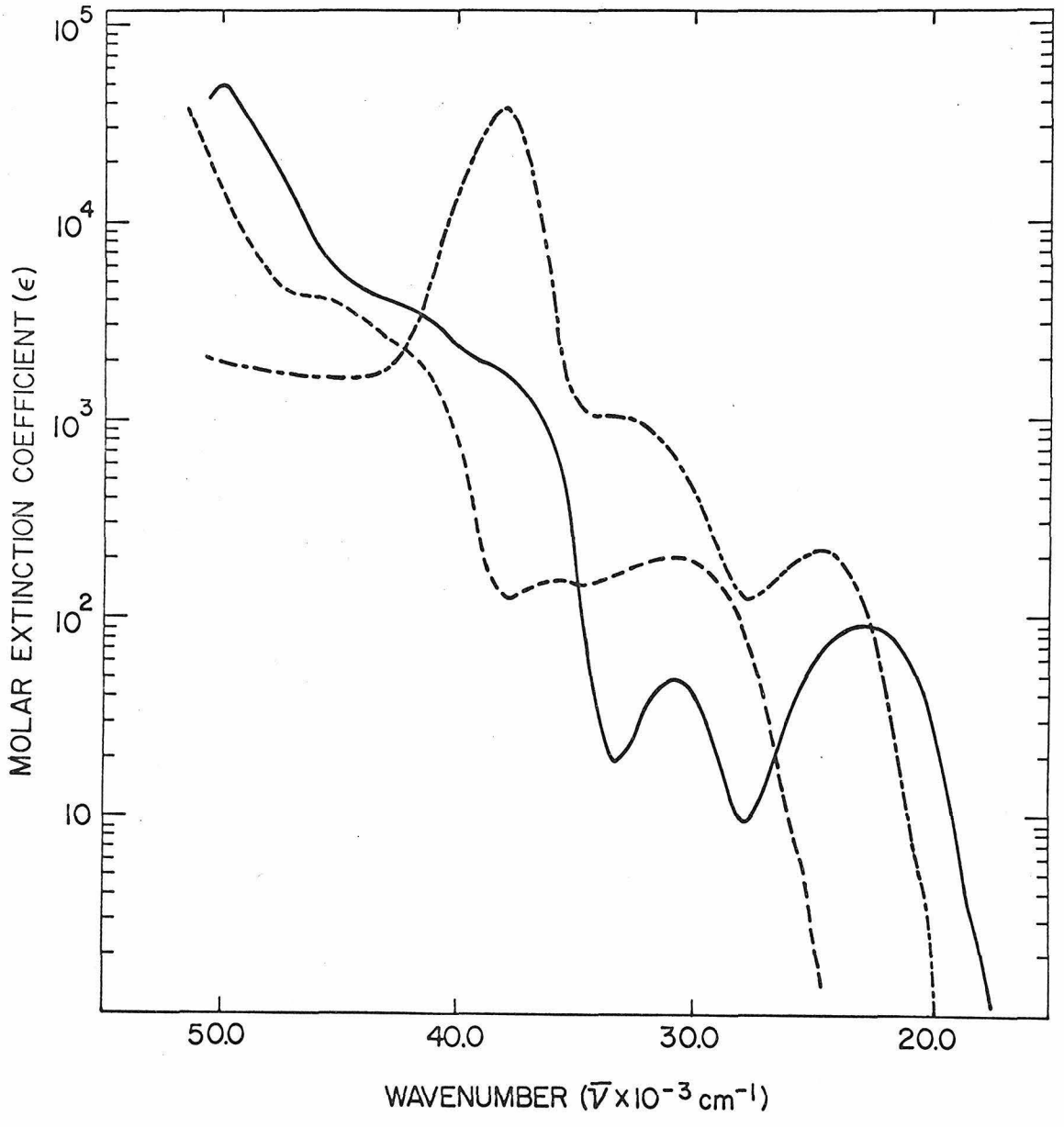
MOLAR EXTINCTION COEFFICIENT (ε)
10^5
10^4
10^3
10^2
10
50.0
40.0
30.0
20.0
WAVENUMBER ($\bar{\nu}$ x 10^-3 cm^-1)

TABLE II. The Ultraviolet and Visible Absorption Spectra of Four d^6 Metallocenes

Molecule	Band Identification	Band, cm^{-1}	ϵ	$f \times 10^3$
$Fe(cp)_2$	I[a]	18,900	~7	
	II[a, b]	22,700 (21,800 / 24,000)	91.0 (36 / 72)	1.9 (0.39 / 1.1)
	III[a]	30,800	49.0	0.75
	IV[c, d]	37,700	1,600	
	V[c, d]	41,700	3,500	
	VI[d]	50,000	51,000	730
$Ru(cp)_2$	I[a]	26,000	~5	
	II[a, b]	31,000 (30,000 / 32,900)	200 (120 / 160)	5.0 (1.5 / 2.4)
	III[a]	36,000	150	
	IV[c, d]	42,000	2,000	
	V[c, d]	46,100	4,200	
	VI[d]	>51,300	>50,000	

TABLE II. (Continued)

Molecule	Band Identification	Band, cm^{-1}	ϵ	$f \times 10^3$
$Co(cp)_2^+$	I[e]	21,800	~7	
	II[b, e]	24,600 (24,300 / 26,400)	220 (140 / 120)	3.8 (1.3 / 1.5)
	III[e]	33,300	1,200	
	VI[e]	38,000	38,000	500
Fe(ϕ-cp)(cp)	I[a]	~17,500	~5	
	II[a, b]	22,400 (20,800 / 23,000	310 (160 / 320)	6.1 (1.3 / 4.3)
	III[a]	29,500	850	
	IV[a]	31,400	1,250	
	V[d]	36,100	10,100	
	VI[d]	42,000	16,300	
	VII[d]	>50,000	>30,000	

[a]Measured in EPA. [b]Band can be resolved into two submaxima at 77°K; Gaussian resolution gives the bands in parenthesis. [c]Shoulder. [d]Measured in isopentane. [e]Measured as the perchlorate salt in aqueous solution.

our ferrocene communication and generalize to other ferrocene-like molecules.

Band system II in the 4.2°K single crystal ferrocene spectrum (see Figure 3) appears as a vibrationally structured band shouldering a more intense, unstructured band. Band system III also develops vibrational structure at liquid helium temperature. Details of peak position and spacing for the vibrational structure in these band systems are given in Table III. Absorption spectra at 4.2°K were also obtained for thick single crystals of ferrocene to insure that we had detected all the vibrational bands in the structure. The spacing of the vibrational structure in each band is 240 ~ 300 cm^{-1}, which is the excited state totally symmetric ring-metal vibration (a_{1g}, the ground state value is 309 cm^{-1}).[38] The non-uniformity in spacing in each system is seemingly outside of the experimental uncertainty in peak location and is possibly attributable to having more than one vibronic origin.

We have been able to resolve into two bands the low energy band system (corresponding to system II of ferrocene) in both phenylferrocene and ruthenocene. In Figure 4 the temperature dependence of band system II of phenylferrocene is depicted. The 77°K spectrum of phenylferrocene is not shown in Figure 4 but could be obtained using either an EPA glass or a single crystal. The single crystal spectrum of phenylferrocene at 4.2°K shows no vibrational structure, but in this case it is more apparent that band system II is composed of two transitions. Similar comments can be made concerning band system II in ruthenocene. The 77°K absorption spectrum

TABLE III. Vibrational Structure of Ferrocene Bands IIa and III

System	$\bar{\nu}(cm^{-1})$	$\Delta\bar{\nu} = \bar{\nu}_n - \bar{\nu}_{n-1}$
IIa	19,870 ± 20	
	20,120 ± 10	250
	20,400 ± 10	280
	20,670 ± 10	270
	20,970 ± 10	300
	21,240 ± 10	270
	21,510 ± 10	270
	21,770 ± 10	260
	22,050 ± 10	280
	22,330 ± 10	280
	22,640 ± 20	310
III	29,590 ± 20	
	29,860 ± 20	270
	30,150 ± 20	290
	30,450 ± 20	300
	30,690 ± 20	240
	30,950 ± 20	260
	31,210 ± 20	260
	31,500 ± 20	290
	31,760 ± 20	260
	32,020 ± 20	260

Fig. 3. Visible absorption spectra of ferrocene at various temperatures: a, EPA solution at 300°K; b, EPA glass at 77°K; c, single crystal at 4.2°K. The intensity of the curve c is not to scale.

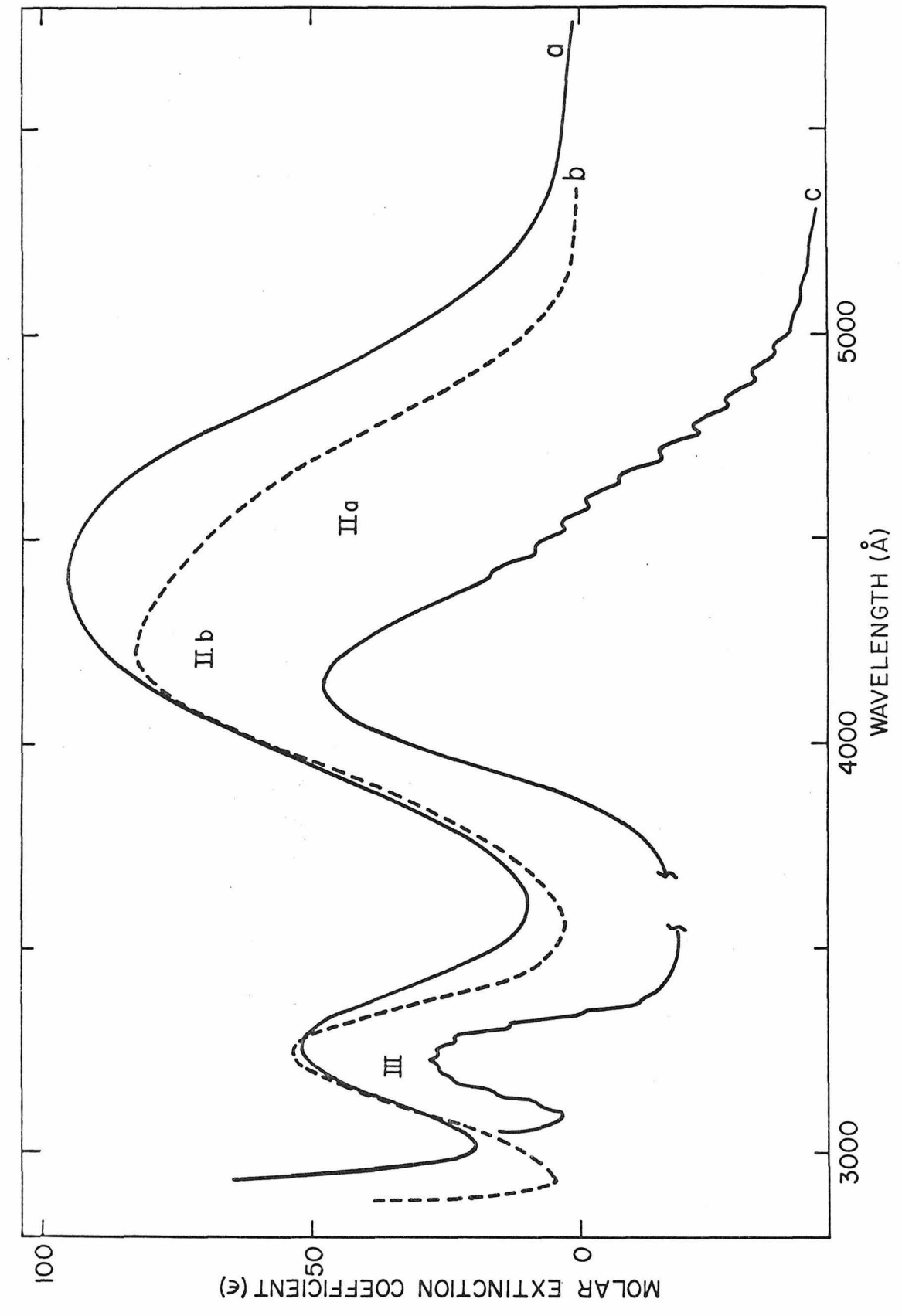
MOLAR EXTINCTION COEFFICIENT (ε)
100
50
0
3000
4000
5000
WAVELENGTH (Å)
a
b
c
III
IIb
IIa

Fig. 4. Visible absorption spectra of phenylferrocene: a, EPA solution at 300°K; b, single crystal at 4.2°K.

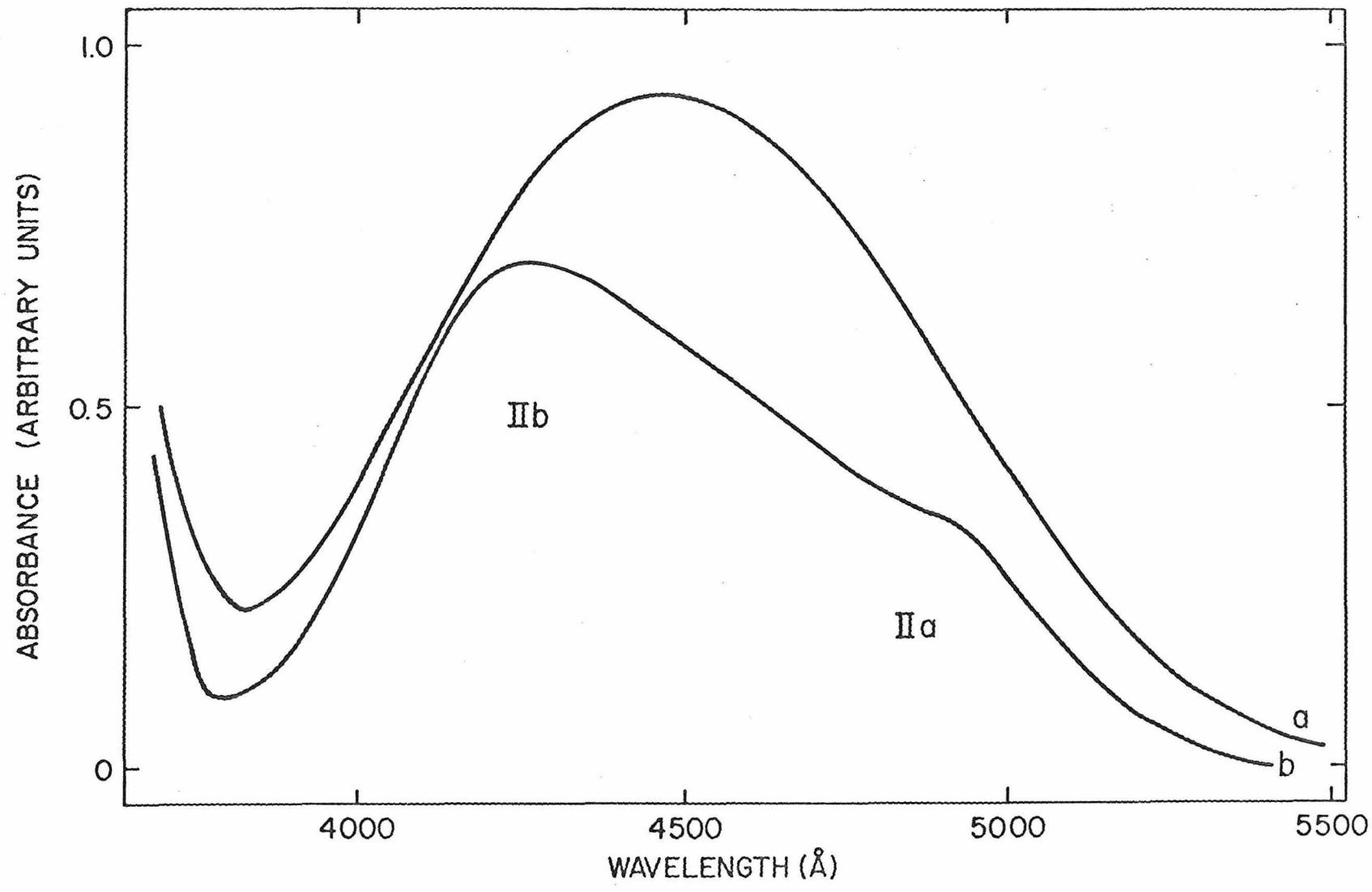
1.0
0.5
0
ABSORBANCE (ARBITRARY UNITS)
IIb
IIa
a
b
4000
4500
5000
5500
WAVELENGTH (Å)

of ruthenocene in EPA glass, as reproduced in Figure 5, shows clearly two peaks in band system II. The probability of an impurity as the explanation for the shoulder in ferrocene has been eliminated. In the cobalticenium ion, the resolution of bands IIa and IIb is poor; nevertheless, the asymmetric band at 77°K could be resolved into two Gaussian curves.

The three expected d-d transitions have thus been located in these d^6 metallocenes. Franck-Condon maxima were obtained in each case by Gaussian analysis of the 77°K spectra (plotted in units of ϵ vs. frequency) and were used as transition energies. The three observed d-d bands are assigned in Table IV to the three spin-allowed d-d transitions. This assignment scheme for the three bands is unique in the sense that it is the only one which yields a physically realistic value for the Racah parameter B. The proposed interpretation is also consistent with the observed temperature behavior of these bands. Band IIa decreases more in intensity than bands IIb and III when the temperature is lowered (see Figure 3). In agreement with this observation our assignment has attributed more d-d character to band IIa than the other two bands (i.e., band IIa results from the one-electron transition $2a_{1g} \rightarrow 2e_{1g}$). The ligand field parameters B, $\Delta_1 = \epsilon^c(e_{2g} - 2a_{1g})$, and $\Delta_2 = \epsilon^c(2e_{1g} - 2a_{1g})$ have been evaluated for the four d^6 metallocene complexes and are given in Table IV. It seems worthwhile to point out that the parameters B and Δ_1 were evaluated without any assumptions from appropriate combinations of the three equations. In order to evaluate Δ_2 it is necessary to assume

Fig. 5. Near-ultraviolet absorption spectra of ruthenocene: a, EPA solution at 300°K; b, EPA glass at 77°K.

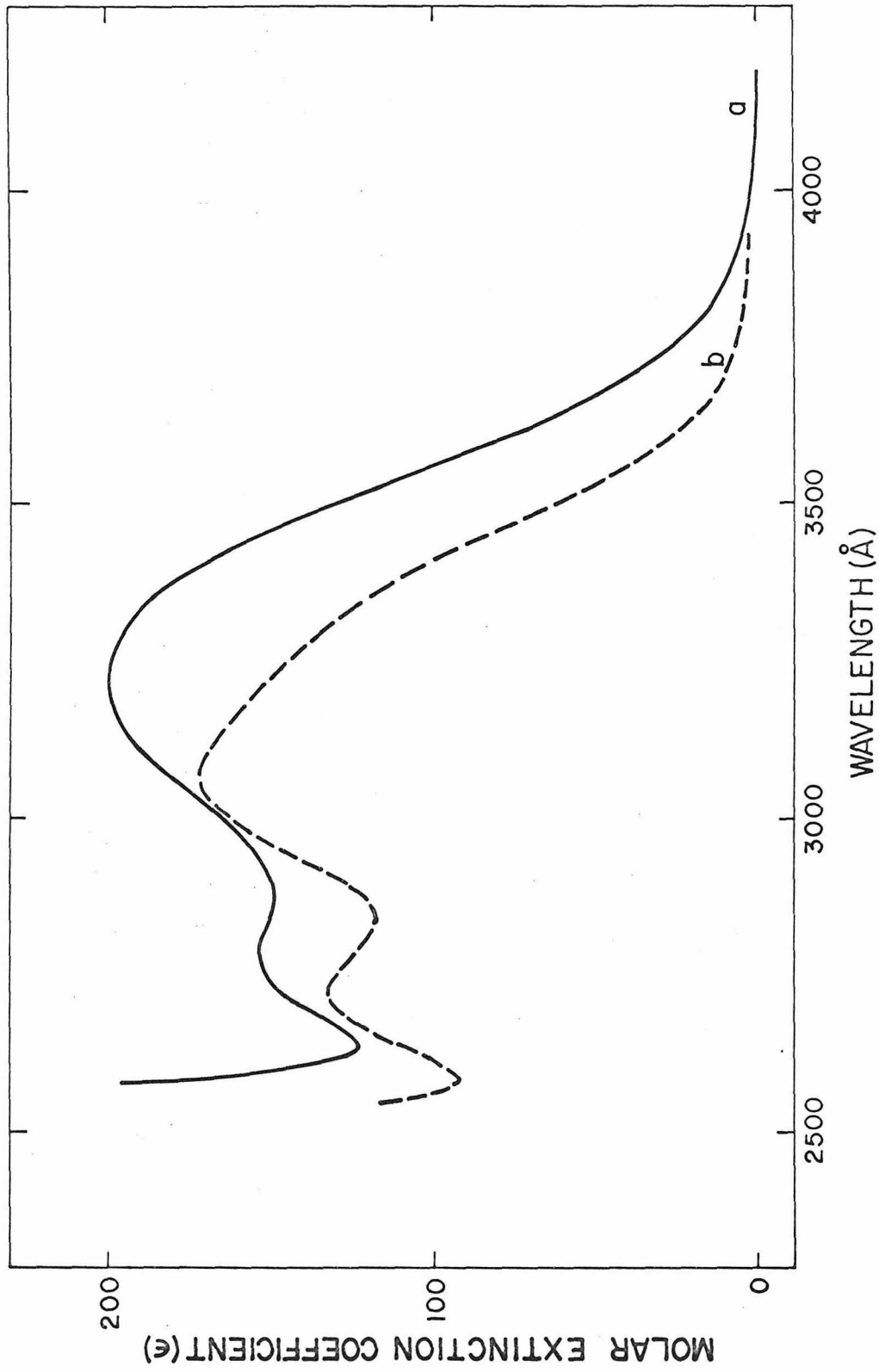
MOLAR EXTINCTION COEFFICIENT (ε)
200
100
0
2500
3000
3500
4000
WAVELENGTH (Å)
a
b

TABLE IV. Spin-Allowed Ligand Field Absorption Transitions and Parameters for d^6 Metallocenes[a]

	$Fe(cp)_2$	$Ru(cp)_2$	$Co(cp)_2^+$	$Fe(\phi\text{-}cp)(cp)$
$^1A_{1g} \rightarrow a^1E_{1g}$	21,800	29,500	24,300	20,800
$^1A_{1g} \rightarrow {}^1E_{2g}$	24,000	32,500	26,400	23,000
$^1A_{1g} \rightarrow b^1E_{1g}$	30,800	36,600	33,300	29,500
Δ_2	22,000	29,800	24,400	21,000
Δ_1	- 7,100	- 6,600	- 7,200	- 6,900
B	390	260	400	374
β	0.42	0.42	0.36	0.40

[a]Energies in cm^{-1}.

a value for the ratio C/B. We have taken C/B = 4.0, which is generally reasonable for the case of transition metal complexes. The Δ_2 values thus obtained are only slightly affected by changing the C/B ratio, since the value of B is small in these metallocenes.

The values of the ligand field parameters for the d^6 metallocenes are of some interest. The three transitions move to higher energy in the series Fe < Co < Ru, reflecting the increasing ligand field splitting. Thus Δ_2 increases parallel to the probable increase in ring → metal bonding, Fe < Co < Ru. The relatively small Racah electron repulsion parameters B in these d^6 metallocenes indicate appreciable covalency. The B value for ferrocene (390 cm^{-1}) compares closely with that for $Fe(CN)_6^{4-}$ (380 cm^{-1}).[39] Finally, it can be seen in Table IV that in every case the one-electron energy of the a_{1g} orbital is higher than that of the e_{2g} level. This is in agreement with qualitative molecular orbital theory, because the filled, primarily metal e_{2g} level is expected to derive some stabilization from $d\pi \rightarrow$ ring bonding with the unfilled ligand level of e_{2g} symmetry. Finally, we note that Δ_1 is approximately the same for $Fe(cp)_2$ and $Co(cp)_2^+$, whereas in $Ru(cp)_2$ Δ_1 is appreciably smaller. This probably reflects a balance between increased $d\pi \rightarrow$ ring bonding in $Ru(cp)_2$, which lowers $\epsilon^c(e_{2g})$, and increased participation of the metal 4s orbital, which lowers $\epsilon^c(a_{1g})$.

The ligand field parameters are also useful in predicting the location of the spin-forbidden absorption transitions and interpreting emission data, a subject to which we now turn.

Emission and Spin-Forbidden d-d Transitions. The phosphorescence of ferrocene was not detectable in 3-methylpentane glass (77°K) at the highest sensitivity of the instrument we used. However, ruthenocene exhibited a clear phosphorescence in the visible region when illuminated with ~ 36, 000 cm^{-1} light. The band maximum is located at 23, 300 cm^{-1}. The half life of the ruthenocene phosphorescence was estimated to be relatively short (< 1 sec). During these emission measurements it was found that many unpurified organic solvents (even the spectrograde) such as EPA and ethanol showed a relatively strong phosphorescence in the region of interest at the highest instrument sensitivity, whereas the purified 3-methylpentane showed negligible phosphorescence in this region.

Phosphorescence and three very week spin-forbidden absorption bands (spin-forbidden d-d bands) of ferrocene were reported by Scott and Becker.[24] It was concluded[25] that the observed emission was not compatible with the energy scheme deduced from the observed absorption transitions within the framework of the present theory of phosphorescence. Another recent paper[26] reported the phosphorescence of ferrocene in different solvents, including inert gases. In both cases, phosphorescence of ferrocene was observed with the exciting light in the region of absorption band III (~31, 000 cm^{-1}).

Ruthenocene has shown phosphorescence also with exciting light in the region of band III ($\sim 36,000\ cm^{-1}$). Therefore, the emissions of ferrocene and ruthenocene probably occur via the same mechanism. We are presently studying this mechanism in detail for ruthenocene and will report our findings in a separate paper.

Of the three very weak absorption bands of ferrocene reported by Scott and Becker,[24, 25] the existence of the first two ($\epsilon < 1$), which could only be produced by Gaussian analysis, is doubtful. A careful absorption measurement below 4000 Å on ruthenocene failed to detect any bands corresponding to these alleged ferrocene bands. Band I ($\epsilon \sim 7$) of ferrocene, on the other hand, has been characterized by iodine perturbation experiments.[24, 40] This band system has been observed in all four d^6 metallocenes under investigation here. Therefore, we conclude that band I is the only singlet-triplet transition which can be observed in the absorption spectra of these molecules.

The positions of the three spin-forbidden d-d transitions were calculated using the expressions in Table I and the values of Δ_1, Δ_2, and B which were evaluated in the previous section. As seen in Table V, the predicted lowest singlet-triplet transitions in each of the d^6 metallocenes are in good agreement with the observed spin-forbidden absorption positions of band I.

TABLE V. Spin-Forbidden d-d Transitions for d^6 Metallocenes[a]

	$Fe(cp)_2$	$Ru(cp)_2$	$Co(cp)_2^+$	$Fe(\phi\text{-}cp)(cp)$
$^1A_{1g} \rightarrow b\,^3E_{1g}$	22.4	30.9	24.8	21.5
$^1A_{1g} \rightarrow {}^3E_{2g}$	20.9	30.3	23.2	20.1
$^1A_{1g} \rightarrow a\,^3E_{1g}$	18.6 (18.9)[b]	27.3 (26.0)[b]	20.8 (21.8)[b]	17.7 (17.5)[b]

[a]Transition energies ($\bar{\nu} \times 10^{-3}$, cm^{-1}) were calculated using the ligand field parameters resultant from the analysis of the spin-allowed d-d bands.

[b]Experimentally observed in absorption in this work.

Charge Transfer Bands. In the ultraviolet region of the ferrocene solution absorption spectrum (see Figure 2) a strong band (ϵ = 51, 000) at 50, 000 cm^{-1} (band VI) and two shoulders at 37, 700 and 41, 700 cm^{-1} (bands IV and V) have been observed as reported.[24,25] In Figure 2 and Table II it can be seen that ruthenocene exhibits a similar ultraviolet absorption spectrum, with the three bands slightly blue-shifted. However, in the isoelectronic cobalticenium ion only a single strong band appears at 38, 000 cm^{-1}, with no apparent shoulders. Band VI (ϵ = 38, 000) of the cobalticenium ion has an oscillator strength similar to that of band VI of ferrocene and ruthenocene and most probably is due to the same type of fully allowed charge transfer transition. Two different types of charge transfer occur in metal complexes. For instance, in the d^6 hexacyanometalate complexes $Fe(CN)_6^{2-}$ and $Co(CN)_6^{3-}$ M $\rightarrow$ L charge transfer bands have been observed[40, 41] and the charge transfer transition energy increases on increasing the positive charge of the central metal ion. On the other hand, L $\rightarrow$ M charge transfer bands have been observed in d^6 hexahalometalate systems.[42] Here the transition energy decreases markedly with increasing positive charge of the metal atom. The energy of band VI in the d^6 metallocenes is in the order $Co(cp)_2^+ < Fe(cp)_2 < Ru(cp)_2$, which is the order of decreasing metal electronegativity. Thus we conclude that band VI is a L $\rightarrow$ M charge transfer.

In terms of the energy level scheme in Figure 1 there is only one possible L → M assignment for band VI, $1e_{1u} \rightarrow 2e_{1g}$, since the $1a_{2u}$ level is estimated to be too far from the $2e_{1g}$ level. The one-electron transition $1e_{1u} \rightarrow 2e_{1g}$ results in three excited states, $^1A_{1u}$, $^1A_{2u}$, and $^1E_{2u}$, but only the transition to the $^1A_{2u}$ state is allowed. Therefore, band system VI in the d^6 metallocenes is assigned as a $^1A_{1g} \rightarrow {}^1A_{2u}$ ($1e_{1u} \rightarrow 2e_{1g}$) transition.

The characterization of the two shoulders, systems IV and V, is not as definitive, since the band positions and intensities are both difficult to determine accurately and the reported[24, 43, 44] substitutional effects are doubtful. For instance, in phenylferrocene, one shoulder and three strong bands have been observed (see Table II), but the two bands at 36,100 and 42,000 cm^{-1} are probably due to the primarily phenyl-group transitions $^1A_{1g} \rightarrow {}^1B_{2u}$ (39,400 cm^{-1}) and $^1A_{1g} \rightarrow {}^1B_{1u}$ (49,000 cm^{-1}). These two bands[45, 46] are quite variable, both in band position and intensity, when benzene is substituted.

Electronic Spectra of d^5 Metallocenes

An aqueous solution of ferricenium ion, $Fe(cp)_2^+$, exhibits at room temperature four bands and at least four shoulders, as can be seen in Table VI and Figure 6. The ground electronic state $(1e_{2g})^3 (2a_{1g})^2$ of the ferricenium ion has been investigated by various techniques.[20,21,36] In this section we will show how absorption spectroscopy applied to various ferricenium compounds will give information as to the location and character of various excited states. In some instances this information about excited states will be shown to give insight into the ferricenium ion ground electronic state. In particular, ferricenium band I is a new feature, not observable in ferrocene, which will be valuable in the characterization of electronic structure.

Band System I. This ferricenium band system has moderate intensity and exhibits vibrational structure at 77°K in a LiCl glass (see Figure 7). In our communication[21] the observed vibrational progression was assigned to the symmetric ring-metal stretching frequency (the corresponding ground state ferrocene a_{1g} frequency is 309 cm^{-1}). Details of the peak positions in this 77°K LiCl glass spectrum are given in Table VII. It can be seen that the vibrational spacings in the band system are approximately the same, but on the higher energy side irregular intensities complicate matters. The oscillator strength of band I increases approximately 20% in going from 300 to 77°K (2.3×10^{-3} to 2.7×10^{-3}). This type of temperature dependence rules against a d-d transition. We have assigned this band

Fig. 6. Electronic absorption spectrum of ferricenium ion in 0.01 M $HClO_4$ aqueous solution at 300°K.

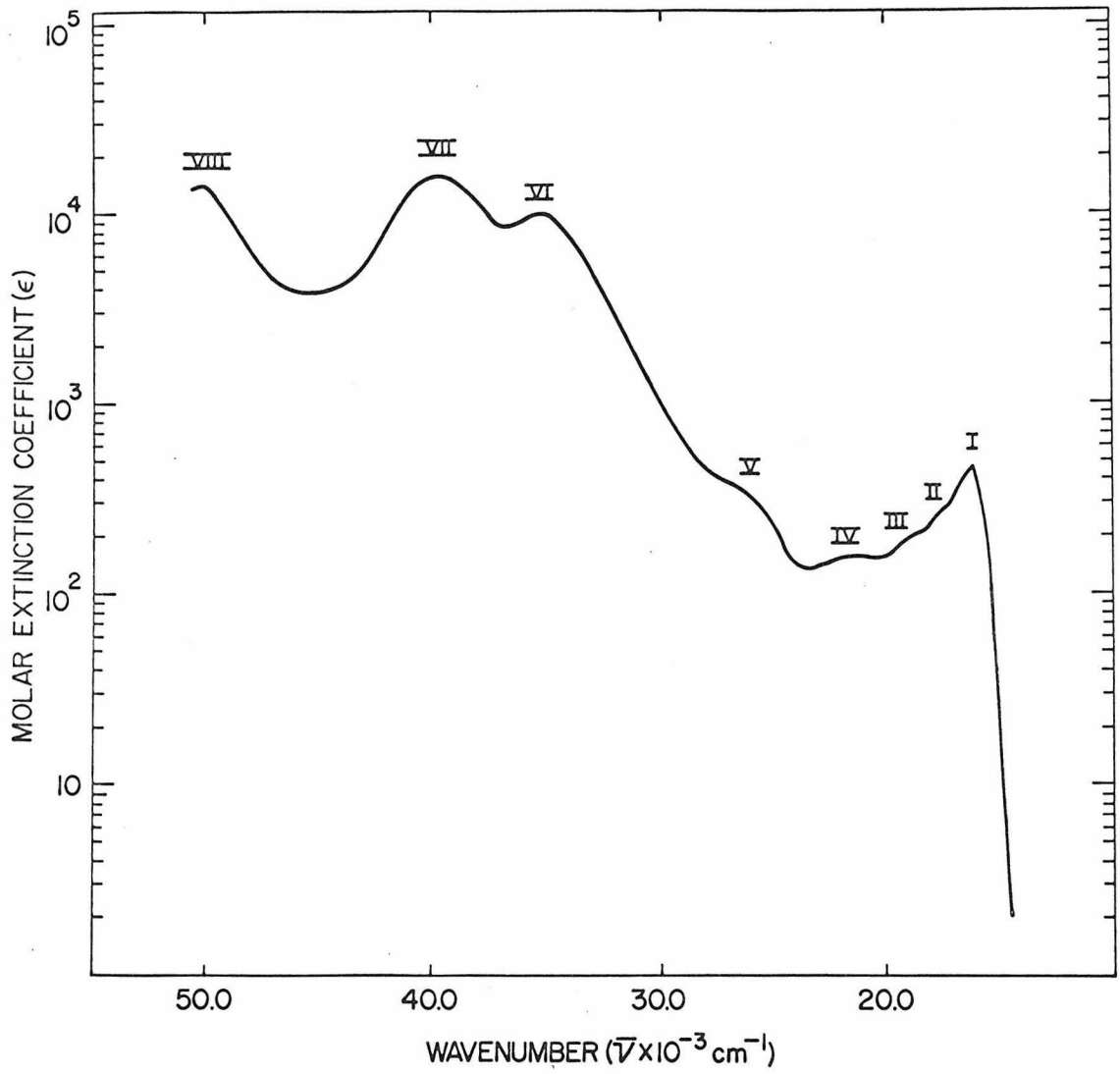
MOLAR EXTINCTION COEFFICIENT (ε)
10^5
10^4
10^3
10^2
10
VIII
VII
VI
V
IV
III
II
I
50.0
40.0
30.0
20.0
WAVENUMBER (ν̄ x 10^-3 cm^-1)

TABLE VI. Electronic Absorption Spectrum of Aqueous $Fe(cp)_2^+$[a]

	$\bar{\nu}(cm^{-1})$	ϵ	$f \times 10^3$
I	16,200	450	2.3
II[b]	17,700	250	
III[b]	19,100	190	
IV[b]	21,400	150	
V[b]	26,300	350	
VI	35,300	9,700	~120
VII	39,900	16,000	162
VIII	50,500	14,000	

[a] 10 M LiCl aqueous solution.

[b] Shoulder.

Fig. 7. Visible absorption spectra of $[Fe(cp)_2](BF_4)$ in 10 M LiCl aqueous solution: (-·--), 300°K; (——), 77°K.

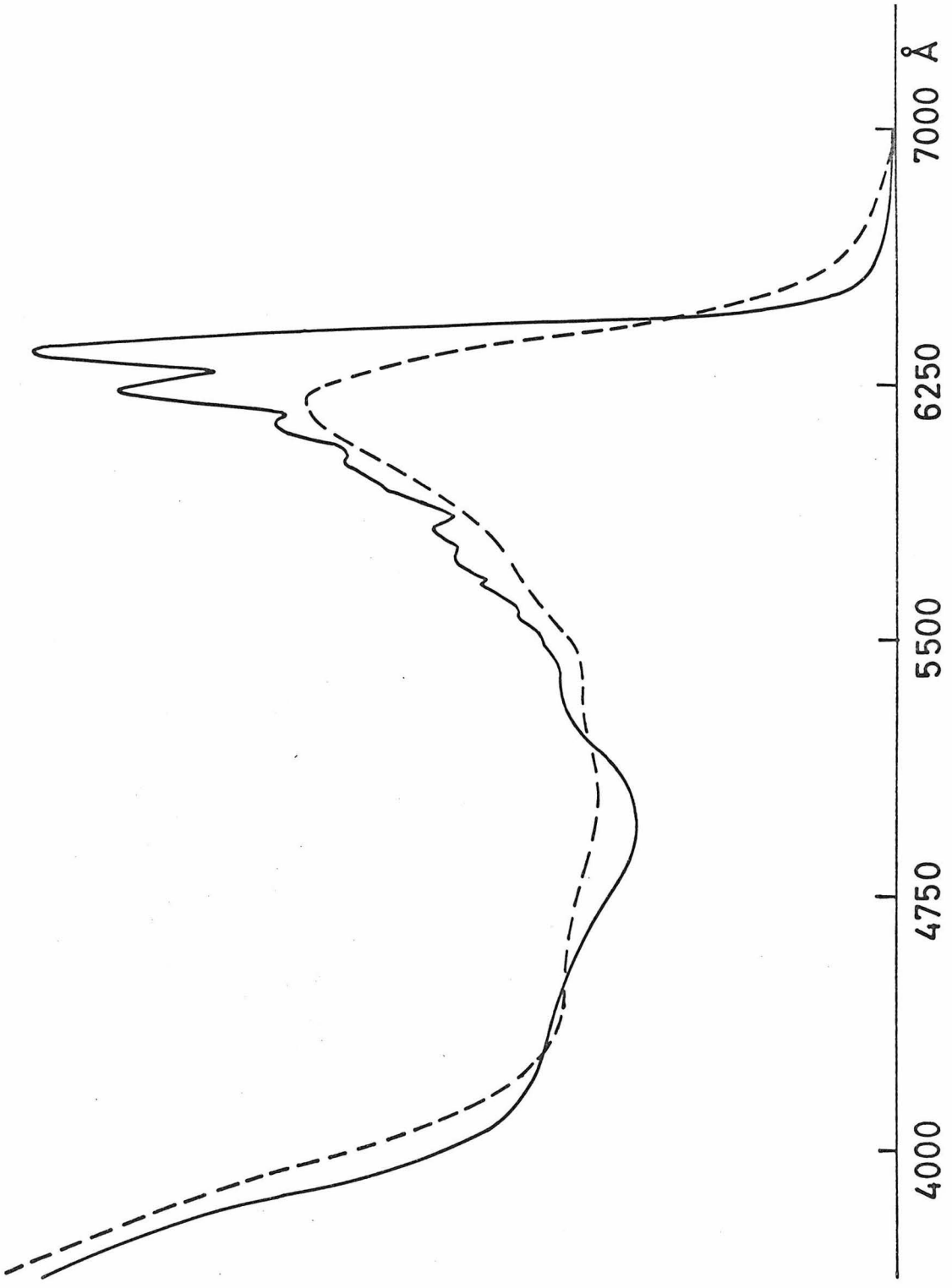
7000 Å
6250
5500
4750
4000

TABLE VII. Vibrational Structure of Band I of $Fe(cp)_2^+$ in Solution[a]

$\bar{\nu}(cm^{-1})$	$\Delta\bar{\nu} = \bar{\nu}_n - \bar{\nu}_{n-1}$	Assignment
15,730 ± 10		(0,0)
16,020 ± 10	290	(1,0)
16,290 ± 10	270	(2,0)
16,590 ± 10	300	(3,0)
16,860 ± 10[b]	270	
17,150 ± 10	290	
17,420 ± 10	270	
17,700 ± 20	280	
17,950 ± 20	250	
18,240 ± 20	290	
18,550 ± 20	290	
18,800 ± 20	250	

[a]10 M LiCl aqueous solution at 77°K.

[b]This component is not clearly resolved from the 16,590 cm^{-1} band.

as the ligand-to-metal charge transfer $^2E_{2g} \rightarrow {}^2E_{1u}$. The above evidence as well as an analogy with ferricyanide were the reasons for our assignment of the ferricenium band I to the transition of an electron from the bonding ring level $1e_{1u}$ to the hole in the essentially non-bonding metal $1e_{2g}$ orbital (see Figure 8). The validity of the above assignment was further checked by studying the substitutional behavior of band I. Two substituted ferricenium salts were prepared: $[Fe(n\text{-}Bu\text{-}cp)(cp)]PF_6$ and $[Fe(n\text{-}Bu\text{-}cp)_2]PF_6$. It was found convenient to perform the absorption spectroscopic studies of these two salts and $[Fe(cp)_2]PF_6$ in KBr pellets. The results of these studies can be seen in Figures 9-11. The 16,200 cm^{-1} band system of $[Fe(cp)_2]PF_6$ in KBr pellet undergoes a red shift upon ring substitution, a result that is apparent from either a comparison of the room temperature or 77°K absorption spectra. Thus this band system appears at 16,000 cm^{-1} for $[Fe(n\text{-}Bu\text{-}cp)(cp)]PF_6$ and shows a drastic shift to 14,800 cm^{-1} for $[Fe(n\text{-}Bu\text{-}cp)_2]PF_6$ at room temperature. The apparent origins (0, 0) in the progressions at 77°K for the monobutylated and dibutylated ferricenium hexafluorophosphates appear at 14,950 and 14,160 cm^{-1}, respectively, compared to 15,630 cm^{-1} for $[Fe(cp)_2]PF_6$. This substitution trend provides further support for our $^2E_{2g} \rightarrow {}^2E_{1u}$ assignment.

As can be seen in Figure 9, band system I of the ferricenium ion shows markedly better resolution of vibrational structure when the compound is pelleted in KBr than we had obtained for a LiCl glass. In fact, in appearance each peak in the LiCl glass spectrum

Fig. 8. Energy level scheme for the $^2E_{2g}$ ground and $^2E_{1u}$ excited states of ferricenium ion. The primed symbols are appropriate for D_5' symmetry; see reference 22.

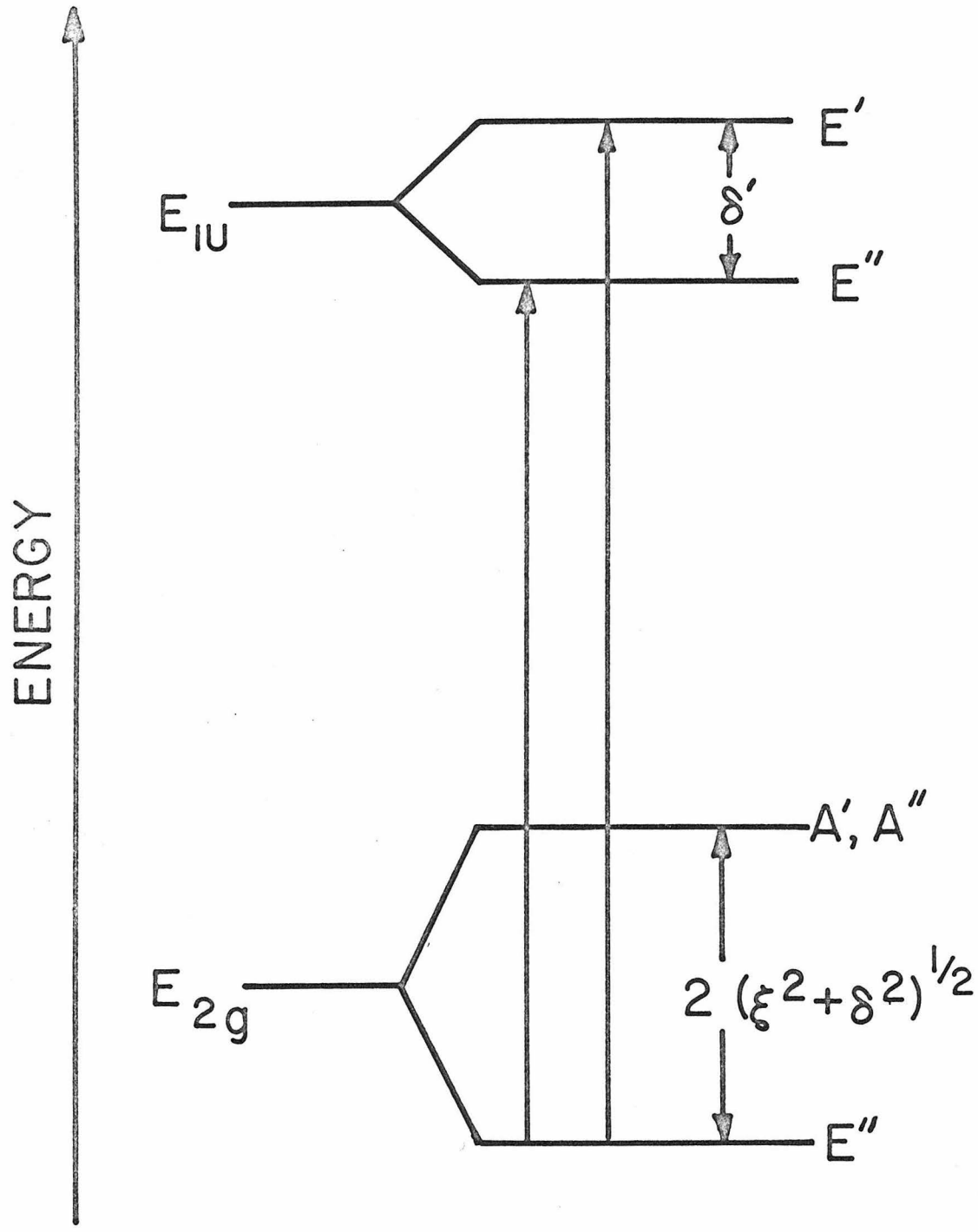
ENERGY
E'
δ'
E''
E1u
A', A''
E2g
2 (ξ2+δ2)1/2
E''

Fig. 9. Vibrational structure of Band I for a KBr pellet of $[Fe(cp)_2]PF_6$ at 77°K.

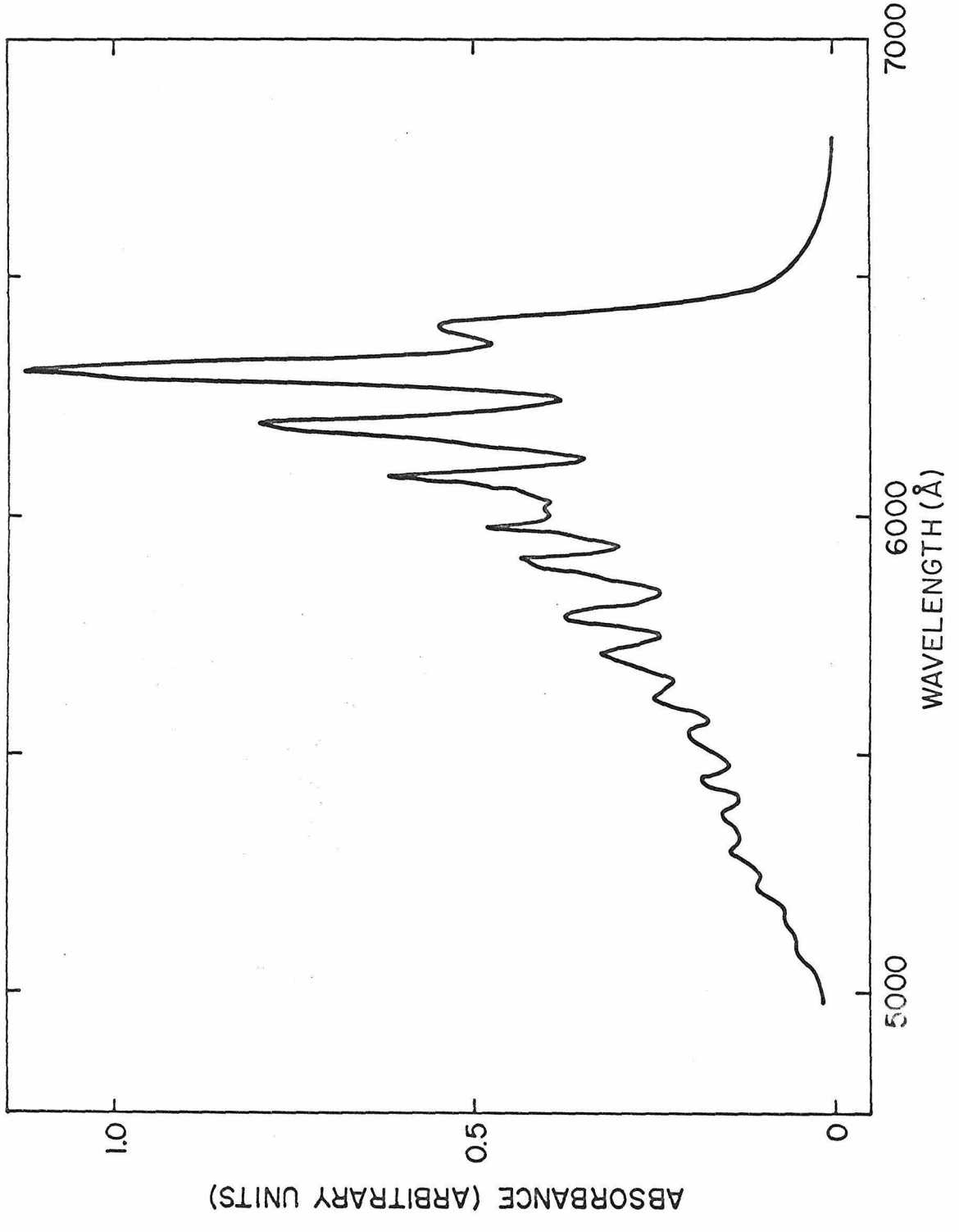
ABSORBANCE (ARBITRARY UNITS)
1.0
0.5
0
5000
6000
7000
WAVELENGTH (Å)

Fig. 10. Visible absorption spectra of [Fe(n-Bu-cp)(cp)](PF_6) in KBr pellet: (----), 300°K; (——), 77°K.

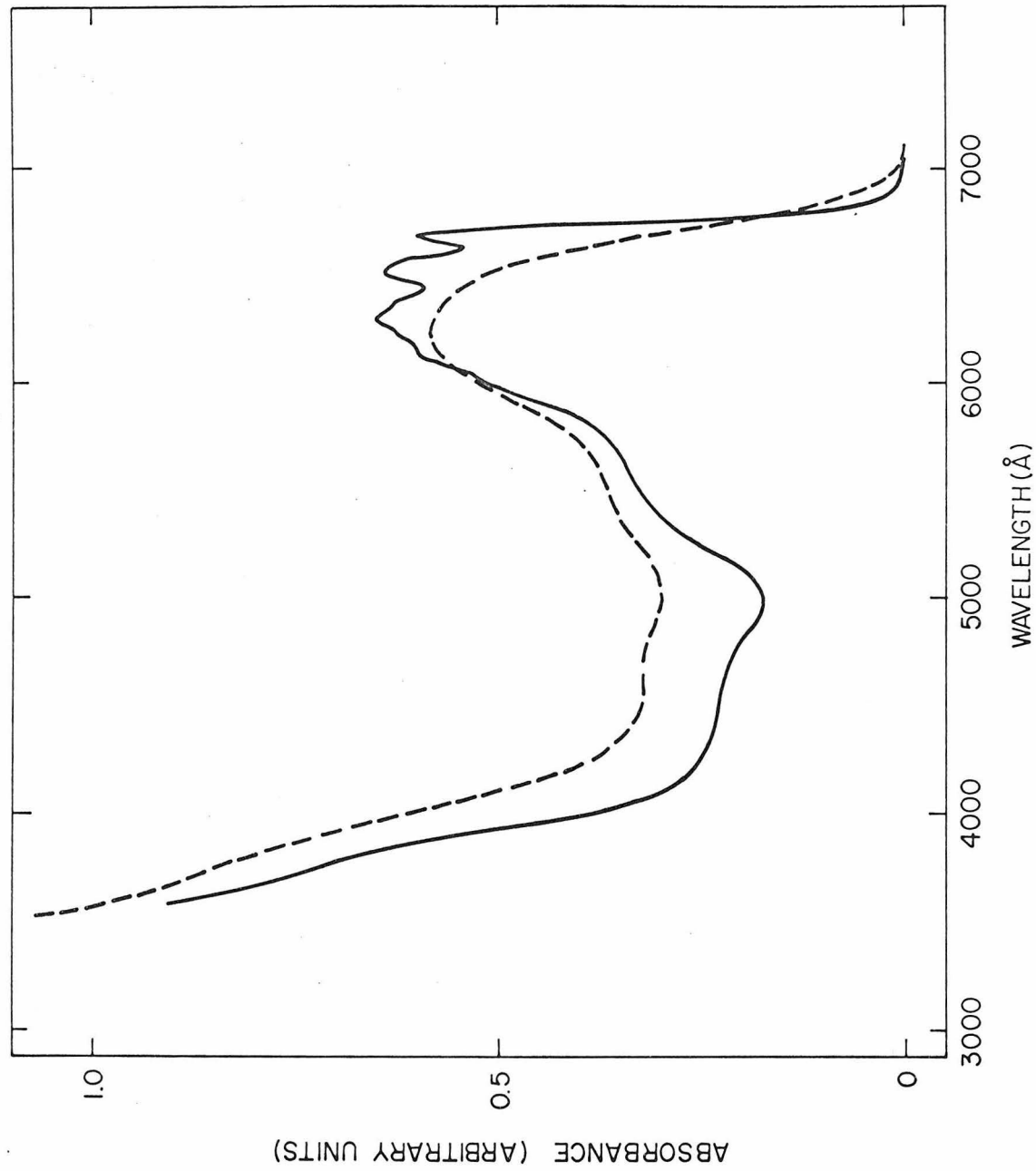
ABSORBANCE (ARBITRARY UNITS)
1.0
0.5
0
3000
4000
5000
6000
7000
WAVELENGTH (Å)

Fig. 11. Visible absorption spectra of $[Fe(n\text{-}Bu\text{-}cp)_2](PF_6)$ in KBr pellet: (----), 300°K; (——), 77°K.

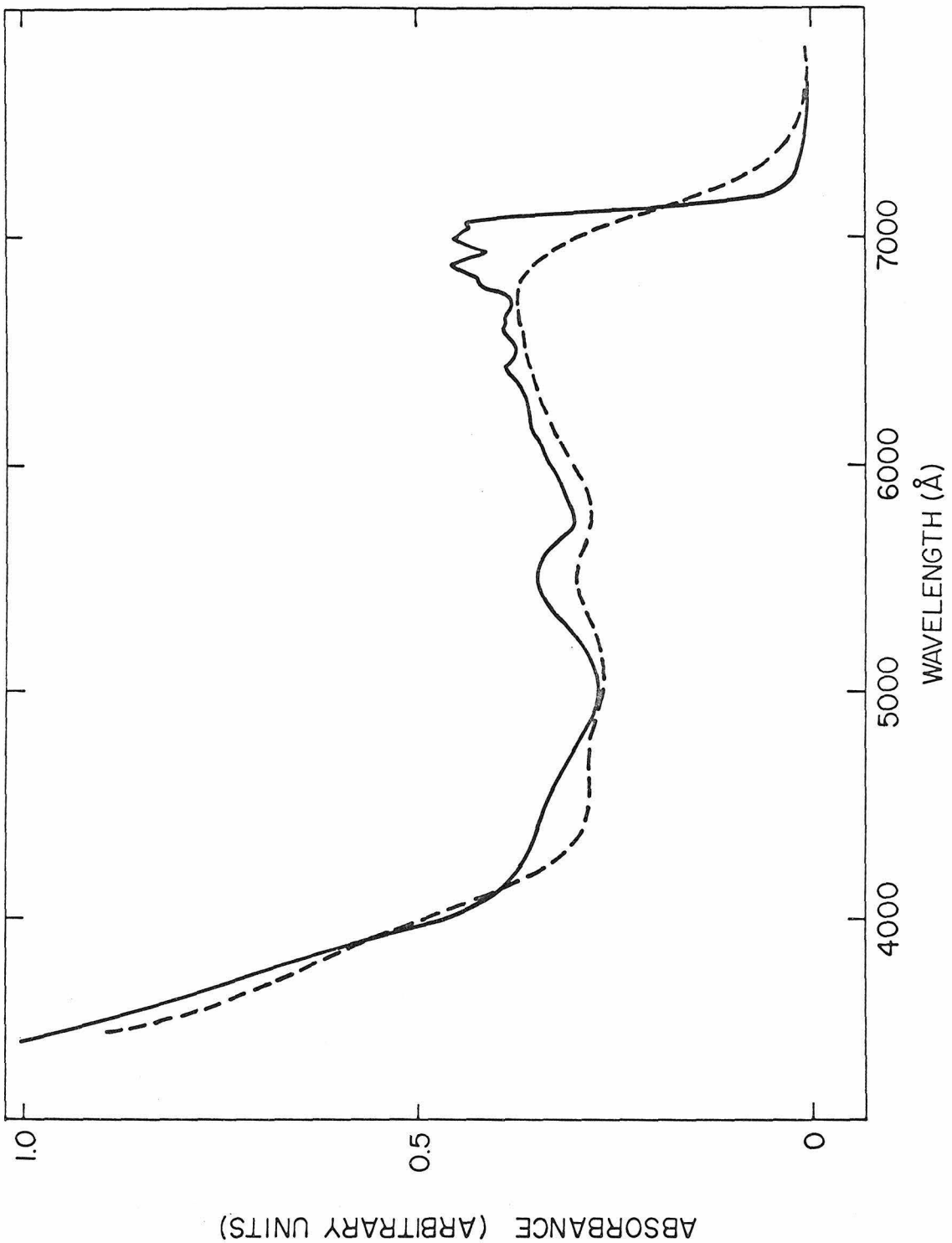
ABSORBANCE (ARBITRARY UNITS)
1.0
0.5
0
4000
5000
6000
7000
WAVELENGTH (Å)

seems to be split into two. This doubling of peaks can be best seen in the 77°K spectrum of $[Fe(cp)_2](CCl_3CO_2H)_3$, depicted in Figure 12. It seems worthwhile, at this time, to point out that $[Fe(cp)_2]BF_4$ gives the same 77°K absorption spectrum in either a KBr pellet or in a LiCl glass. We will return to this point later in the discussion.

Before we begin to develop a detailed assignment of the vibrational structure in these ferricenium spectra, it is helpful to review what is known about the ground state of the ferricenium ion. Such a review will aid our speculation as to the expected appearance of the ferricenium $^2E_{2g} \rightarrow {}^2E_{1u}$ transition under moderate resolution. As indicated in the Theory section the ground electronic state of the ferricenium ion is a $^2E_{2g}(a_{1g})^2(e_{2g})^3$ state which is split into two Kramers doublets by spin-orbit coupling and crystal fields of symmetry lower than D_5. Thus it would be reasonable to expect the $^2E_{1u}$ excited state to be split by components of the low-symmetry crystal field, as shown in the schematic energy diagram of Figure 8. Since both $E''(^2E_{2g}) \rightarrow E'(^2E_{1u})$ and $E''(^2E_{2g}) \rightarrow E''(^2E_{1u})$ are allowed transitions, a doubled vibrational progression could result from a progression of the totally symmetric vibration on each origin. The splitting of the excited state $^2E_{1u}$ would be due essentially to a distortion which influences the energy of the carbon p-orbitals, $\delta' = \langle e^+_{1u} | H'_{eff} | e^-_{1u} \rangle$.

The vibrational structure which appears in the 77°K spectrum of $[Fe(cp)_2](CCl_3CO_2H)_3$ is the easiest to explain. As noted previously,

Fig. 12. Vibrational structure of Band I for a KBr pellet of $[Fe(cp)_2](CCl_3CO_2H)_3$ at 77°K.

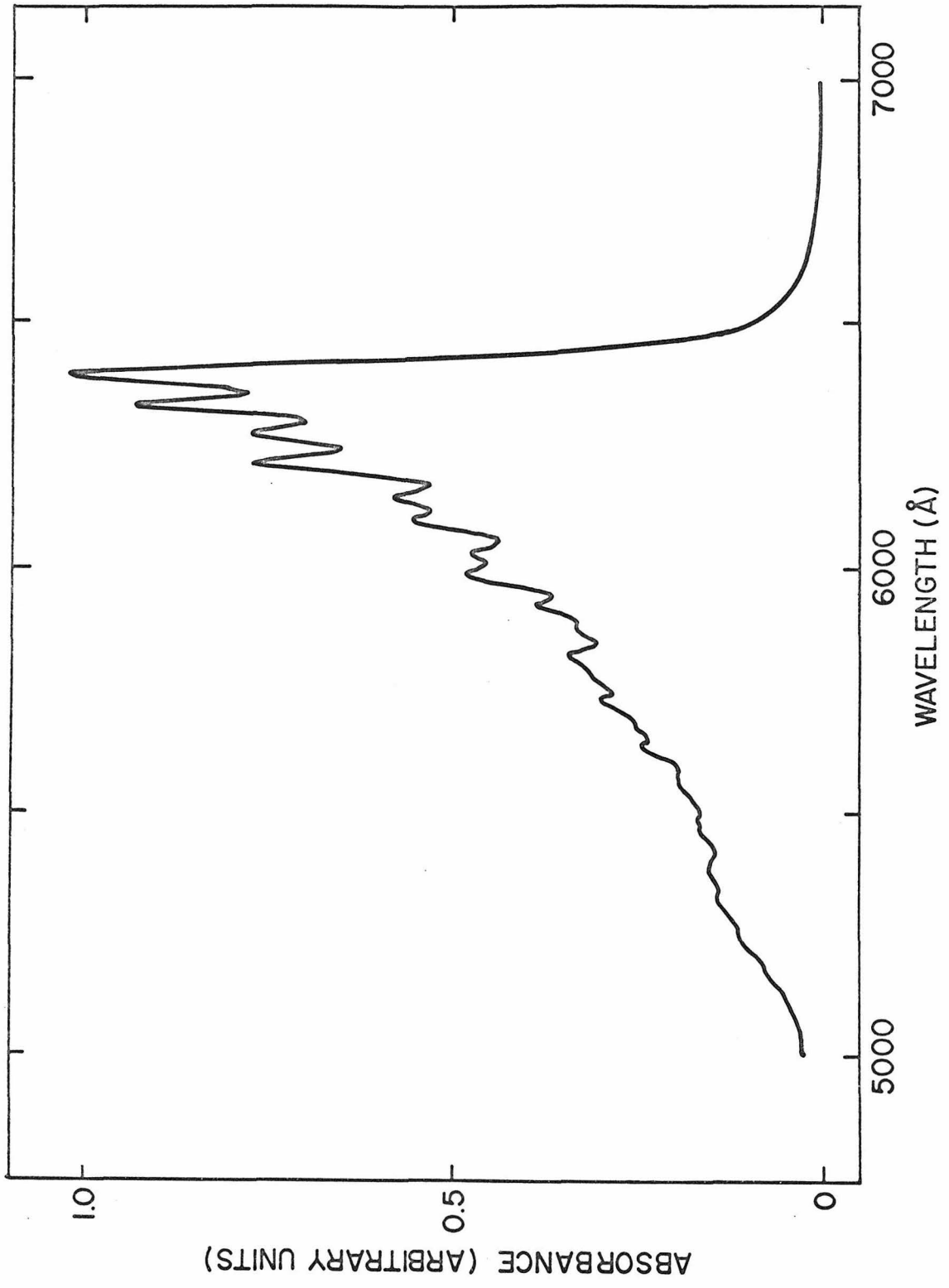
ABSORBANCE (ARBITRARY UNITS)
1.0
0.5
0
5000
6000
7000
WAVELENGTH (Å)

TABLE VIII. Vibrational Structure of Band I of $[Fe(cp)_2](CCl_3CO_2H)_3$[a]

$\bar{\nu}(cm^{-1})$	$\Delta\bar{\nu} = \bar{\nu}_n - \bar{\nu}_{n-1}$	$\Delta\bar{\nu}' = \bar{\nu}_{n'} - \bar{\nu}_{n'-1}$	Assignment
			$A_{1g}(W_4)$
15,640 ± 10			(0, 0)
15,800 ± 10			(0, 0)′
15,940 ± 10	300		(1, 0)
16,100 ± 10		300	(1, 0)′
16,270 ± 10	330		(2, 0)
16,410 ± 10		310	(2, 0)′
16,580 ± 10	310		(3, 0)
16,710 ± 10		300	(3, 0)′
16,880 ± 10	300		(4, 0)
17,020 ± 20		310	(4, 0)′
17,190 ± 20	310		(5, 0)
17,320 ± 20		300	(5, 0)′
b			

[a]KBr pellet spectrum at 77°K.

[b]The progression continues down to ~5100 Å but the structure is poorly resolved.

band system I in this spectrum is most likely a progression of doublets resulting from a splitting of the excited state ($^2E_{1u} \rightarrow E'$ and E''). The first two peaks, 15,640 and 15,800 cm^{-1}, are probably the origins (0, 0) of the $E'' \rightarrow E'$ and $E'' \rightarrow E''$ transitions. The distortion parameter of the $^2E_{1u}$ excited state, δ', may be estimated as 140 cm^{-1} (average of the spacings of the doublets) for $[Fe(cp)_2](CCl_3CO_2H)_3$. The details of our tentative assignment are given in Table VIII. The 77°K single crystal spectrum of $[Fe(cp)_2](CCl_3CO_2H)_3$ shows essentially the same vibrational structure for band system I. In addition, at higher energy two new bands (20,600 and 22,400 cm^{-1}) appear which were either not present in the KBr pellet or solution spectra or have gained appreciable intensity. The intensity of these two bands is slightly in excess of that of band system I. One possible explanation is that these two bands in the single crystal spectrum are intermolecular charge transfer bands.

In the case of $[Fe(cp)_2]PF_6$ each vibrational component (see Figure 9) in the 77°K KBr pellet spectrum is not symmetric (some appear to be shouldered). The two electronic origins are not easy to locate in this case. However, we have made a tentative assignment (see Table IX) analogous to that proposed for band system I of $[Fe(cp)_2](CCl_3CO_2H)_3$. If the first two components at 15,630 and 15,850 cm^{-1} are taken as the two origins, the distortion in the excited state, δ', is estimated as 200 cm^{-1}. It seems that the first progression with an origin at 15,630 cm^{-1} has a lower intensity than the second progression and probably causes shoulders on each of the

TABLE IX. Vibrational Structure of Band I of $[Fe(cp)_2]PF_6$[a]

$\bar{\nu}(cm^{-1})$[c]	$\Delta\bar{\nu} = \bar{\nu}_n - \bar{\nu}_{n-1}$	$\Delta\bar{\nu} = \bar{\nu}_{n'} - \bar{\nu}_{n'-1}$	Assignment
15,630 ± 10			(0, 0)
15,850 ± 10			(0, 0)′
(15,930)	(300)		(1, 0)
16,150 ± 10		300	(1, 0)′
(16,230)	(300)		(2, 0)
16,440 ± 10		290	(2, 0)′
(16,530)	(300)		(3, 0)
16,730 ± 10		290	(3, 0)′
16,810[b]			
16,920			
17,010[b]			
17,220[b]			
17,290			
17,520			
17,580[b]			
17,810			
18,050			
18,130[b]			
18,370			
18,600			
18,690[b]			
18,910			

TABLE IX. (Continued)

$\bar{\nu}(cm^{-1})$	$\Delta\bar{\nu} = \bar{\nu}_n - \bar{\nu}_{n-1}$	$\Delta\bar{\nu} = \bar{\nu}_{n'} - \bar{\nu}_{n'-1}$	Assignment
19,140			
19,420			
19,690			

[a]KBr pellet spectrum at 77°K, the frequencies in parentheses were calculated assuming an a_{1g} progression on the (0, 0) origin.

[b]Shoulder.

[c]Uncertainties in peak positions are ± 20 cm^{-1} unless otherwise specified.

components of the second progression. Further study of this band system I at 4.2°K may be helpful in better understanding the vibrational structure.

It is clear from the above two cases that we are in fact dealing with a split excited state. In the substituted ferricenium ion salts the low temperature spectrum also has the appearance of a doubled progression (see Figures 10 and 11). Band system I in the ferricenium spectrum is a reasonably sensitive function of the counter-ion as well as ring substitution. Similar results were found in the magnetic susceptibility studies,[36] where the distortion in the ferricenium $^2E_{2g}$ ground state (i.e., $\delta = \langle e^+_{2g} | H'_{eff} | e^-_{2g} \rangle$), was found to be sensitive to counter-ion interchange as well as ring substitution.

Finally, we return to the LiCl glass spectrum and indulge in a brief discussion. The 77°K LiCl glass spectrum of the ferricenium ion and the 77°K KBr pellet spectrum of $[Fe(cp)_2]BF_4$ exhibit far less vibrational structure than the other cases; peaks are broader also. Two explanations come to mind: a) There is an averaging of several environments and lower resolution ensues, or b) The distortion δ' approaches equality with the vibrational frequency causing excessive overlapping. Explanation (a) seems viable for the LiCl glass case but is difficult to accept for the KBr spectrum of $[Fe(cp)_2]BF_4$. Magnetic susceptibility measurements have indicated[21, 36] that the ground state distortion experienced by the

ferricenium ion in an aqueous solution is comparable to that felt by the ion in the tetrafluoroborate salt. Thus until further study, explanation (b) is the more attractive of the two.

Spin-Allowed d-d Transitions. In the visible region of the ferricenium ion spectrum four shoulders at 17,700, 19,100, 21,400 and 26,300 cm^{-1} (bands II-V) have been observed. These weak peaks appear at the same positions in all of the ferricenium salts, both in solutions and in KBr pellets. Their intensities and positions are nearly insensitive to ring substitution. Therefore, these shoulders may be assigned as essentially metal d-d transitions.

Theoretically, seven different d-d transitions are predicted for the ferricenium ion in the visible and ultraviolet region (see Theory section), excluding the lowest $^2A_{1g}$ transition which is expected[21] to be in the IR range. Since we have fewer observed bands, the approach that we have taken is to calculate theoretical transition energies for different values of the three ligand field parameters, B, Δ_1, and Δ_2. Computer diagonalization was employed to account for configurational interaction in the case of the $^2E_{1g}$ transitions. Using the ferrocene parameters as guides the ranges of the parameters investigated were: $-2,000 > \Delta_1 > -14,000$ cm^{-1}; $22,000 < \Delta_2 < 35,000$ cm^{-1}; $400 < B < 700$ cm^{-1}. We found that the transition energies are in the order (giving only the symbol for the excited state): $a^2A_{1g} \ll a^2E_{1g} < a^2E_{2g} < b^2E_{1g} \sim b^2A_{1g} \sim {}^2A_{2g} < c^2E_{1g} \sim b^2E_{2g}$. Calculated ferricenium transition energies are given in Table X for the case

TABLE X. Ligand Field Bands of $Fe(cp)_2^+$

Transitions	Calculated Energy I[a]	Calculated Energy II[b]	Experimental[c]
$^2E_{2g} \rightarrow a^2E_{1g}$	20,000	14,700	17,700
$\rightarrow a^2E_{2g}$	22,100	21,000	19,100
$\rightarrow b^2E_{1g}$	25,000	23,900	21,400
$\rightarrow b^2A_{1g}$	26,400	24,200	26,300
$\rightarrow {}^2A_{2g}$	26,400	24,200	
$\rightarrow c^2E_{1g}$	28,600	29,800	
$\rightarrow b^2E_{2g}$	29,800	31,600	

[a] $\Delta_1 = -7,100\ cm^{-1}$, $\Delta_2 = 22,000\ cm^{-1}$ and $B = 390\ cm^{-1}$.

[b] $\Delta_1 = -7,100\ cm^{-1}$, $\Delta_2 = 22,000\ cm^{-1}$ and $B = 700\ cm^{-1}$.

[c] Ordered in increasing energy.

where the parameters (B, Δ_1, Δ_2) are assumed to be the same as in ferrocene. Results are also tabulated for the calculation where Δ_1 and Δ_2 were taken from ferrocene but B was increased to 700 cm^{-1}. This latter treatment is based on the assumption that the parameter change in going from $Fe(cp)_2$ to $Fe(cp)_2^+$ is analogous to changes observed[40] in going from $Fe(CN)_6^{4-}$ to $Fe(CN)_6^{3-}$. Although neither calculation gives particularly good agreement with the experimental peak positions, the assignments for the first three ligand field bands are reasonably satisfactory.

Further work is needed to better resolve these weak peaks. Perhaps the ferricenium ion should be substituted such that band system I moves to much lower energy. This would make possible an improved definition in peak position for the lower energy d-d bands.

Charge Transfer Bands. The solution spectrum of the ferricenium ion shows three bands at 35, 300, 39, 900 and 50, 500 cm^{-1} (bands VI-VIII) in the ultraviolet region (see Figure 6). These three bands have large oscillator strengths ($f > 0.1$) and as such they result from allowed transitions. In comparison with band VI of ferrocene ($f \sim 0.7$), the ferricenium band VIII has a somewhat lower oscillator strength. However, it is probable that band VIII arises from a $1e_{1u} \rightarrow 2e_{1g}$ transition. The band systems VI and VII of the ferricenium ion, which appear in the region of the ferrocene shoulders IV and V, may be regarded as allowed charge transfer transitions which are either forbidden or do not occur in the ferrocene molecule.

Bands VI and VII may be assigned after consideration of the allowed charge transfer transitions. By group theory we know that to be allowed a transition from the $^2E_{2g}$ ground state must be to an excited state of $^2E_{1u}$ or $^2E_{2u}$ symmetry. We have summarized in Table XI the energetically feasible charge transfer transitions (see the MO diagram, Figure 1) which give $^2E_{1u}$ or $^2E_{2u}$ excited states.

We have already assigned the low energy charge transfer band at 16,200 cm^{-1} in $Fe(cp)_2^+$ as the allowed transition from the $1e_{1u}$ level to the hole in the $1e_{2g}$ level (see Figure 8). Bands VI and VII of the ferricenium ion could be envisioned as transitions from some other low-lying bonding levels to the same hole in the essentially metal e_{2g} orbital. However, no such transitions are electric dipole allowed. Two types of transitions remain as candidates: Metal-to-ligand transitions from the two essentially nonbonding orbitals $2a_{1g}$ and $1e_{2g}$ to e_{2u}; and the ligand-to-metal charge transfer transitions from $1e_{1u}$ to $2e_{1g}$.

Since the metal-to-ligand transitions to e_{2u} are allowed but not observed in the case of ferrocene, we much prefer the ligand-to-metal charge transfer assignment for bands VI and VII of the ferricenium ion. It is our contention that band VI in the ferrocene spectrum results from the $1e_{1u} \rightarrow 2e_{1g}$ transition and that this same band is present in the ferricenium spectrum. The $1e_{1u} \rightarrow 2e_{1g}$ transition results in only one allowed excited state ($^1A_{2u}$) in ferrocene but gives three allowed states ($^2E_{1u}$ and two $^2E_{2u}$) in the ferricenium case. Therefore, the three strong bands (VI, VII, and VIII) in the ferricenium

TABLE XI. Selected Charge Transfer Transitions of d^5 and d^6 Metallocenes

One Electron Transitions	$Fe(cp)_2$		$Fe(cp)_2^+$	
	Allowed (A) Forbidden (F)	Excited States[a]	Allowed (A) Forbidden (F)	Excited States[a]
$2a_{1g} \rightarrow e_{2u}$	F	$({}^1E_{2u})$	A	${}^2E_{1u} + ({}^2A_{1u}) + ({}^2A_{2u})$
$1e_{2g} \rightarrow e_{2u}$	A	${}^1E_{1u} + {}^1A_{2u} + ({}^1A_{1u})$	A	$3{}^2E_{2u} + {}^2E_{1u}$
$1e_{1u} \rightarrow 1e_{2g}$	-	-	A	${}^2E_{1u}$
$1e_{1u} \rightarrow 2e_{1g}$	A	${}^1A_{2u} + ({}^1A_{1u}) + ({}^1E_{2u})$	A	$2{}^3E_{2u} + {}^2E_{1u} + ({}^2A_{1u}) + ({}^2A_{2u})$
$1a_{2u} \rightarrow 1e_{2g}$	-	-	F	$({}^2A_{2u})$

[a]Transitions to the excited states in parentheses are orbitally forbidden.

spectrum are nicely accounted for by the single one-electron transition $1e_{1u} \rightarrow 2e_{1g}$. Strong evidence in support of this assignment is found in the observation that all of the three bands show red shifts upon ring substitution (see Table XII) by an energy comparable to the observed shifts of band system I of the ferricenium ion. This latter band system is definitely a ligand-to-metal charge transfer transition. Finally, we note that the ratio of the intensities of the two highest energy ferricenium bands ($\epsilon_{VII}/\epsilon_{VIII}$) is almost constant among the unsubstituted and substituted ferricenium ions.

Acknowledgments.

This research was supported by the National Science Foundation. We thank Professor C. J. Ballhausen for several stimulating discussions.

TABLE XII. Charge Transfer Bands of Substituted and Unsubstituted Ferricenium Ions[a]

Band	$Fe(cp)_2^+$		$Fe(n\text{-}Bu\text{-}cp)(cp)^+$		$Fe(n\text{-}Bu\text{-}cp)_2^+$	
	$\bar{\nu}(cm^{-1})$	ϵ	$\bar{\nu}(cm^{-1})$	ϵ	$\bar{\nu}(cm^{-1})$	ϵ
I	16,190	450	16,000	330	15,390	340
VI[b]	35,310	9,700	34,770	8,600	34,360	9,400
VII	39,900	15,900	39,310	13,600	38,610	13,300
VIII	50,450	14,200	50,000	12,300	49,630	12,000
ϵ(VII)/ϵ(VIII)	1.11		1.10		1.11	

[a] 0.01 M $HClO_4$ aqueous solution.

[b] Appears as a shoulder in substituted ferricenium ions.

References

(1) T. J. Kealy and P. L. Panson, Nature, 168, 1039 (1951).

(2) S. A. Miller, J. A. Tebboth, and J. F. Tremaine, J. Chem. Soc., 632 (1952).

(3) H. H. Jaffe, J. Chem. Phys., 21, 156 (1953).

(4) J. D. Dunitz and L. E. Orgel, J. Chem. Phys., 23, 954 (1955).

(5) W. Moffit, J. Amer. Chem. Soc., 76, 3386 (1954).

(6) M. Yamasaki, J. Chem. Phys., 24, 1260 (1956).

(7) E. Ruch, Rec. Trav. Chem., 75, 638 (1956).

(8) E. M. Shustorovich and M. E. Dyatkina, Doklady Akad. Nauk SSSR, 128, 1234 (1959); ibid., 131, 113 (1960); and ibid., 133, 141 (1960).

(9) J. P. Dahl and C. J. Ballhausen, Kgl. Danske Vid. Selsk, Mat-Fys. Medd., 33 (1961).

(10) R. D. Fischer, Theoret. Chim. Acta, 1, 418 (1963).

(11) A. T. Armstrong, D. G. Carroll, and S. P. McGlynn, J. Chem. Phys., 47, 1104 (1967).

(12) J. H. Schachtschneider, R. Prins, and P. Ros, Inorg. Chim. Acta , 1, 462 (1967).

(13) A. D. Liehr and C. J. Ballhausen, Acta Chem. Scand., 11, 207 (1957).

(14) F. A. Matsen, J. Amer. Chem. Soc., 81, 2023 (1959).

(15) R. E. Robertsen and H. M. McConnell, J. Phys. Chem., 64, 70 (1960).

(16) D. R. Scott and R. S. Becker, J. Organometal. Chem., 4, 409 (1965).

(17) M. Rosenblum, "Chemistry of the Iron Group Metallocenes," Interscience-Wiley, Inc., New York, 1965.

(18) D. A. Brown, Transition Metal Chem., 3 (1966).

(19) C. J. Ballhausen and H. B. Gray, Chapter 1 in "Chemistry of the Coordination Compounds," Vol. I, A. E. Martell, ed., van Nostrand-Reinhold, in press.

(20) R. Prins and F. J. Reinders, J. Amer. Chem. Soc., 91, 4929 (1969).

(21) Y. S. Sohn, D. N. Hendrickson, and H. B. Gray, J. Amer. Chem. Soc., 92, 3233 (1970).

(22) A. H. Maki and T. E. Berry, J. Amer. Chem. Soc., 87, 4437 (1965).

(23) R. Prins and J. D. W. van Voorst, J. Chem. Phys., 49, 4465 (1968).

(24) D. R. Scott and R. S. Becker, J. Chem. Phys., 35, 516 (1961).

(25) A. T. Armstrong, D. G. Carroll, and S. P. McGlynn, J. Chem. Phys., 46, 4321 (1967).

(26) J. J. Smith and B. Meyer, J. Chem. Phys., 48, 5436 (1968).

(27) P. B. Stephenson and W. E. Winterrowd, J. Chem. Phys., 52, 3308 (1970).

(28) Y. S. Sohn, D. N. Hendrickson, J. H. Smith, and H. B. Gray, Chem. Phys. Lett., in press.

(29) D. A. Levy and L. E. Orgel, Mol. Phys., 4, 93 (1961).

(30) D. R. Scott and R. S. Becker, J. Phys. Chem., 69, 3207 (1965).

(31) G. Wilkinson, J. Amer. Chem. Soc., 74, 6148 (1952).

(32) G. D. Broadhead and P. S. Pauson, J. Chem. Soc., 367 (1955).

(33) M. Rosenblum, J. Amer. Chem. Soc., 81, 4530 (1959).

(34) M. Aly, R. Bramley, J. Upadhyay, A. Wasserman, and P. Woolliams, Chem. Comm., 404 (1965).

(35) D. N. Hendrickson, Y. S. Sohn, and H. B. Gray, submitted to Inorg. Chem.

(36) C. J. Ballhausen, "Introduction to Ligand Field Theory," McGraw-Hill, New York, N.Y., 1962.

(37) L. D. Dave, D. F. Evans, and G. Wilkinson, private communication quoted in Ref. 22.

(38) J. Bodenheimer, E. Loewenthal, and W. Low, Chem. Phys. Lett., 3, 715 (1969).

(39) J. J. Alexander and H. B. Gray, J. Amer. Chem. Soc., 91, 4260 (1968).

(40) A. N. Nesmeyanov, E. G. Perevalova, and O. A. Nesmeyanova, Doklady Akad. Nauk SSSR, 100, 1099 (1955).

(41) H. B. Gray and N. A. Beach, J. Amer. Chem. Soc., 85, 2922 (1963).

(42) C. K. Jorgensen, Mol. Phys., 2, 309 (1959).

(43) V. Weinmayr, J. Amer. Chem. Soc., 77, 3012 (1955).

(44) K. I. Grandberg, S. P. Gubin, and E. G. Perevalova, Izv. Akad. Nauk SSSR, Ser. Khim., 549 (1966).

(45) H. H. Jaffe and M. Orchin, "Theory and Application of Ultraviolet Spectroscopy," John Wiley and Sons, Inc., New York, N.Y. 1962.

(46) A. R. Gillam and E. S. Stern, "Electronic Absorption Spectroscopy," E. Arnold Ltd., London, 1958.

PART II. MAGNETIC SUSCEPTIBILITY STUDY OF THE FERRICENIUM ION

Part II was partly published in J. Am. Chem. Soc., 92, 3233 (1970). The whole manuscript has been submitted for publication in Inorg. Chem.

Magnetic Susceptibility Study of the Ferricenium Ion

David N. Hendrickson, Y. S. Sohn, and Harry B. Gray

Contribution No. 4064 from the Arthur Amos Noyes Laboratory of Chemical Physics, California Institute of Technology, Pasadena, California 91109

Abstract

The ground electronic state [$^2E_{2g}(a_{1g})^2(e_{2g})^3$] of the ferricenium ion has been further characterized by a variable-temperature (40-300°K) magnetic susceptibility study of nine ferricenium and two analogous Fe(III) dicarbollide ($1,2\text{-}B_9C_2H_{11}^{2-}$) compounds. The observed temperature independence of the effective magnetic moments for these ferricenium compounds is explicable in terms of either a temperature-dependent, low-symmetry crystal field distortion or thermal population of the $^2A_{1g}(a_{1g})^1(e_{2g})^4$ state. Solvent and counter ion effects on the magnetic properties of the ferricenium ion are appreciable.

Introduction

The electronic structure of the ferricenium ion has been a subject of continuing interest. Theoretical molecular orbital investigations have provided some insight into the bonding of the ferricenium ion, but are not reliable as a means of characterizing the fine details of the ground and lowest electronic states. Unfortunately, the electronic absorption spectrum of the ferricenium ion is complicated[3-5] and to date has yielded little detailed electronic structural information.

The esr studies of ferricenium compounds by Prins and Reinders[6] and analogous Fe(III) dicarbollide compounds by Maki and Berry[7] have been of greatest value in elucidating the ground electronic configuration of these systems. Both of these low temperature esr studies have indicated, on the basis of an anisotropic g tensor, that the ground state of the ferricenium ion is a $^2E_{2g}(a_{1g})^2(e_{2g})^3$ state which is split into two Kramers doublets by spin-orbit coupling and crystal fields of symmetry lower than D_5. Contrary to these reports, Saito[8] has obtained an essentially isotropic g tensor for ferricenium ion, which was supposedly produced by gamma-irradiation of ferrocene.

We have recently communicated[5] certain results of variable temperature magnetic susceptibility studies which support and further characterize the $^2E_{2g}$ ground state of the ferricenium ion. In this

paper we will expand on this communication; new magnetic susceptibility data will be presented for some substituted ferricenium compounds as well as for two Fe(III) dicarbollide compounds. A brief discussion of the effects of ring-substitution and anion environment on the magnetic properties of the ferricenium ion will be given.

Experimental Section

Compound Preparations. Ferrocene (Eastman Kodak) was purified by recrystallization from ethanol, followed by sublimation. Chemically pure (Research Inorganic Chem.) mono- and 1,1′-dibutylferrocene were used without further purification. Phenylferrocene was synthesized by Broadhead and Pauson's recipe[9] and recrystallized from n-hexane (m.p. = 111°, lit. 109-110°). All other chemicals were reagent grade unless specified. All chemical analyses were performed by Schwarzkopf Microanalytical Labs.

Samples of $[Fe(C_5H_5)_2]I_3$, $[Fe(n\text{-}C_4H_9\text{-}C_5H_4)(C_5H_5)]I_3$, and $[Fe(C_6H_5\text{-}C_5H_4)(C_5H_5)]I_4$ were prepared by mixing 1 mmol of ferrocene or substituted ferrocene with 2.5 mmol of iodine, both dissolved in cyclohexane. The resulting dark red precipitate was recrystallized from nitromethane. Anal. Calcd for $[Fe(C_5H_5)_2]I_3$: Fe, 9.85%; I, 67.17%. Found: Fe, 9.66%; I, 67.52%. Calcd for $[Fe(n\text{-}C_4H_9\text{-}C_5H_4)(C_5H_5)]I_3$: Fe, 8.97%; I, 61.12%; C, 27.00%; H, 2.91%. Found: Fe, 9.18%; I, 61.11%; C, 26.64%; H, 2.95%. Calcd for $[Fe(C_6H_5\text{-}C_5H_4)(C_5H_5)]I_4$: Fe, 7.26%; I, 65.95%; C, 24,36%; H, 1.83%. Found: Fe, 7.36%; I, 63.86%; C, 24.36%; H, 2.11%.

Samples of $[Fe(C_5H_5)_2](C_6H_2N_3O_7)$ and $[Fe(n\text{-}C_4H_9\text{-}C_5H_4)(C_5H_5)](C_6H_2N_3O_7)$ were prepared using the method of Pavlik and Klikorka.[10] Ferricenium picrate could also be made by mixing 1 mmol of ferrocene in 50 ml benzene with 30 ml of benzene

in which 2 mmol p-benzoquinone and a large excess of picric acid had been dissolved. Anal. Calcd for $[Fe(C_5H_5)_2](C_6H_2N_3O_7)$: Fe, 13.47%; C, 46.40%; N, 10.15%; H, 2.92%. Found: Fe, 13.67%; C, 46.11%; N, 10.33%; H, 3.05%. Calcd for $[Fe(n\text{-}C_4H_9\text{-}C_5H_4)(C_5H_5)](C_6H_2N_3O_7)$: Fe, 11.88%; C, 51.08%; N, 8.94%; H, 4.29%. Found: Fe, 11.72%; C, 51.29%: N, 8.67%; H, 4.26%.

The hexafluorophosphates, $[Fe(C_5H_5)_2]PF_6$, $[Fe(n\text{-}C_4H_9\text{-}C_5H_4)(C_5H_5)]PF_6$, and $[Fe(n\text{-}C_4H_9\text{-}C_5H_4)_2]PF_6$ were prepared from ferricenium sulfate solution by precipitation with a 4-fold excess of $(NH_4)PF_6$ dissolved in a minimum of water. The resulting precipitates were dried over P_4O_{10}. Ferricenium hexafluorophosphate could also be made by mixing concentrated solutions of ferricenium tetrafluoroborate and ammonium hexafluorophosphate. Anal. Calcd for $[Fe(C_5H_5)_2]PF_6$: Fe, 16.87%: C, 36.29%; F, 34.44%; H, 3.05%. Found: Fe, 16.88%; C, 36.23%; F, 34.17%; H, 3.07%. Calcd for $[Fe(n\text{-}C_4H_9\text{-}C_5H_4)(C_5H_5)]PF_6$: Fe, 14.43%; C, 43.44%; F, 29.45%; H, 4.69%. Found: Fe, 14.57%; C, 43.20%; F, 29.34%; H, 4.53%. Calcd for $[Fe(n\text{-}C_4H_9\text{-}C_5H_4)_2]PF_6$: Fe, 12.60%, C, 48.78%; F, 25.72%; H, 5.91%. Found: Fe, 12.62%; C, 48.86%; F, 25.50%; H, 5.88%.

A sample of $[Fe(C_5H_5)_2]BF_4$ was prepared by oxidizing ferrocene in Et_2O with p-benzoquinone in the presence of HBF_4. A 30 ml Et_2O solution of ferrocene (1 mmol) was mixed with 30 ml of an etherial solution of p-benzoquinone (2 mmol) and tetrafluoroboric

acid (4 mmol, 50% aqueous soln). The resulting blue precipitate was filtered and washed thoroughly with ether. Anal. Calcd for $[Fe(C_5H_5)_2]BF_4$: Fe, 20.47%; C, 44.02%; F, 27.85%; H, 3.69%. Found: Fe, 20.64%; C, 44.18%; F, 27.56%; H, 3.92%.

$[(CH_3)_4N][(\pi\text{-}(3)\text{-}1,2\text{-}B_9C_2H_{11})_2Fe]$ and $[Fe(C_5H_5)(\pi\text{-}(3)\text{-}1,2\text{-}B_9C_2H_{11})]$. The method of Hawthorne et al.[11] was used in the preparation of these compounds. Purification was accomplished by three recrystallizations from acetone/water or two from cyclohexane/benzene. Anal. Calcd for $[(CH_3)_4N][(DCB)_2Fe]$: Fe, 14.15%; B, 49.29%; C, 24.34%; N, 3.55%; H, 8.68%. Found: Fe, 14.06%; B, 48.74%; C, 24.49%; N, 3.62%; H, 8.58%. Calcd for [Fe(cp)(DCB)]: Fe, 22.04%; B, 38.40%; C, 33.19%; H, 6.37%. Found: 22.08%; B, 38.27%; C, 33.42%; H, 6.57%.

Magnetic Measurements. A Princeton Applied Research FM-1 vibrating sample magnetometer, coupled with an Andonian Associates liquid helium dewar, was used in the determinations of the magnetic susceptibilities of solid materials. Temperatures were measured using a copper-constantan thermocouple; the insensitivity of this thermocouple at very low temperatures necessitated the reporting of magnetic susceptibility data only down to 40°K (here the accuracy of a single measurement is ca. 10%).

Room temperature effective magnetic moments (ca. 3% accuracy) for solids were measured vs. $CuSO_4 \cdot 5H_2O$ standard on the

FM-1 magnetometer. These were used to convert the relative machine data resultant from liquid nitrogen runs (300-80°K in 2 hrs) and indirectly the relative machine data from liquid helium runs (40-125°K in 1 hr). Duplicate determinations were made for freshly prepared samples of each compound in each range. Empty-holder diamagnetic corrections were applied throughout the whole temperature range.

The Evans' nmr method[12] was used to measure the room temperature (i.e., the ambient probe temperature was 42°C) solution magnetic moments. A Varian A-60 spectrometer was used. Both $[Fe(cp)_2]^+$ and $[Fe(n\text{-}Bu\text{-}cp)(cp)]^+$ were prepared in situ by oxidizing the appropriate ferrocene (~ 3 mmol) with 1 ml conc. H_2SO_4, then diluting to 25 ml with H_2O containing ~ 2% t-BuOH. Filtration (and in the case of the butyl-substituted compound extraction with benzene) preceded the nmr measurements. A dilute sulfuric acid solution of $[Fe(cp)_2]BF_4$ was also used to determine the solution effective magnetic moment of the $[Fe(cp)_2]^+$ ion. In all cases the concentration of the ferricenium ion was measured optically. Density corrections[12] were also applied.

Theory

The $^2E_{2g}\ (a_{1g})^2\ (e_{2g})^3$ state of the ferricenium ion is split into two Kramers doublets [E″ and (A′, A″)] under the influence of spin-orbit coupling and crystal fields of symmetry lower than D_5. The

wavefunctions (hole formalism) and energies for these two Kramers doublets have been given.[7]

$$\Psi_{\pm}(E'') = \begin{cases} N(e_{2g}^{+} + \zeta e_{2g}^{-})\alpha \\ N(e_{2g}^{-} + \zeta e_{2g}^{+})\beta \end{cases} \qquad W(E'') = -(\xi^2 + \delta^2)^{\frac{1}{2}}$$

$$\Psi_{\pm}(A', A'') = \begin{cases} N(e_{2g}^{-} - \zeta e_{2g}^{+})\alpha \\ N(e_{2g}^{+} - \zeta e_{2g}^{-})\beta \end{cases} \quad W(A', A'') = +(\xi^2 + \delta^2)^{\frac{1}{2}}$$

Here the mixing parameter (ζ), spin-orbit coupling constant (ξ), and low-symmetry distortion parameter (δ) are the same as defined previously.[7]

The symmetry of the ferricenium ion will be taken as D_{5d} with the z-axis as the five-fold axis. To calculate the parallel ($\chi_{\parallel}$) and perpendicular ($\chi_{\perp}$) components of the paramagnetic susceptibility we introduce the perturbations $\beta H_z(\hat{L}_z + 2\hat{S}_z)$ and $\beta H_x(\hat{L}_x + 2\hat{S}_x) = \beta H_y(\hat{L}_y + 2\hat{S}_y)$, respectively. The resulting secular equations are solved for the eigenvalues, which are then used to evaluate the parallel and perpendicular components of the paramagnetic susceptibility of the ferricenium ion by Van Vleck's formula.[13]

$$\chi_{\alpha} = \frac{N\beta^2}{kT\omega_0} \sum_{m} \left\{ (\langle \psi_{0m} | L_{\alpha} + 2S_{\alpha} | \psi_{0m} \rangle)^2 + 2kT \sum_{n \neq 0} \frac{(\langle \psi_n | L_{\alpha} + 2S_{\alpha} | \psi_{0m} \rangle)^2}{E_n - E_0} \right\}$$

The α component of the magnetic susceptibility tensor χ_α is evaluated by summing the appropriate expectation values over the m components of the ψ_0 ground state (with degeneracy ω_0) and the n excited states ψ_n.

Considering only the two Kramers doublets from the ferricenium $^2E_{2g}$ ground state, we find for the lower doublet E″

$$\chi_{\parallel}(E'') = \frac{N\beta^2}{kT}\left[\left(1 + \frac{2k'(1-\zeta^2)}{(1+\zeta^2)}\right)^2 + \frac{16\zeta^2 k'^2 (kT)}{(\xi^2+\delta^2)^{\frac{1}{2}}(1+\zeta^2)^2}\right]$$

$$\chi_{\perp}(E'') = \frac{N\beta^2}{kT}\left[\frac{4\zeta^2}{(1+\zeta^2)^2} + \frac{2kT(1-\zeta^2)^2}{(1+\zeta^2)^2\,(\xi^2+\zeta^2)^{\frac{1}{2}}}\right]$$

Here the symbols ζ, k', ξ, and δ are again as defined earlier.[7] The average magnetic susceptibility (χ) and the effective magnetic moments (μ_{eff}) are readily found.

$$\chi = \tfrac{1}{3}(\chi_{\parallel} + 2\chi_{\perp})$$

$$\mu_{eff} = 2.828(\chi T)^{\frac{1}{2}}$$

The effective magnetic moment, μ_{eff}, of the ferricenium ion, assuming a $^2E_{2g}$ ground state, would be expected then to be dependent on temperature (see Figure 1), the low-symmetry distortion parameter (δ), and the orbital reduction factor (k'). The mixing parameter, ζ, depends on the ratio of δ and ξ; the latter is given by $\xi = -k'\xi_0$,

Fig. 1. Theoretical effective magnetic moment (μ_{eff}) vs. temperature curves for E″($^2E_{2g}$) ferricenium ground state experiencing different low-symmetry distortions δ. In all cases the orbital reduction parameter k′ = 0.80.

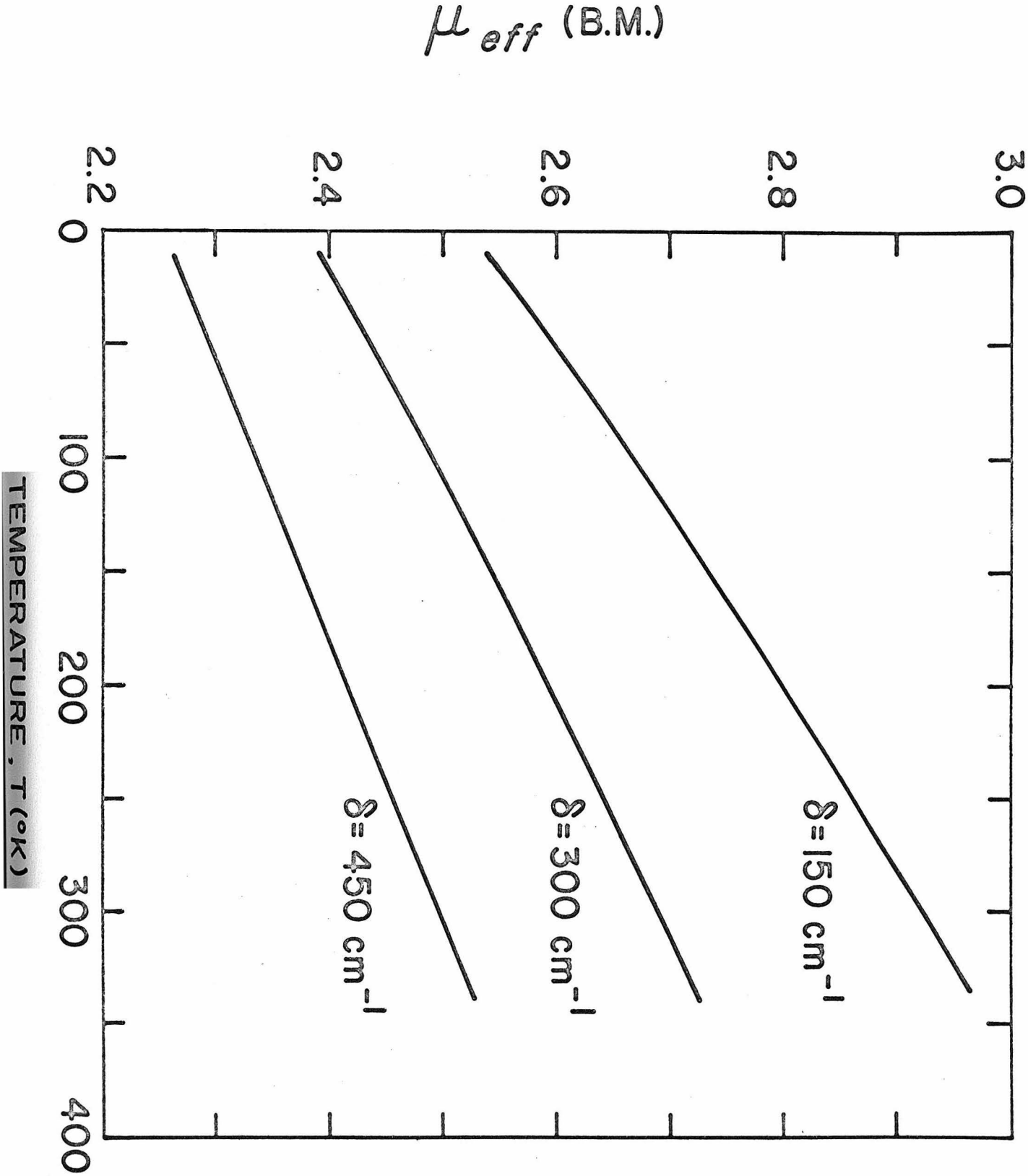
μ_{eff} (B.M.)
3.0
2.8
2.6
2.4
2.2
0
100
200
300
400
TEMPERATURE, T (°K)
δ = 150 cm⁻¹
δ = 300 cm⁻¹
δ = 450 cm⁻¹

where ξ_0 is the one-electron spin-orbit coupling constant of a free iron atom.

In anticipation of the Results section the above susceptibility expressions for the ferricenium ion will be modified to account for two possibilities. As depicted in Figure 1, μ_{eff} for the ferricenium ion is sensitive to changes in the component of the low-symmetry crystal field which affects the $^2E_{2g}$ manifold, that is, $\delta = \langle e^+_{2g} | H'_{eff} | e^-_{2g} \rangle$. If δ increases with increasing temperature, it is possible to select the temperature functionality of δ such that the μ_{eff} for the ferricenium ion would be essentially temperature independent.

Another means of securing a temperature-independent μ_{eff} is the introduction of a low-lying electronic state. Thermal population of the $^2A_{1g}\,(a_{1g})^1\,(e_{2g})^4$ state[14] at the higher temperatures would have the desired effect. The magnetic susceptibility expressions then appear as

$$\chi_\alpha = \frac{\chi_\alpha[E''(^2E_{2g})] + e^{\frac{-\Delta E}{kT}}\,\chi_\alpha(^2A_{1g})}{1 + e^{\frac{-\Delta E}{kT}}}$$

where χ_α is either the parallel or perpendicular component of the susceptibility, $\Delta E = \Delta E[^2A_{1g} - E''\,(^2E_{2g})]$, and the susceptibilities of the $^2A_{1g}$ state are those of a spin-only state

$$\chi_{\parallel}(^2A_{1g}) = \chi_{\perp}(^2A_{1g}) = \frac{N\beta^2}{kT}$$

If $\Delta E \simeq kT$ thermal population of the $^2A_{1g}$ state will dramatically affect the shape of the μ_{eff} vs. T curve at higher temperatures; μ_{eff} can become essentially independent of temperature under these conditions.

As pointed out by Maki and Berry[7] there is a further complication to be considered when the $^2E_{2g}$ and $^2A_{1g}$ are nearly degenerate. Components of the low-symmetry crystal field will mix the $^2E_{2g}$ and $^2A_{1g}$ states introducing another distortion parameter $\epsilon = \langle e^{\pm}_{2g} | \mathcal{H}' | a_{1g} \rangle$. The data at our disposal are not sufficient to include this configuration interaction; but we recognize that our parameter evaluation (δ, k', and ΔE) in the thermal population model is not unique.

Results and Discussion

Room Temperature Measurements. Room temperature magnetic susceptibility measurements were completed for nine ferricenium and two Fe(III) dicarbollide (i.e., $B_9C_2H_{11}^{2-}$) solid compounds. The requisite ligand and counter-ion diamagnetic corrections were obtained from either direct measurement or from a table[15]; the results are given in Table I. These diamagnetic corrections were used in the calculations of the room temperature effective magnetic moments for the compounds listed in Table II. Here we also give the 42°C nmr solution moments for the $[Fe(cp)_2]^+$ and $[Fe(n\text{-}Bu\text{-}cp)(cp)]^+$ ions in dilute sulfuric acid.

The room temperature moments of the low-spin d^5 iron in these ferricenium and dicarbollide complexes range from ~ 2.3 to

Table I. Various Diamagnetic Corrections Used in the Treatment of Experimental Data

	Diamagnetism ($\times 10^6$ cgs)
PF_6^-	-23.0[a]
BF_4^-	-122.0[a]
pic^-	-147.6[a]
$[Co(DCB)_2]^-$	-257.1[a]
$[(CH_3)_4N]^+$	-60.3[a]
I_3^-	-139.5[a]
I_4^-	-184.1[b]
$[Fe(cp)_2]$	-125.0[c]
[Fe(n-Bu-cp)(cp)]	-172.4[d]
$[Fe(n\text{-}Bu\text{-}cp)_2]$	-219.8[d]
[Fe(ϕcp)(cp)]	-172.7[d]

a) Determined by direct measurement of appropriate compound.

b) Taken as $\chi_M(I_3^-) + \frac{1}{2}\chi_M(I_2)$, the latter value from tables.[15]

c) F. Englemann, Z. Naturforsch., 8b, 775 (1953).

d) Taken as χ_M (ferrocene) + χ_M (substituent), the latter value from tables.[15]

Table II. Room Temperature Effective Magnetic Moments for Various Ferricenium and Analogous Compounds

Compound[a]	μ_{eff} at 298°K (B.M.)
$[Fe(cp)_2]PF_6$	2.62
$[Fe(cp)_2]$pic	2.60
$[Fe(cp)_2]I_3$	2.47
$[Fe(cp)_2]BF_4$	2.44
$[Fe(cp)_2]ClO_4$	2.34[b]
$[Fe(n\text{-}Bu\text{-}cp)(cp)]PF_6$	2.54
$[Fe(n\text{-}Bu\text{-}cp)(cp)]$pic	2.48
$[Fe(n\text{-}Bu\text{-}cp)(cp)]I_3$	2.53
$[Fe(n\text{-}Bu\text{-}cp)_2]PF_6$	2.59
$[Fe(\phi\text{-}cp)(cp)]I_4$	2.58
$[(CH_3)_4N][Fe(DCB)_2]$	2.58
$[Fe(DCB)_2]^-$ (soln)[c]	2.10[d]
$[Fe(DCB)(cp)]$[c]	2.23
$[(CH_3)_4N]\{Fe[1,2\text{-}B_9H_9C_2(CH_3)_2]_2\}$	2.45[b]
$\{Fe[1,2\text{-}B_9H_9C_2(CH_3)_2]_2\}^-$ (soln)	1.99[d]
$[Fe(cp)_2]^+$ (soln)	2.31[e]
$[Fe(cp)_2]BF_4$ (soln)	2.48[e]
$[Fe(n\text{-}Bu\text{-}cp)(cp)]^+$ (soln)	2.38[e]

a) All compounds are solids unless otherwise stated.

b) J. S. Little, P. S. Welcker, N. J. Soy, and S. J. Todd, Inorg. Chem., 9, 63 (1970).

Table II (continued)

c) The ligand DCB^{2-} is 1, 2-$B_9C_2H_{11}^{2-}$.

d) From Ref. 11; magnetic moments measured in acetone solution.

e) Measured in dilute H_2SO_4 by Evans nmr method,[12] at an ambient probe temperature of 42° C.

~ 2.6 B. M. This degree of deviation from the spin-only value of 1.73 B. M. establishes the $^2E_{2g}$ ground state for the ferricenium ion, in agreement with two esr studies.[6,7] Sufficient precautions were taken to rule out the alternative possibility of a $^2A_{1g}$ ground state with paramagnetic impurities. The solution moments measured for the two different ferricenium ions are relatively low. In the case of two iron dicarbollide complexes both solid and solution moments are known and the latter are appreciably smaller. These data suggest that in solution the ferricenium ion is significantly distorted (see Figure 1).

Some support for this proposal was found in the nmr experimentation. In our application of the nmr method for solution magnetic moments t-BuOH (2% in H_2O) was used as the monitor of the bulk susceptibility of the solution. We have found that for aqueous solutions of $[Fe(cp)_2]^+$ and $[Fe(n\text{-}Bu\text{-}cp)(cp)]^+$ the shift in the water peak greatly exceeded (~ 70%) that observed in the t-BuOH peak. Close radial (i. e., x-y plane) approach would result in a pseudocontact interaction causing a larger peak shift for the water protons. Thus there is clear indication of a specific interaction of water with the ferricenium ion. Our conclusion is further supported by evidence which shows that the aqueous ferricenium ion is bound by certain carboxylic acids.[16] It appears that in solution the ferricenium ion is coordinated to a solvent molecule and that this coordination results in a distortion greater than that experienced in the solids. Any consideration of the temperature dependence of the solution μ_{eff} or other magnetic property (e. g., pseudocontact nmr shift) of the ferricenium ion would require a careful evaluation of this effect.

Variable Temperature Measurements. Variable temperature magnetic susceptibility studies in the range of 40-300°K resulted in the μ_{eff} vs. T curves depicted in Figures 2-5. In the case of four compounds, data were only collected down to 80°K. It is clear from these figures, however, that all eleven μ_{eff} vs. T curves have essentially the same shape. Ring-substitution and counter-ion interchange have the effect only of displacing the curve for a particular compound to higher or lower effective magnetic moment. Thus mono-butylation leads to a ~0.1 B. M. change for the hexafluorophosphates (see Figure 3), whereas, 1, 1′-dibutylation leaves the moment essentially unchanged. It seems that the more asymmetric the ion as a result of substitution, the more pronounced is the change in μ_{eff}. Monobutylation in the picrate and triiodide series (see Figures 3 and 4) gives the same order of change in μ_{eff} as observed for the hexafluorophosphates. Unfortunately, we were not able to prepare the disubstituted ferricenium picrate and triiodide compounds. Total interchange of the dicarbollide ion for the cyclopentadienide ion results in no dramatic change (compare the position of the curve for the bis-dicarbollide compound in Figure 2 with those for various unsubstituted ferricenium salts in Figures 3-5). Replacement of one of the cyclopentadienyl ligands by dicarbollide, giving the non-ionic compound $[Fe(cp)(1,2\text{-}B_9C_2H_{11})]$, results in a low magnetic moment (see Figure 2). Since this is the only non-ionic d^5 ferricenium-like complex considered, it is reasonable to suggest that the low moment is due to a distortion caused by packing the asymmetric molecule into the crystal.

Fig. 2. Curves of the effective magnetic moment (μ_{eff}) vs. temperature for two Fe(III) dicarbollide (i.e., $1,2\text{-}B_9C_2H_{11}^{2-} \equiv DCB^{2-}$) compounds: ○, $[(CH_3)_4N][Fe(DCB)_2]$; □, [Fe(cp)(DCB)]. The solid line is a theoretical curve for the thermal population model with $\delta = 240\ cm^{-1}$ and $\Delta E[E'(^2A_{1g}) - E''(^2E_{2g})] = 280\ cm^{-1}$.

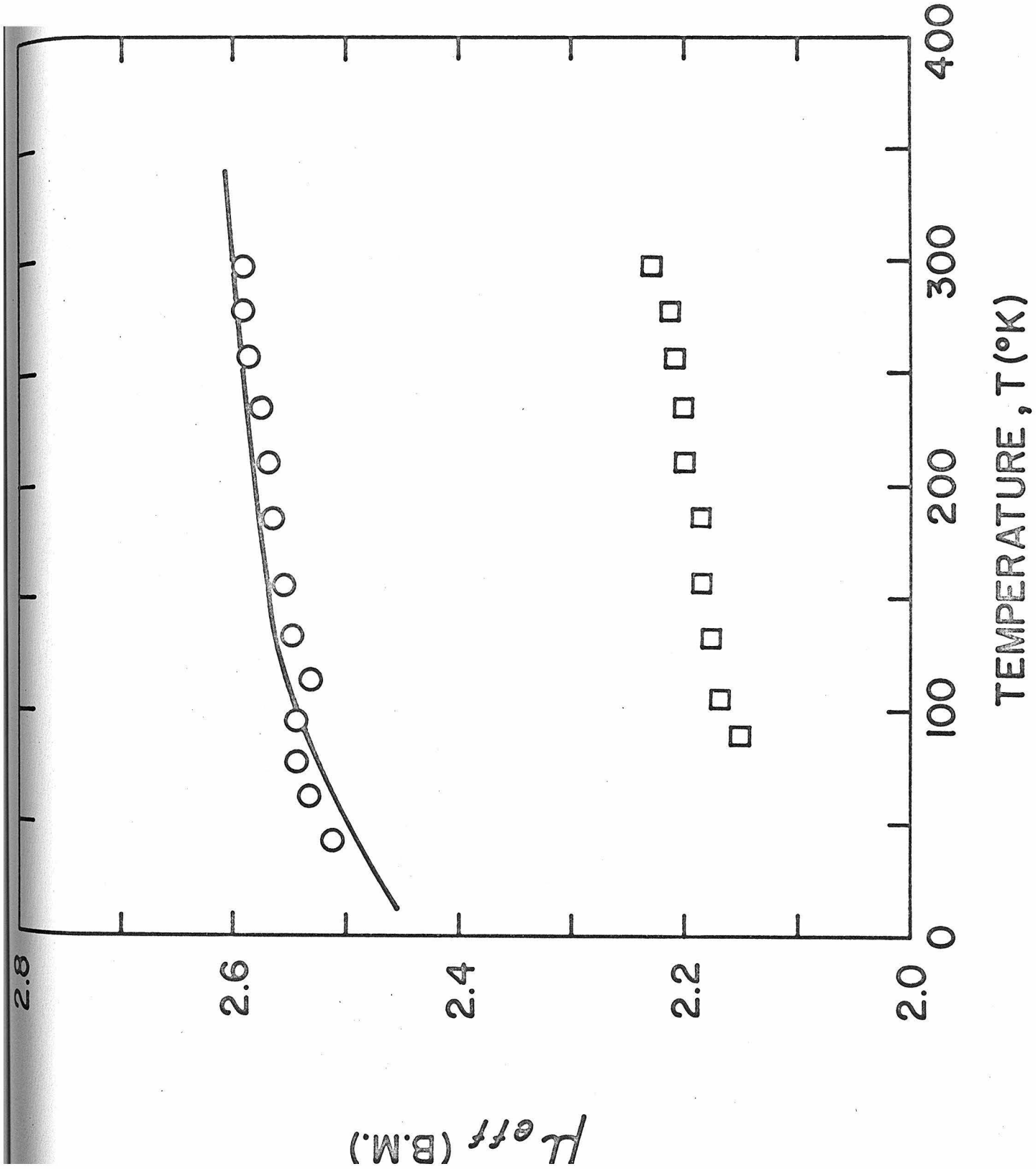
2.8
2.6
2.4
2.2
2.0
0
100
200
300
400
TEMPERATURE, T (°K)
μ_{eff} (B.M.)

Fig. 3. Curves of the effective magnetic moment (μ_{eff}) vs. temperature for three different ferricenium hexafluorophosphates: □, $[Fe(n\text{-}C_4H_9 — C_5H_4)_2]PF_6$; Δ, $[Fe(C_5H_5)_2]PF_6$; ○, $[Fe(n\text{-}C_4H_9 — C_5H_4)(C_5H_5)]PF_6$. The solid lines are theoretical curves for the thermal population model: a, $\delta = 180\ cm^{-1}$ and $\Delta E = 260\ cm^{-1}$; b, $\delta = 160\ cm^{-1}$ and $\Delta E = 200\ cm^{-1}$.

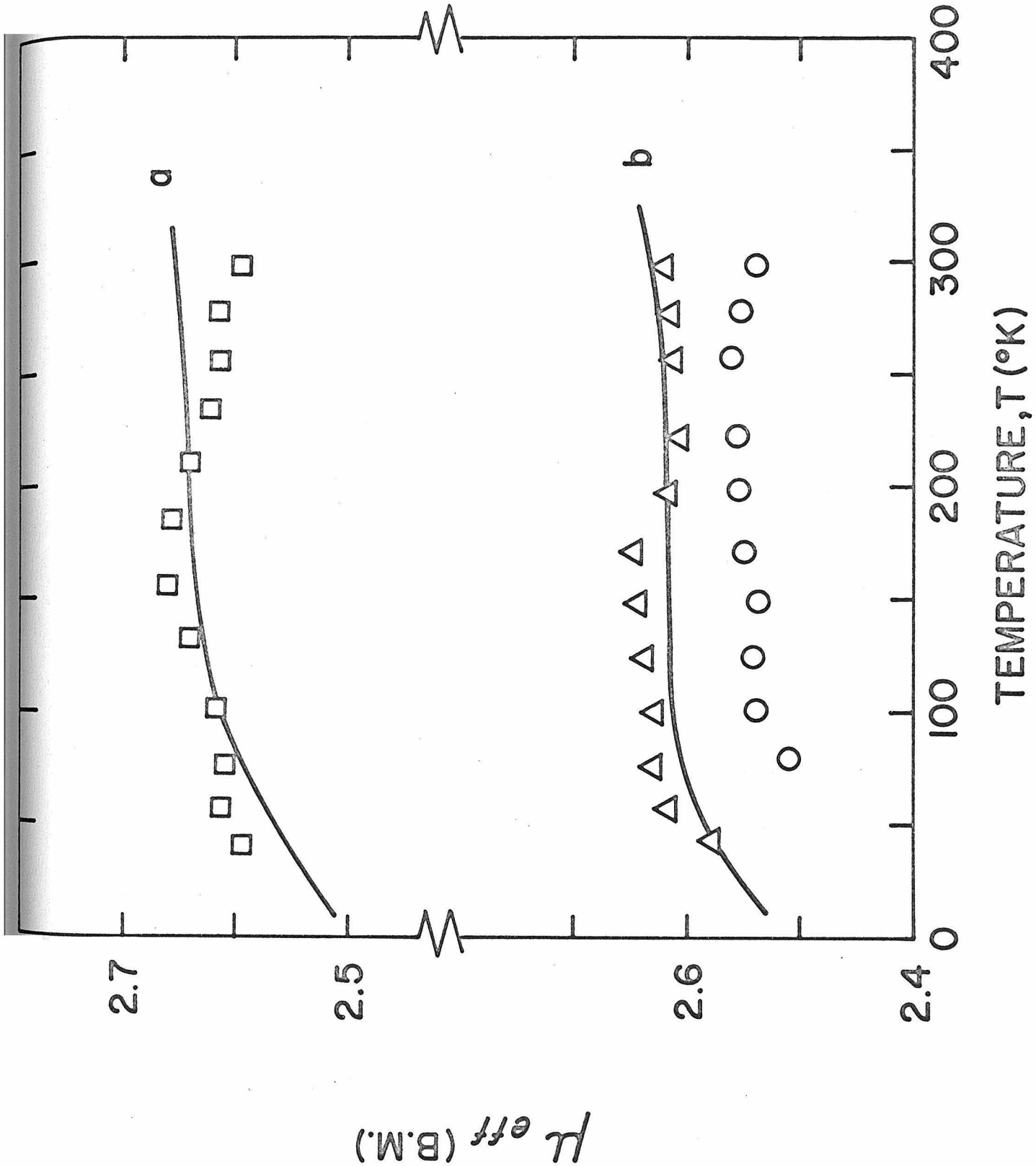
a
b
2.7
2.5
2.6
2.4
0
100
200
300
400
TEMPERATURE, T (°K)
μ eff (B.M.)

Fig. 4. Curves of the effective magnetic moment (μ_{eff}) vs. temperature for three ferricenium salts: □, $[Fe(C_5H_5)_2]pic$; ○, $[Fe(n\text{-}C_4H_9 - C_5H_4)(C_5H_5)]pic$; Δ, $[Fe(C_5H_5)_2]BF_4$. The solid lines are theoretical curves for the thermal population model: a, $\delta = 200\ cm^{-1}$ and $\Delta E = 240\ cm^{-1}$; b, $\delta = 330\ cm^{-1}$, $\Delta E = 260\ cm^{-1}$; c, $\delta = 330\ cm^{-1}$ and $\Delta E = 200\ cm^{-1}$. The mark × represents the μ_{eff} obtained by esr in reference 3 for frozen DMF and acetone solutions of $[Fe(C_5H_5)_2]BF_4$.

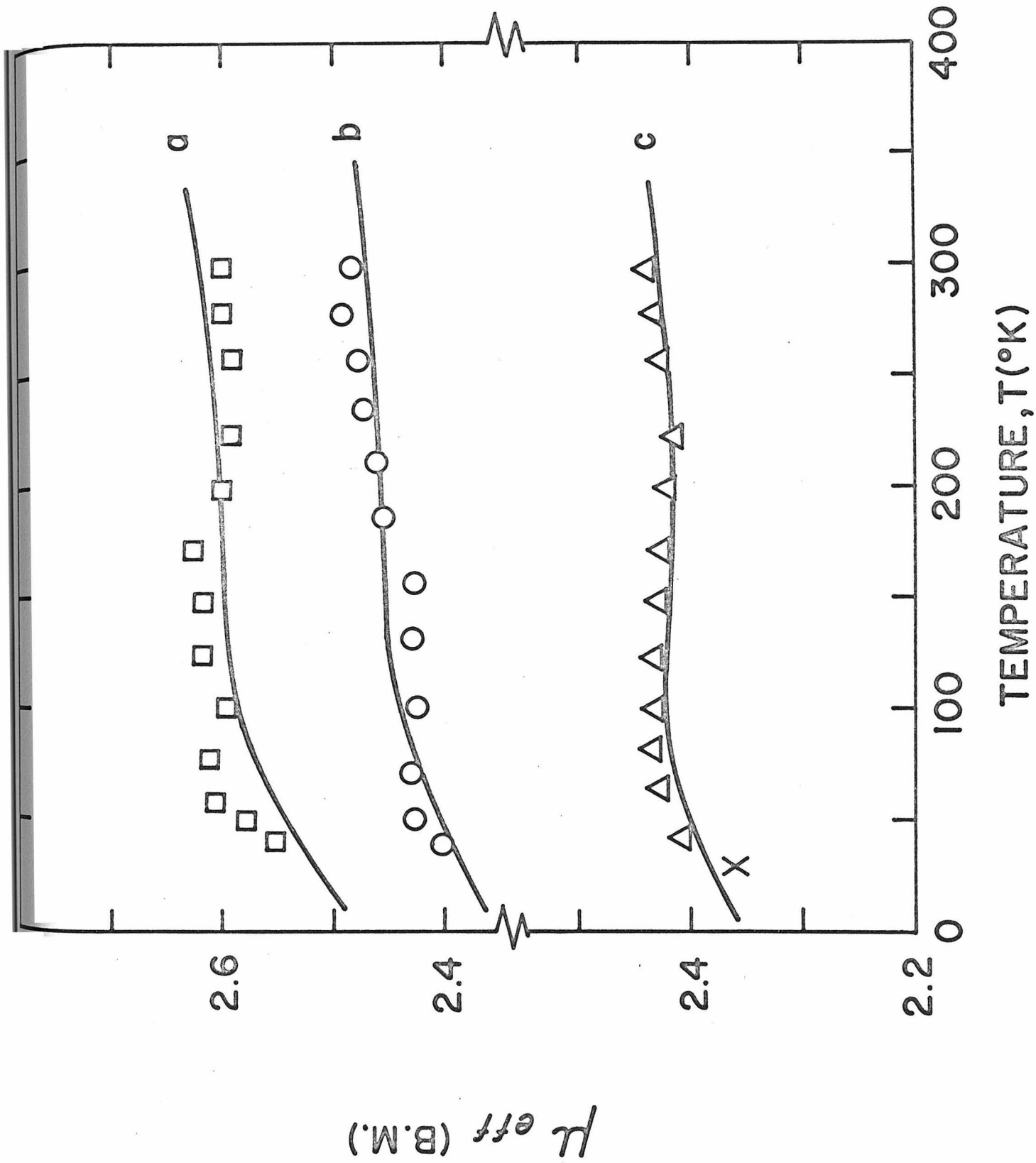
a
b
c
X
2.6
2.4
2.4
2.2
0
100
200
300
400
TEMPERATURE, T(°K)
μ_{eff} (B.M.)

Fig. 5. Curves of the effective magnetic moment (μ_{eff}) vs. temperature for three ferricenium salts: □, $[Fe(n\text{-}C_4H_9\text{-}C_5H_4)(C_5H_5)]I_3$; ○, $[Fe(C_5H_5)_2]I_3$; △, $[Fe(C_6H_5\text{-}C_5H_4)(C_5H_5)]I_4$. The solid line is a theoretical curve for the thermal population model with $\delta = 330\ cm^{-1}$ and $\Delta E = 260\ cm^{-1}$. The mark × represents the μ_{eff} obtained by esr in reference 3 for frozen DMF and acetone solutions of $[Fe(C_5H_5)_2]I_3$.

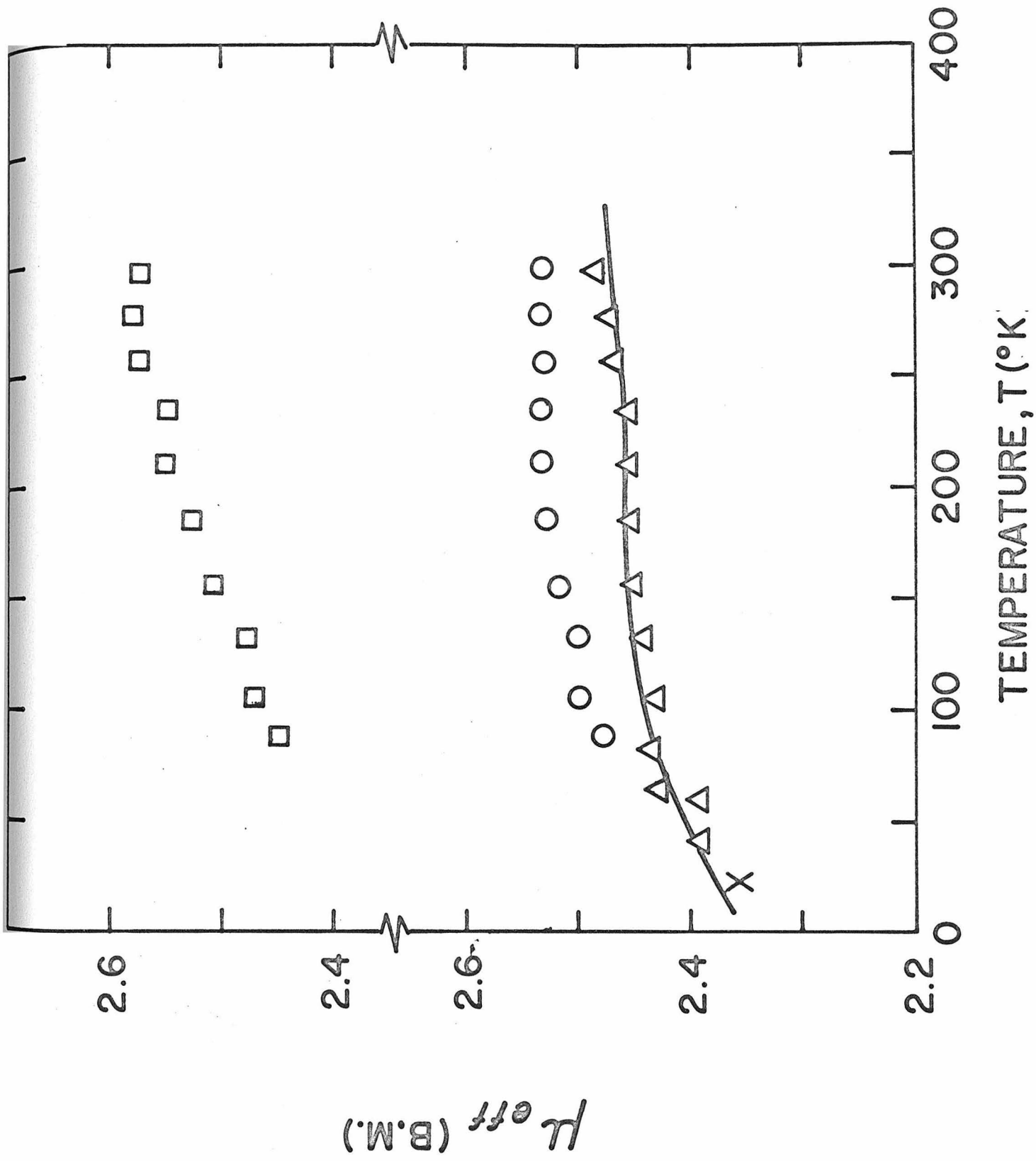
2.6
2.4
2.6
2.4
2.2
0
100
200
300
400
TEMPERATURE, T(°K
μ_{eff} (B.M.)

The solution moment (Table II) determined for the ferricenium ion is essentially that found for either $[Fe(cp)_2]BF_4(s)$ or $[Fe(cp)_2]I_3(s)$. It appears that the distortion felt by the ferricenium ion in solution is the same as that in the triiodide and tetrafluoroborate solids. Prins and Reinders[6] measured the esr spectra for these same two solids in frozen solutions of dimethylformamide and acetone at 20° K. Their g-values give $\mu_{eff} = 2.36$ B.M. at 20° K for the ferricenium ion; it is thus not surprising that this μ_{eff} value fits on our μ_{eff} vs. T curves for both $[Fe(cp)_2]BF_4(s)$ and $[Fe(cp)_2]I_3(s)$ (see Figures 4 and 5).

A comparison of the experimental μ_{eff} vs. T data (Figures 2-5) with the theoretical curves (Figure 1) generated for the $^2E_{2g}$ ground state ferricenium ion experiencing a temperature-independent, low-symmetry distortion (δ) is instructive. Theoretically μ_{eff} should increase with increasing temperature, but experimentally μ_{eff} is found to be relatively temperature independent. In the Theory section two different modifications of the theoretical susceptibility expression were proposed to give a temperature-independent μ_{eff}. Perhaps the simplest approach would be to take δ as temperature dependent. From Figure 1 we can see that if δ increases with increasing temperature the experimental curves can be fit. Thus as the crystal expands with increasing temperature the low-symmetry distortion increases, possibly due to increased motion of the cyclopentadienyl rings.

The second modification of the susceptibility expression given in the Theory section involves consideration of the low-lying $^2A_{1g}$ state.[14] If this state becomes thermally populated as the temperature increases, a temperature-independent μ_{eff} could result. Assuming $\epsilon = 0$ (see Theory), theoretical curves (see Figs. 2-5) have been visually fit to the experimental data for seven of the compounds. We have elected to assume the same orbital reduction parameter ($k' = 0.80$) in each case. Within the framework of this thermal population model the distortion parameter δ for these seven compounds varies from $\sim$ 160 to $\sim$ 330 cm^{-1}, whereas $\Delta E[\,^2A_{1g} - E''(^2E_{2g})]$ varies from $\sim$ 200 to $\sim$ 280 cm^{-1}. The variation in δ is well outside the range of experimental uncertainties; the distortion seems to reflect changes in the anion environment mainly, where small anions and water solvent molecules cause the larger distortions. Thus changing the anion from PF_6^- to the relatively small BF_4^- results in a difference of $\sim$ 0.2 B.M. in μ_{eff} for the unsubstituted ferricenium ion.

In summary, it is clear that the experimental magnetic susceptibility curves obtained for various ferricenium compounds cannot be explained by considering only the two Kramers doublets from the $^2E_{2g}$ ground state with a temperature-independent distortion δ. It is necessary to introduce $\delta(T)$ or thermal population of the $^2A_{1g}$ state to explain the relative temperature independence of μ_{eff}. We are planning further experimentation to distinguish between these possibilities. Single crystal susceptibility work would be valuable.

Acknowledgments

This research was supported by the National Science Foundation.

References

(1) For ferricenium MO treatment: E. M. Shustorovich and M. E. Dyatkina, Doklady Akademii Nank. SSSR, 144, 141 (1960).

(2) For ferrocene MO treatments: D. R. Scott and R. S. Becker, J. Chem. Phys., 35, 516 (1961), and references therein; J. P. Dahl and C. J. Ballhausen, Mat. Fys. Medd. Dan Vid. Sels., 33, No. 5 (1961); R. D. Fischer, Theoret. Chim. Acta, 1, 418 (1963); A. T. Armstrong, D. G. Carroll, and S. P. McGlynn, J. Chem. Phys., 47, 1104 (1967); and J. H. Schactschneider, R. Prins, and P. Ros, Inorg. Chim. Acta, 1, 462 (1967).

(3) D. A. Levy and L. E. Orgel, Mol. Phys., 4, 93 (1961).

(4) D. R. Scott and R. S. Becker, J. Phys. Chem., 69, 3207 (1965).

(5) Y. S. Sohn, D. N. Hendrickson, and H. B. Gray, J. Amer. Chem. Soc., in press.

(6) R. Prins and F. J. Reinders, J. Amer. Chem. Soc., 91, 4929 (1969).

(7) A. H. Maki and T. E. Berry, J. Amer. Chem. Soc., 87, 4437 (1965).

(8) E. Saito, J. Chem. Phys., 50, 3539 (1969).

(9) G. D. Broadhead and P. S. Pauson, J. Chem. Soc., 367 (1955).

(10) T. Pavlik and J. Klikorka, Coll. Czech. Chem. Commun., 30, 664 (1965).

(11) M. F. Hawthorne, D. C. Young, T. D. Andrews, D. V. Howe, R. L. Pilling, A. D. Pitts, M. Reintjes, L. F. Warren, Jr., and P. A. Wegner, J. Amer. Chem. Soc., 90, 879 (1968).

(12) D. F. Evans, J. Chem. Soc., 2003 (1959).

(13) J. H. Van Vleck, "The Theory of Electric and Magnetic Susceptibilities", Oxford University Press (1932).

(14) The proximity of the $^2E_{2g}$ and $^2A_{1g}$ states in the ferricenium ion has been alluded to briefly in reference 5; further details will follow in another paper.

(15) J. Lewis and R. G. Wilkins, "Modern Coordination Chemistry", Interscience Inc. (1960).

(16) T. D. Smith, J. Inorg. Nucl. Chem., 14, 290 (1960).

PART III. SYNTHESIS AND CHARACTERIZATION OF SEVERAL OXIDATION PRODUCTS OF RUTHENOCENE

Part III has been prepared for publication in Inorg. Chem.

Synthesis and Characterization of Several Oxidation Products of Ruthenocene

Y. S. Sohn, David N. Hendrickson, and Harry B. Gray

Contribution No. from the Arthur Amos Noyes Laboratory of Chemical Physics, California Institute of Technology, Pasadena, California 91109

Abstract

Attempts to prepare ruthenicenium salts have resulted in the synthesis and characterization of several interesting ruthenocene derivatives. Contrary to a previous report, electrochemical oxidation of ruthenocene employing a mercury anode yields the mercury-bridged dimer $[(cp)_2Ru—Hg—Ru(cp)_2](ClO_4)_2$. Analytical, infrared, Raman, and electronic absorption spectral data were utilized in assigning the molecular structure. In particular, a Raman band at 110 cm^{-1} was assigned to the symmetrical Ru—Hg—Ru stretching mode. Preliminary X-ray crystallographic data for the hexafluorophosphate salt, which was obtained by anion exchange, are in agreement with the above dimeric formulation. Chemical oxidation of ruthenocene by iodine and bromine gives $[Ru(cp)_2I]I_3$ and $[Ru(cp)_2Br]Br_3$, respectively, as indicated by analytical and spectral data.

Introduction

Recent studies of the electronic structures of metallocenes[1-3] have provided convincing evidence that the ground state of the ferricenium ion, $Fe(cp)_2^+$, is $^2E_{2g}$. There are also some magnetic susceptibility data[4] on various $Fe(cp)_2^+$ salts which can be understood if a $^2A_{1g}$ state lies within a few hundred wavenumbers of the $^2E_{2g}$ ground state. From the observed energy level patterns in going from $Fe(cp)_2$ to $Ru(cp)_2$, we might expect a reversal of the $^2E_{2g} < {}^2A_{1g}$ order and therefore a $^2A_{1g}$ ground state in the case of $Ru(cp)_2^+$. Consequently, low temperature ESR and magnetic suceptibility measurements on the ruthenicenium ion would be very useful in developing a better overall electronic structural picture of metallocene complexes. Thus we have attempted to prepare a series of ruthenicenium salts.

The synthesis of the ruthenicenium ion was reported in 1952 by Wilkinson.[5] In our laboratory several attempts, including Wilkinson's method for the oxidation of ruthenocene, have failed to yield the desired complex. Instead, we have obtained several diamagnetic oxidation products. These diamagnetic species are not interesting insofar as the ruthenicenium electronic structure is concerned, but they are important as a means of providing insight into some aspects of ruthenocene chemistry. In this paper we report the synthesis and characterization of the products of electrochemical oxidation of ruthenocene at a mercury anode and two halogen-oxidized compounds.

Experimental

Compound Preparation. Ruthenocene (Orgmet) was purified by recrystallization in ethanol and sublimation twice in vacuum. All other chemicals used were reagent grade unless specified. Chemical analyses were performed by Schwartzkopf Microanalytical Laboratory.

Electrochemical oxidation of ruthenocene was carried out following Wilkinson's method.[5] A sample of ruthenocene (0.10 g) was dissolved in ~200 ml of a supporting electrolyte consisting of 90% ethanol with added perchloric acid and then oxidized on a mercury anode by a controlled potential of + 0.4 v vs. SCE using a potentiostat (Electronische Potentiostat Nach Wenking). The initial current reading was 27 mA and the reaction was terminated at 3.8 mA after ~50 min. The quantity of electricity consumed during this process was 39 coulombs in agreement with the theoretical value of 42 coulombs calculated assuming a one-electron oxidation of $Ru(cp)_2$. This is in accord with a previous report.[6] A yellow perchlorate salt (compound I) precipitated out during the electrolysis. Caution: This perchlorate salt is highly explosive when shocked in the dry state. Scratching the glass filter proved dangerous. Compound I was confirmed to be the same product as reported[5] previously by comparing the ultraviolet-visible absorption spectrum of its aqueous solution with that reported. It was possible to prepare the hexafluorophophate salt (compound II) by anion exchange with the perchlorate. The electronic absorption spectra of compounds I and II are identical.

Chemical oxidation of ruthenocene was carried out using halogens as oxidizing agents. A sample of ruthenocene (0.5 mmol) dissolved in 50 ml of CCl_4 was added to a 500 ml CCl_4 solution containing 1.5 mmol of iodine. A dark red crystalline precipitate (compound III) slowly formed. This iodide compound was found to be diamagnetic. Several attempts using different ratios of the reactants [$Ru(cp)_2/I_2$] and different solvents such as cyclohexane, n-hexane, and benzene failed to produce any paramagnetic oxidation products. Bromine oxidation of ruthenocene proceeded in a similar fashion. To a 150 ml of a cyclohexane solution of ruthenocene (0.10 g), bromine was added dropwise until the reaction was complete. A greenish-yellow precipitate (compound IV) was formed. This compound was also found to be diamagnetic.

Both of the halide complexes (III and IV) as well as the two electrochemically-produced complexes (I and II) are soluble in polar organic solvents. The bromide complex (IV) is unstable as a solid, decomposing after a few days at room temperature, and dissolves with reaction in water. On the other hand, the iodide (III) is so stable that it can be purified by recrystallization in nitromethane; well-formed needles were grown from this solvent. Analytical data for compounds III and IV are consistent with the following formulas: III, Calcd for $Ru(C_5H_5)_2I_4$: Ru, 13.68%; I, 68.70%; C, 16.26%; H, 1.36%. Found: Ru, 13.39%; I, 68.04%; C, 16.07%; H, 1.50%. IV, Calcd for $Ru(C_5H_5)_2Br_4$: Ru, 18.34%; Br, 58.02%; C, 21.80%; H, 1.83%. Found: Ru, 18.02%; Br, 57.44%; C, 21.97%; H, 1.89%.

We were not able to reconcile the analytical data for compound I with any reasonable empirical formula: Found: Ru, 14.83%; Hg, 14.53%; Cl, 8.30%; C, 26.85%; H, 2.88%.

Physical Measurements. The electronic absorption spectra of compounds I and II were measured on a Cary Model 14 CMRI spectrophotometer. A Cary Model 14 was employed for spectral measurements near 2000Å. An aqueous $HClO_4$ solution (0.01 M) was used in the room temperature absorption measurements. Low temperature (77°K) absorption spectra were determined using a quartz dewar and a solvent mixture of propionitrile, ethanol and ethyl ether (1:1:3). Bubbling of the coolant (liquid nitrogen) was eliminated by operating under reduced pressures.

Infrared spectra of the four compounds were obtained with a Perkin-Elmer Model 225 Grating Spectrophotometer. Nujol mulls were used for the 200-450 cm^{-1} region and both KBr pellets and Nujol mulls for the 450-4000 cm^{-1} region. The Raman spectrum of compound II was measured on a Cary Model 81 spectrophotometer using both solid and acetonitrile solution samples. Room temperature magnetic susceptibilities of solid materials were determined with a Princeton Applied Research FM-1 vibrating sample magnetometer.

Results and Discussion

Electrochemical Oxidation. Electrochemical oxidation of ruthenocene employing a mercury anode and a perchloric acid electrolyte yields a yellow perchlorate salt (compound I). Wilkinson[5] reported that compound I is $[Ru(cp)_2]ClO_4$. It is clear that this is not the case, because we have found that compound I is diamagnetic and contains an appreciable amount of mercury (14.53%). Nevertheless, we confirmed Wilkinson's[6] finding that there is one-electron equivalent per ruthenocene involved in the electrochemical production of compound I. This finding is equally explicable in terms of a mercury oxidation, $Hg \xrightarrow{-2e^-} Hg(II)$, as it is an oxidation of ruthenocene. If this is the case, compound I may be formulated as $[(cp)_2Ru-Hg-Ru(cp)_2](ClO_4)_2$. The analytical data for this compound (see Experimental section) suggest but poorly fit this formulation. However, preliminary X-ray work on compound II is consistent with the suggested structure of the cation.[7]

The infrared spectra (see Table I) of compounds I and II are essentially the same as those obtained for compounds III and IV (see Figures 1 and 2). It is apparent that compound II is the hexafluorophosphate salt of the same cation incorporated in compound I. In the case of compound II a Raman spectrum was taken (see Table I). A strong Raman band at 110 cm^{-1} was observed both in solid and solution. This band is not observable in ruthenocene and may be assigned to the symmetrical Ru—Hg—Ru stretching mode. The next

Table I. Infrared and Raman Bands of Oxidation Products of Ruthenocene[a]

$Ru(cp)_2$		Compound I	II		III	IV
IR	R	IR	IR	R	IR	IR
				110(s)		
		~ 190(s)	~ 190(s)		211(M)	225(W)
	330(s)			338(s)		
379(W)					379(M)	377(M)
	402(M)	407(M)	410(M)			
446(s)		427(M)	425(M)		419(M)	429(M)
	600(W)	585(W)	585(W)	602(W)	578(W)	579(W)
806(s)		811(s)[c]	812(M)[c]		819(W)	818(W)
834(W)		854(M)	853(M)		844(s)	840(s)
864(M)		863(M)	878(M)			864(W)
					920(W)	920(W)
					976(W)	975(W)
	996(W)					

Table I. (Continued)

$Ru(cp)_2$		Compound I	II		III	IV
IR	R	IR	IR	R	IR	IR
1002(s)[b]		1005(M)[b]	1012(s)[b]		1020(M)	1013(M)
1050(W)[b]	1056(M)	1050(M)	1062(W)[b]	1070(W)	1045(W)[b]	1050(W)[b]
1100(s)[b]	1105(s)		1100(s)[b]	1108(M)	1107(W)	1112(W)
	1200(W)					
	1360(W)					
1402(s)	1408(M)	1405(s)	1408(s)[b]	1408(W)	1402(s)	1404(s)
		1420(s)[b]	1423(s)[b]	1423(W)	1436(M)[c]	1440(s)[c]
1620(W)						
1660(W)						
1675(W)						
1755(W)						
1790(W)						
3080(M)[b]	3085(W)	3105(s)[b]	3128(s)[b]	3130(W)	3090(s)	3085[b]
	3103(W)					
	3110(W)					

Table I. (Continued)

[a]Positions of infrared bands were taken from the spectra made in Nujol mull.

[b]This band shows further structure in a KBr pellet.

[c]Band position taken from KBr pellet spectrum.

Fig. 1. Infrared spectrum of compound III: KBr pellet in the 4000-450 cm^{-1} region; Nujol mull in the 450-200 cm^{-1} region.

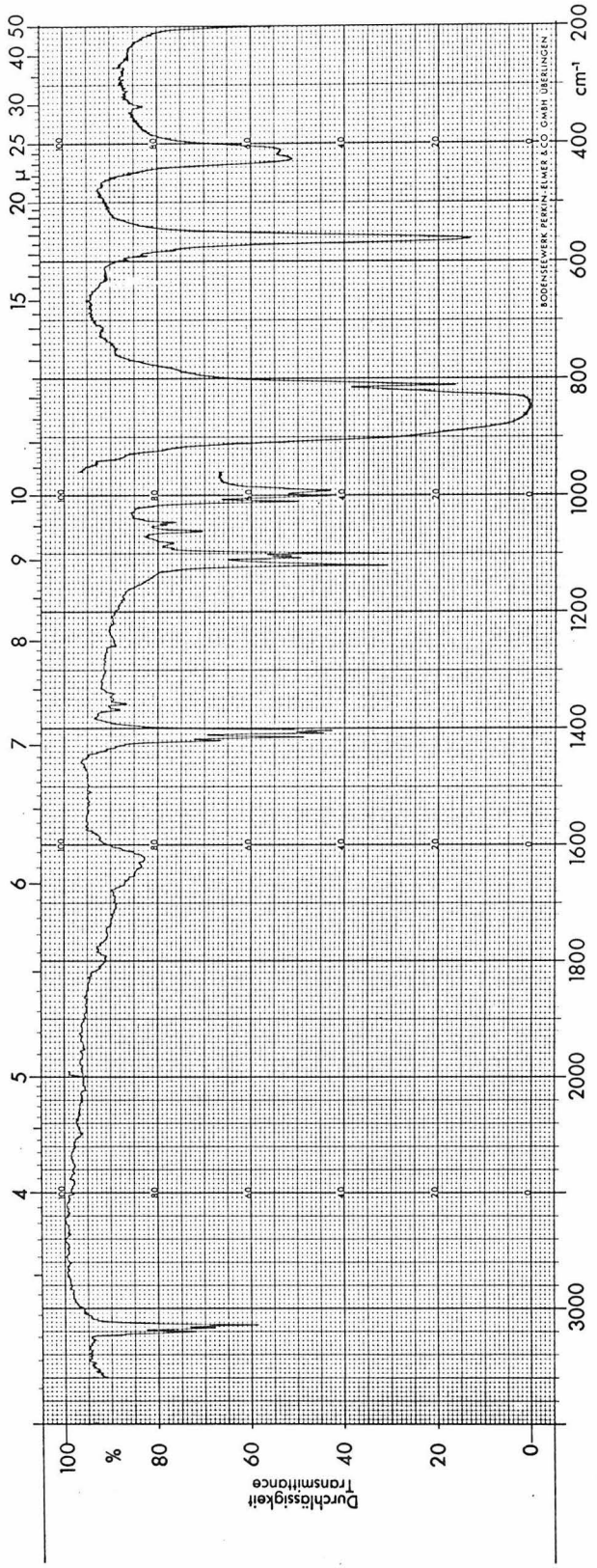
Durchlässigkeit
Transmittance
%
100
80
60
40
20
0
4
5
6
7
8
9
10
15
20 μ
25
30
40
50
3000
2000
1800
1600
1400
1200
1000
800
600
400
200
cm⁻¹
BODENSEEWERK PERKIN-ELMER & CO. GMBH ÜBERLINGEN

Fig. 2. Infrared spectrum of compound III: KBr pellet in the 4000-450 cm^{-1} region; Nujol mull in the 450-200 cm^{-1} region.

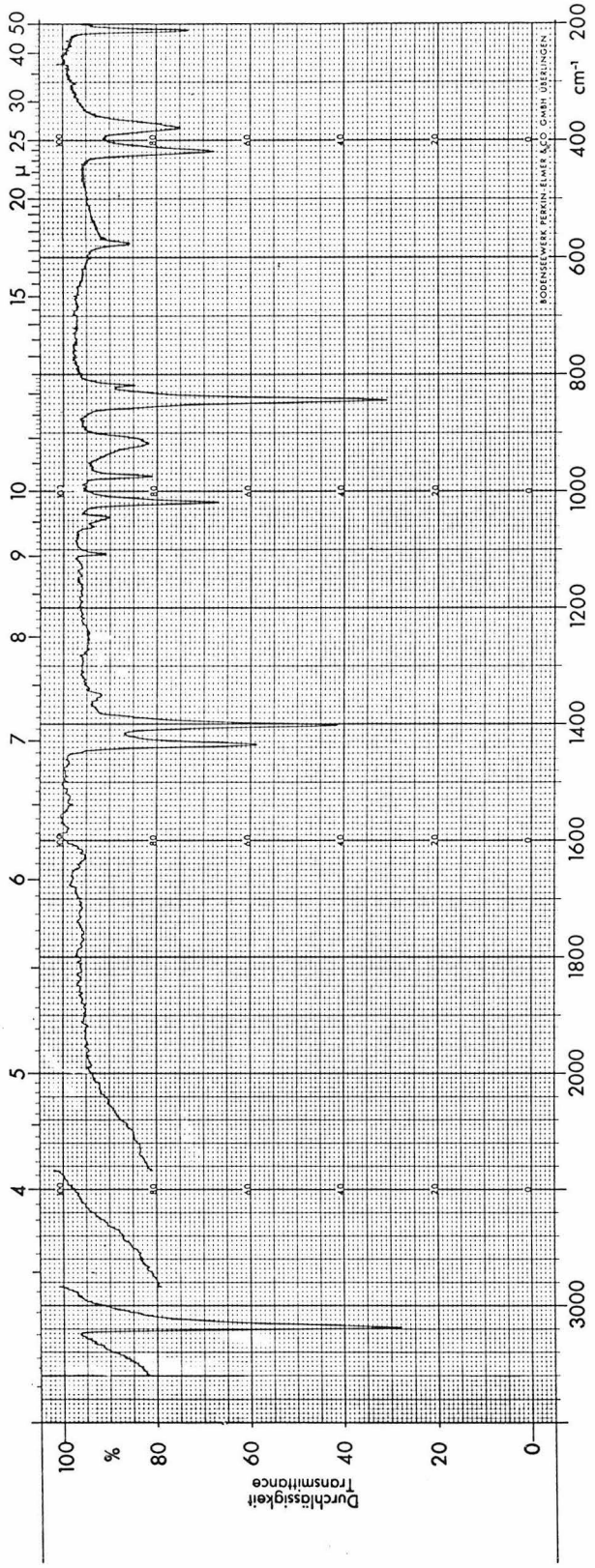
Durchlässigkeit
Transmittance
%
100
80
60
40
20
0
μ
cm⁻¹
BODENSEEWERK PERKIN-ELMER & CO GMBH ÜBERLINGEN

higher energy Raman band (338 cm^{-1}) observed for compound II may be assigned as the symmetrical ring-metal-ring stretch, ω_4,[8] which is observed at 330 cm^{-1} in ruthenocene. To a good approximation, then, we can consider the cation to be $[(cp)_2Ru(II)-Hg(II)-Ru(II)(cp)_2]^{2+}$. The IR band at 190 cm^{-1} can be assigned as the ring-metal-ring bending vibration, ω_{22}. The ring-metal-ring bending motion of ruthenocene was calculated[8] to be $\sim$185 cm^{-1} by using the ω_4/ω_{22} ratio of ferrocene. This ratio is 1.78 for ferrocene and is 338/190 = 1.78 for compound II, confirming the assignment. The higher energy bands (> 400 cm^{-1}), representing various ring motions in the mercury compounds, appear at almost the same positions as they do in the ruthenocene spectrum. However, it may be noted that the IR bands observed at at 407 and 1001 cm^{-1} for compound I (410 and 1002 cm^{-1} for compound II) correspond to two Raman-active vibrations in ruthenocene (402 and 996 cm^{-1}, respectively) that have become IR-active, presumably due to the lower molecular symmetry.

The room-temperature ultraviolet-visible absorption spectrum of compound I was measured in 0.01 M $HClO_4$ solution (see Figure 3 and Table II). A strong band at 31,200 cm^{-1} appears which was missing in the ruthenocene spectrum.[1] The 77°K spectrum of $[(cp)_2Ru-Hg-Ru(cp)_2](PF_6)_2$ shows that this band is blue shifted ($\sim$300 cm^{-1}) and dramatically sharpened (the half-width changes from 4300 cm^{-1} at room temperature to 2500 cm^{-1} at 77°K). It is

Fig. 3. Electronic absorption spectra of compound I: (——), 0.01 M $HClO_4$ aqueous solution at 300°K; (----), dissolved in solvent mixture of ethanol, ether and propionitrate (1:1:3) at 77°K (the intensity is not to scale in this case).

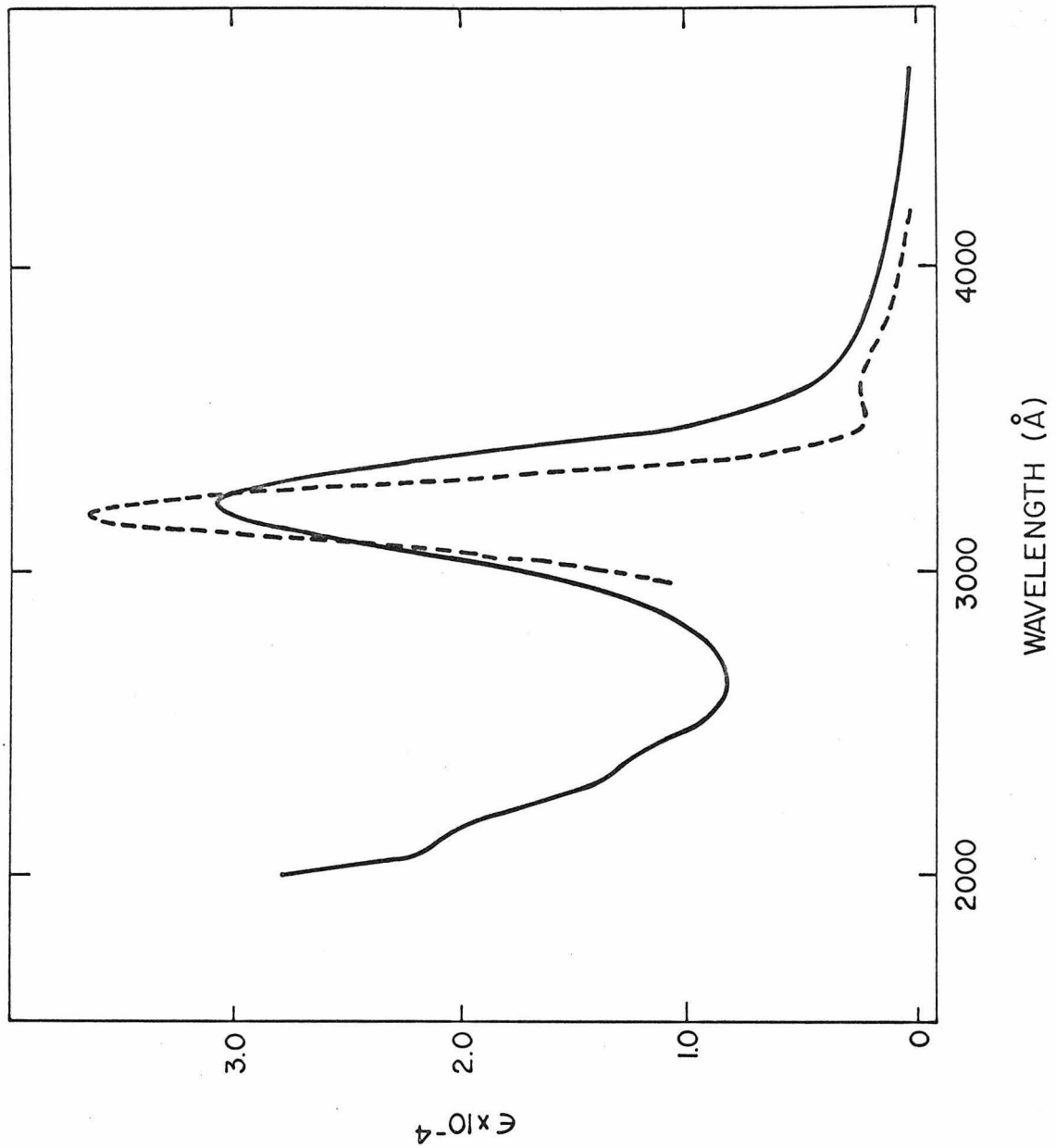
3.0
2.0
1.0
0
ε x10⁻⁴
2000
3000
4000
WAVELENGTH (Å)

Table II. Electronic Absorption Bands of Ruthenocene and $[(cp)_2Ru - Hg - Ru(cp)_2]^{++}$ Ion

	$Ru(cp)_2$			$[(cp)_2Ru - Hg - Ru(cp)_2]^{++}$		
System	Assignment	$\bar{\nu}(cm^{-1})$	ϵ	$\bar{\nu}(cm^{-1})$	ϵ	$\nu_{\frac{1}{2}}(cm^{-1})$
I	$^1A_{1g} \rightarrow a^3E_{1g}$	26,000	~ 5	26,700[a]	3,800	
II	$\rightarrow \{ a^1E_{1g}$ $^1E_{2g}$	31,000	200			
				31,200	30,000	4,300
				(31,500)[b]		(2,500)[b]
III	$\rightarrow b^1E_{1g}$	36,000	150			
IV		42,000	2,000	42,600[a]	13,000	
V		46,100	4,200	46,500[a]	21,000	
VI	$\rightarrow {}^1A_{2u}$	>51,300	>50,000	>50,000	>30,000	

[a]Shoulder whose intensity (ϵ) is not corrected for tailing by its neighboring band. The position of the 26,700 cm^{-1} band was taken from the resolved spectrum at 77 °K (see Figure 3). The others were

Table II. (Continued)

estimated from the inflection points.

[b]The values in parentheses refer to low temperature (77 °K) data for the 31, 200 cm^{-1} band.

reasonable to assign this band to a transition associated with the metal-metal bond. Similar blue shifts and dramatic sharpening have been observed on lowering the temperature for the bands due to metal-metal transitions in $Mn_2(CO)_{10}$ and $Re_2(CO)_{10}$.[9] Finally, band systems IV, V, and VI of $[(cp)_2Ru—Hg—Ru(cp)_2](PF_6)_2$ appear at almost the same energies as the ruthenocene bands IV, V and VI. This provides further support for considering these mercury-bridged complexes as formally containing Ru(II).

Halides. Oxidation of ruthenocene by iodine and bromine resulted in compounds III and IV, respectively. Analytical data for these halides (see Experimental section) are in excellent agreement with the empirical formulation $Ru(cp)_2X_4$ (X = I and Br). An X-ray structural determination[7] has been completed for the iodide salt. The molecular structure was found to be $[Ru(cp)_2I]I_3$. Since the infrared spectra of the two halides (compounds III and IV) are essentially the same, both in band positions and intensities (see Figure 2 and Table I), it can be concluded that both salts have the same structure, that is, $[Ru(cp)_2X]X_3$. These compounds, therefore, may be viewed as low-spin, seven-coordinate Ru(IV) complexes. This result is not particularly surprising in the light of the observation[10] that oxidation of osmocene by either ferric ammonium sulfate or iodine in aqueous sulfuric acid results in the species $[Os(cp)_2OH]^+$ and $[Os(cp)_2I]^+$, respectively. Furthermore, a recent chronopotentiometric study[11] of various metallocenes has shown that

the oxidation of ruthenocene is a one-step, two-electron process.

The infrared spectra of these halides are interpretable on the basis of the $Ru(cp)_2X^+$ molecular structure. It can be seen in Table I that in the $Ru(cp)_2X^+$ complexes the fundamental modes of the ring-localized motions are in essentially the same positions as in ruthenocene. However, there are additional bands in the oxidized halides. The low energy band (211 cm^{-1}) of $[Ru(cp)_2I]I_3$ represents a skeletal motion not observed for ruthenocene; it is assignable to either Ru-X stretching or ring-metal-ring bending. As mentioned previously, the ring-metal-ring bending energy in ruthenocene was calculated[8] to be ~ 185 cm^{-1}. The low energy band appears at 225 cm^{-1} in $[Ru(cp)_2Br]Br_3$. If this band is the ring-metal-ring bending vibration in ruthenocene shifted to higher energy by ring crowding caused by the halogen substitution, it would be reasonable to expect the iodine-substituted molecule to exhibit the higher energy vibration. Thus the observed shift in this low energy band in going from the iodide to the bromide is in better agreement with the Ru-X stretching mode assignment. It may be pointed out that the anti-symmetrical ring-metal-ring stretching frequency at 446 cm^{-1} in ruthenocene is lowered to 419 cm^{-1} in $[Ru(cp)_2I]I_3$, which indicates that the bonding between the metal and the rings is weakened. This is further support for assigning the 211 cm^{-1} band of $[Ru(cp)_2I]I_3$ as the Ru-I stretch instead of the ring-metal-ring bending vibration. The higher energy bands at 578, 920, 976, and 1436 cm^{-1} observed for

the iodide (579, 920, 975 and 1440 cm^{-1} for the bromide) are all assignable to ring vibrations which do not appear in the more symmetrical ruthenocene molecule.

Acknowledgments: This research was supported by the National Science Foundation. We thank Dr. A. W. Schlueter for communicating the results of the X-ray structural work before publication. We also gratefully acknowledge the assistance of Professor F. C. Anson and Mr. Hong-Sup Lim in carrying out the electrochemical experiments.

References

1. Y.S. Sohn, D.N. Hendrickson and H.B. Gray, submitted to J. Am. Chem. Soc.
2. R. Prins and F.J. Reinders, J. Am. Chem. Soc., 91, 4929 (1969).
3. A.H. Maki and T.E. Berry, J. Am. Chem. Soc., 87, 4437 (1965).
4. D.N. Hendrickson, Y.S. Sohn and H.B. Gray, submitted to Inorg. Chem.
5. G. Wilkinson, J. Am. Chem. Soc., 74, 6146 (1952).
6. G. Wilkinson, J. Am. Chem. Soc., 74, 6149 (1952).
7. A.W. Schlueter and H.B. Gray, unpublished work.
8. E.R. Lippincott and R.D. Nelson, Spectrochim. Acta, 10, 307 (1958).
9. R. Levenson and H.B. Gray, unpublished work.
10. E.O. Fischer and H. Grubert, Ber., 92, 2302 (1952).
11. T. Kuwana, D.E. Bublitz and G. Hoh, J. Am. Chem. Soc., 82, 5811 (1960).

PART IV. PROPOSITIONS I, II, III, IV and V

Proposition I

It is proposed to look for electronic transitions in the infrared region and to measure the anisotropy of the magnetic susceptibility of the ferricencium ion using a single crystal of $[Fe(cp)_2]^+(CCl_3CO_2H)_3^-$. Such an approach would result in a thorough characterization of the ground state of ferricenium ion.

The ground electronic state of the ferricenium ion has been established to be $^2E_{2g}$ by electron spin resonance[1, 2] and magnetic susceptibility[3] studies. There is some evidence that the lowest excited $^2A_{1g}$ state is located very closely (< 500 cm^{-1}) above the ground state ($^2E_{2g}$) of the ferricenium ion. Ligand field calculations for the ferricenium ion[4] indicate that the $^2A_{1g}$ state could lie only 700 cm^{-1} above the ground state, if it is assumed that there are no diastic changes of the ligand field parameters going from ferrocene to ferricenium ion. Further, a magnetic susceptibility study of the ferricenium ion[3] indicates that the separation between these two states ($\Delta E = {}^2A_{1g} - {}^2E_{2g}$) could be only $200 \sim 300$ cm^{-1}. However, the low-lying $^2A_{1g}$ state of the ferricenium ion has only been implicated by these studies; a more direct characterization is desirable.

Locating this low-lying $^2A_{1g}$ ferricenium state is important for the two following reasons. A knowledge of the energy separation $\Delta E(^2A_{1g} - {}^2E_{2g})$ is mandatory for a detailed analysis of the reported magnetic susceptibility data.[3] Thus, the anomalously-high (2.3-2.7 B.M. at 298°K) and temperature-independent effective magnetic

moments of various ferricenium compounds have been accounted for by two possibilities:[3,5] a) thermal population of the low-lying $^2A_{1g}$ state, or b) temperature dependence of a low-symmetry crystal field. A selection between these two models would be possible if the $^2A_{1g}$ state could be directly located. Perhaps the greater significance of locating the $^2A_{1g}$ state in the ferricenium ion is to determine the change in the ligand field parameters (B and Δ_1, see Section I) in going from ferrocene to ferricenium ion. An assessment of the changes in bonding and an assignment of the d-d transitions in the ferricenium ion would ensue.

The best approach to measure ΔE is a direct measurement of the electronic absorption energy of the $^2E_{2g} \rightarrow {}^2A_{1g}$ transition which should appear in the infrared region. The $^2E_{2g}$ state of the ferricenium ion is split into two Kramer's doublets (E″) and (A′, A″), E″ being the lower energy state.[2,4] The $^2A_{1g}$ state corresponds to a E′ state in the double group D_5'. Since the E″ → E′ transition is allowed, the band intensity associated with this transition could be larger or perhaps comparable to that for normal infrared bands. Furthermore, a different band shape might be expected for this electronic transition because it is different in origin than the vibrational transitions. Nevertheless, it still seems a formidable task to identify the E″ → E′ electronic transition if it accidentally appears near some infrared bands with strong intensity. For a better identification of the E″ → E′ transition, it will probably be necessary to cool the system to a lower temperature and to carry out polarization measurements for the observed infrared bands in the region of

interest. The $E'' \rightarrow E'$ transition energy is expected to be less than 1000 cm^{-1}, as pointed out earlier. Five infrared bands of the ferricenium ion were reported[6] in the 400-1000 cm^{-1} region. The polarizations of these infrared bands are known

Mode	Frequency (cm^{-1})	Polarization
ω_{11}	405-423	z
ω_{21}	490-501	z
ω_{9}	779-786	z
ω_{19}	841-860	z
$\omega_{27,33}$	874-886	x, y

The electronic $E'' \rightarrow E'$ transition is x, y polarized. The x, y polarized infrared band ($\omega_{27,33}$) has been observed to be very low in intensity. Therefore, the polarization study will give convincing evidence for identification of the $E'' \rightarrow E'$ transition. To accomplish this goal a single crystal of some ferricenium salt should be available. It is generally difficult to grow single crystals of ferricenium salts because of the instability of the ferricenium ion in solution. Fortunately, recent attempts[4] for preparation of ferricenium salts[7] accidentally resulted in large single crystals of ferricenium trichloroacetic acid, $[Fe(cp)_2]^+(CCl_3CO_2H)_3^-$. Furthermore, the crystal structure of this ferricenium salt has been determined recently by X-ray crystallographic method.[8] The low-temperature infrared spectrum of such crystals would prove fruitful.

These single crystals of $[Fe(cp)_2]^+(CCl_3CO_2H)_3^-$ may also be used in measurements of the anisotropy of the magnetic susceptibility of the ferricenium ion. The temperature dependence of the parallel and perpendicular components of the effective magnetic moments, $\mu_{||}$ and $\mu_{\perp}$, will be useful to distinguish between the two models a) and b) which were mentioned above, since the two models predict different temperature behavior for each anisotropic component. For instance, the thermal population model a) results in the theoretical curves of $\mu_{||}$ and $\mu_{\perp}$ vs. T as are shown in the figure (see next page). The curves in the figure were drawn for a particular set of parameters, $k' = 0.80$, the distortion $\delta = 200\ cm^{-1}$ and $\Delta E = 300\ cm^{-1}$. Similarly, theoretical curves of $\mu_{||}$ and $\mu_{\perp}$ vs. T for model b) can be calculated, in this case thermal population of the $^2A_{1g}$ state is not included. Unfortunately, models a) and b) are not readily distinguished by their temperature behavior. For model a) $\mu_{||}$ changes from 4.12 B.M. at 100 °K to 3.88 B.M. at 300 °K and $\mu_{\perp}$ from 1.27 B.M. at 100 °K to 1.78 B.M. at 300 °K, whereas for model b) $\mu_{||}$ changes from 4.00 B.M. at 100 °K to 3.86 B.M. at 300 °K and $\mu_{\perp}$ from 1.32 B.M. at 100 °K to 1.68 B.M. at 300 °K. Therefore, careful experimentation would be necessary to distinguish between these two models. The single crystal magnetic susceptibility study will at least result in convincing evidence whether either model a or b is applicable.

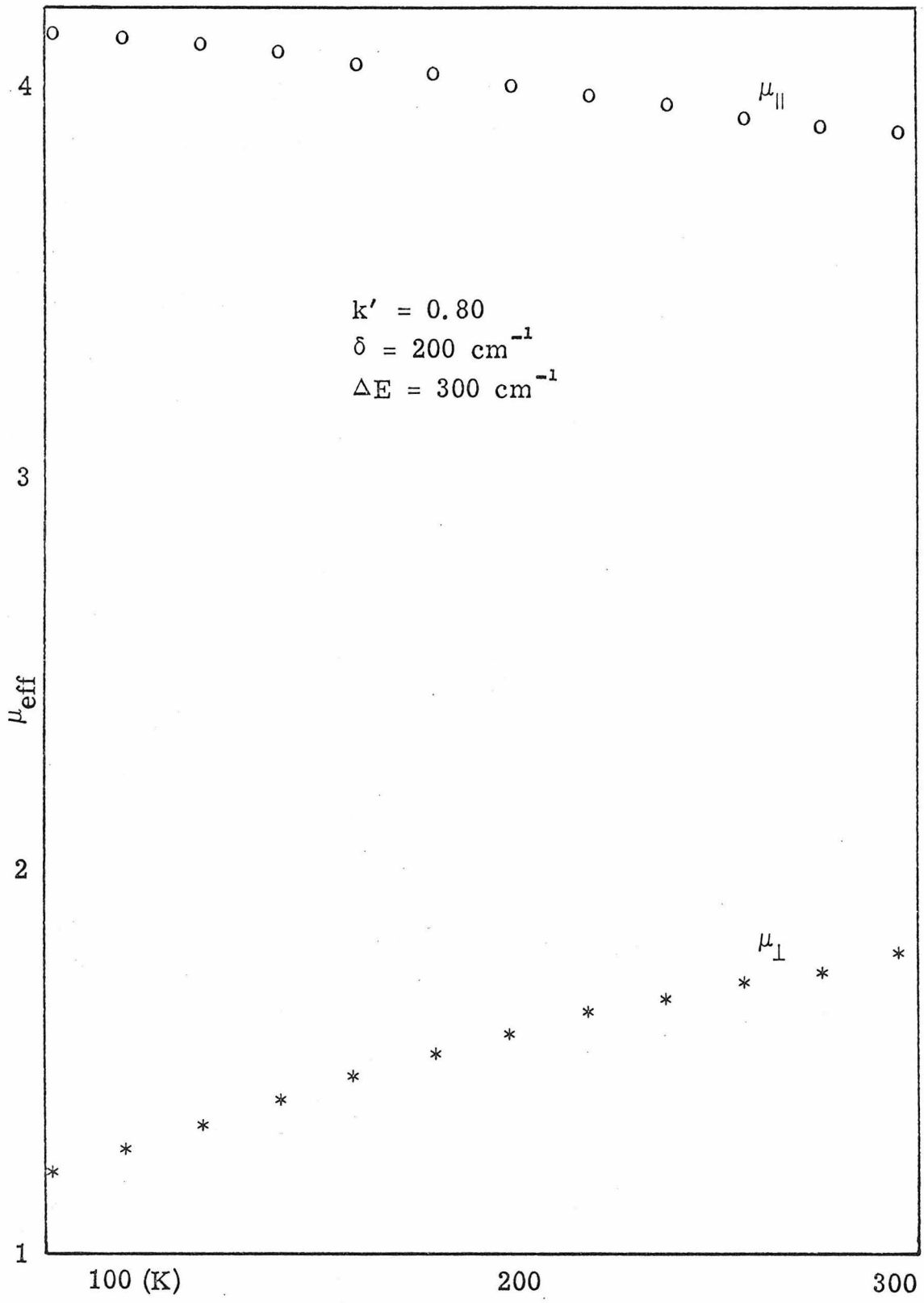
4
3
2
1
μ_{eff}
$\mu_{\parallel}$
$\mu_{\perp}$
k′ = 0.80
δ = 200 cm^{-1}
ΔE = 300 cm^{-1}
100 (K)
200
300

References

1. R. Prins and F. J. Reinders, J. Am. Chem. Soc., 91, 4929 (1969).
2. A. H. Maki and T. E. Berry, J. Am. Chem. Soc., 87, 4437 (1965).
3. Y. S. Sohn, D. N. Hendrickson and H. B. Gray, J. Am. Chem. Soc., 92, 3233 (1970) (see also Part II of this thesis).
4. Y. S. Sohn, D. N. Hendrickson and H. B. Gray, submitted for publication in J. Am. Chem. Soc. (see also Part I of this thesis).
5. D. N. Hendrickson, Y. S. Sohn and H. B. Gray, submitted for publication in Inorg. Chem.
6. I. Pavlik and J. Klikorka, Collection Czechoslov. Chem. Commun., 30, 664 (1965).
7. M. Aly, R. Bramley, J. Upadhyay, A. Wassermann and P. Woolliams, Chem. Comm. 404 (1965).
8. A. W. Schlueter and H. B. Gray, unpublished work.

Proposition II

Syntheses and measurements of physical properties of new monocarbon carborane analogs of ferrocene and ferricenium ion are proposed.

(1) Syntheses. Recently a synthesis of a monocarbon carborane ion $B_{10}CH_{13}^-$ [1], isoelectronic with $B_{11}H_{13}^{2-}$, was reported. The molecular structure of $B_{10}CH_{13}^-$ seems to be an icosahedral fragment with one open face, as proposed by the authors[1] from an analogy with $B_{11}H_{13}^{2-}$, the crystal structure of which has been determined by X-ray crystallography[2] and is shown below.

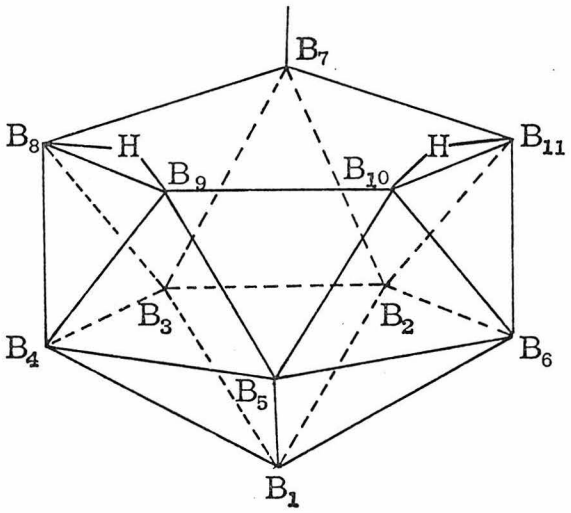

In this figure the external B—H bonds were omitted. There are two bridging hydrogens expected to be chemically active. In fact, these two hydrogens are easily removed by active alkali metals and

$B_{11}H_{11}^{2-}$ [1,3] is obtained. However, the structure of this ion is not icosahedral but octadecahedral[4] formed by a topological rearrangement of the boron framework. Nevertheless, a stable carborane $B_9C_2H_{11}^{2-}$ with icosahedral geometry and isoelectronic with $B_{11}H_{11}^{-4}$ was recently made by reaction of $B_9C_2H_{12}N(CH_3)_3$ with sodium metal in tetrahydrofuran solvent.[3] Using this two-carbon carborane, Hawthorne[3,5,6] has succeeded in the syntheses of carborane analogs of ferrocene and demonstrated their aromatic stability. The crystal structure of one of these analogs, that is, $(C_5H_5)Fe(B_9C_2H_{11})$ has been determined.[7]

From the population analysis of the icosahedral $B_{10}C_2H_{11}$ by Lipscomb and Hoffmann,[8] who predicted aromaticity of this compound, it is indicated that there is greater electron density on the carbon atoms, which means that the participation of the two hetero carbon atoms stabilizes the six electrons delocalized on the open face in the case of the icosahedral fragment. Similarly this analysis explicitly indicates that it is feasible to make an open icosahedral fragment of the monocarbon carborane $B_{10}CH_{11}^{3-}$, but perhaps not as stable as $B_9C_2H_{11}^{2-}$. Evidence of the existence of this anion is presented in the paper.[1] A solvated salt, $Na_3B_{10}CH_{11}\cdot(C_4H_8O)_{1.85}$ was isolated as an intermediate product, although its structure has not been determined yet. This anion is isoelectronic with $B_9C_2H_{11}^{2-}$ and its structure may probably be the same

Hopefully the following reaction for the syntheses of ferrocene-like compounds will be feasible.

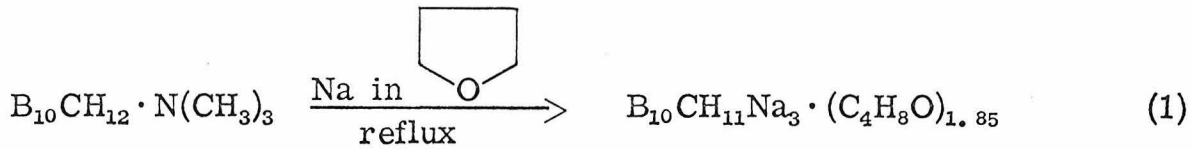

$$B_{10}CH_{12}\cdot N(CH_3)_3 \xrightarrow[\text{reflux}]{\text{Na in THF}} B_{10}CH_{11}Na_3\cdot(C_4H_8O)_{1.85} \qquad (1)$$

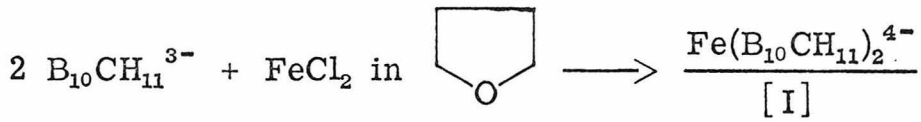

$$2\ B_{10}CH_{11}^{3-} + FeCl_2 \text{ in THF} \longrightarrow \underset{[I]}{Fe(B_{10}CH_{11})_2^{4-}} \qquad (2)$$

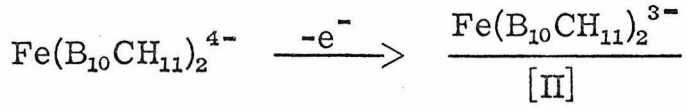

$$Fe(B_{10}CH_{11})_2^{4-} \xrightarrow{-e^-} \underset{[II]}{Fe(B_{10}CH_{11})_2^{3-}} \qquad (3)$$

In the same way

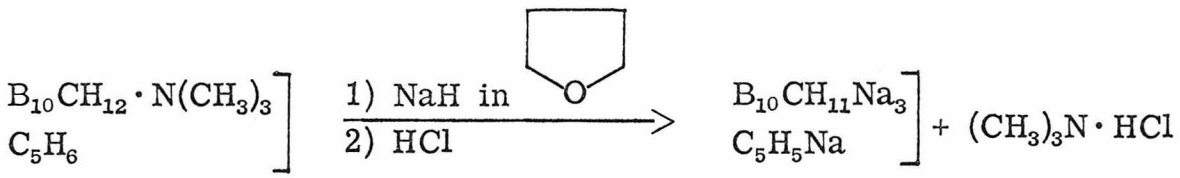

$$\left.\begin{matrix} B_{10}CH_{12}\cdot N(CH_3)_3 \\ C_5H_6 \end{matrix}\right] \xrightarrow[\text{2) HCl}]{\text{1) NaH in THF}} \left.\begin{matrix} B_{10}CH_{11}Na_3 \\ C_5H_5Na \end{matrix}\right] + (CH_3)_3N\cdot HCl$$

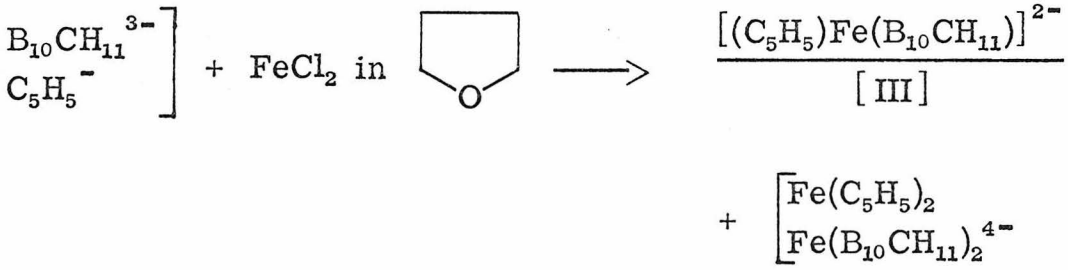

$$\left.\begin{matrix} B_{10}CH_{11}^{3-} \\ C_5H_5^- \end{matrix}\right] + FeCl_2 \text{ in THF} \longrightarrow \underset{[III]}{[(C_5H_5)Fe(B_{10}CH_{11})]^{2-}} + \left[\begin{matrix} Fe(C_5H_5)_2 \\ Fe(B_{10}CH_{11})_2^{4-} \end{matrix}\right]$$

Similarly, the carbonyl compounds of the type, $(B_{10}CH_{11})Fe(CO)_3$ are expected to be easily formed. Nearly all of these compounds are expected to be synthesized in the near future. Now it is interesting

to consider the molecular symmetry of these hypothetical compounds. As far as the interaction of the ligand and the central metal is concerned, we may neglect all the bulk volume except the open face toward the metal, and then this compound may be regarded as a pentagonal antiprism. From consideration of the electron density on the ligand face, it is most probably that the carbons are in such positions that the molecule has an inversion center as is shown overleaf.

(2) Physical properties. It is very interesting to compare various physical and chemical properties of these analogs with those of ferrocene and ferricenium ion, since we can treat these molecules as perturbed by the hetero four boron atoms on each open face. We will first consider the spectral properties.

All the studies concerning electronic absorption measurements of ferrocene[9,10,11] cover the effects of solvent, temperature, and group substitution of the ligand. However, the effect of substitution of hetero atoms for the ligand members has never been considered. It may be expected that the perturbation by the hetero atoms will affect the charge transfer bands of the ferrocene spectrum. As discussed in this research report the charge transfer in the sandwich complex is mainly ligand-to-metal as in the hexahalo complexes of the heavy transition metals.[12] Therefore, higher energy charge transfer bands are expected in the carborane analogs as compared to those of ferrocene. It is also noteworthy to consider the ligand field bands. To see the qualitative features we can simply use the crystal field model. Thus, as suggested by Fischer[13] and also

pointed out by Orgel,[14] the metallocenes may be regarded as an octahedral complex. This concept arises from the fact that in the ligand field picture, the π-bonds on the ring are regarded as polarizable ligands such as CN^-. Consequently, we may approximate the ligand as follows:

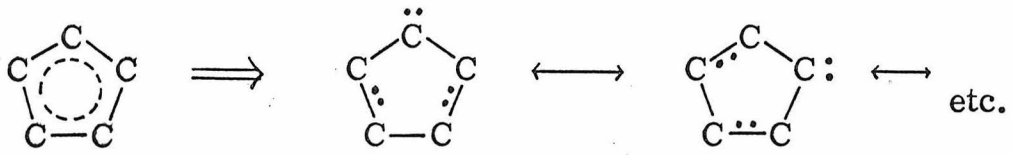

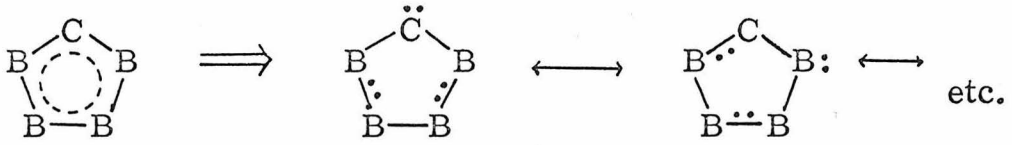

The ferrocene may therefore be approximated as a trigonally-distorted octahedral complex. We take the three-fold axis as the axis of quantization and then the d-orbitals are represented as follows.[15]

$$|e^+> = \sqrt{\tfrac{2}{3}}\,|1> - \sqrt{\tfrac{1}{3}}\,|-2>, \quad |e^-> = \sqrt{\tfrac{2}{3}}\,|-1> + \sqrt{\tfrac{1}{3}}\,|2>$$

$$|t^+> = \sqrt{\tfrac{1}{3}}\,|1> = \sqrt{\tfrac{2}{3}}\,|-2>, \quad |t^-> = \sqrt{\tfrac{1}{3}}\,|-1> - \sqrt{\tfrac{2}{3}}\,|2>$$

$$|t^\circ> = |0>$$

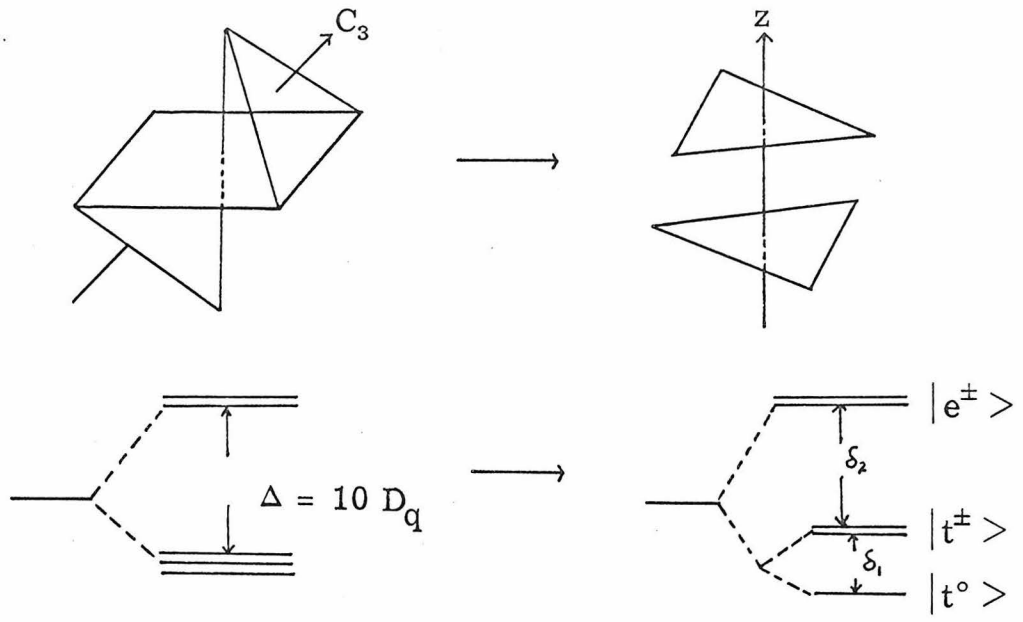

It is seen from the diagram that the lowest level $|t^\circ>$ corresponds to a'_{1g} of the MO's and $|e^\pm>$, $|t^\pm>$ to e^*_{1g}, e_{2g}, respectively. The ground configuration of ferrocene, for instance, is $(12)(a'_{1g})^2(e_{2g})^4$ and the main transitions are

$$a'_{1g} \rightarrow e^*_{1g}, \quad e_{2g} \rightarrow e^*_{1g}.$$

An analysis of the ligand field bands of ferrocene gives $\delta_1 = -7.1$ kK and $\delta_2 = 22.0$ kK (see Part I of this Thesis). It is possible to measure the absorption spectra of the proposed one-carbon carborane transition metal complexes and to extract analogous values for the splitting parameters δ_1 and δ_2. The sum of δ_1 and δ_2 will give a measure of the ligand field strength of the one-carbon carborane ligand and δ_1 will gauge the trigonal distortion in these complexes.

In the ferricenium ion electron repulsion and a negative δ_1 result in a $^2E_{2g}$ ground state (see Part II of this Thesis) and an

anomously high effective magnetic moment. Thus, it would be interesting to carry out a magnetic susceptibility study of these one-carbon carborane complexes to see whether the ground state of these complexes is either $^2E_{2g}$ or $^2A_{1g}$.

References

1. Hyatt, D. A., F. R. Scholer, L. J. Todd and J. L. Warner, Inorg. Chem., 6, 2229 (1967).
2. Fritchie, C. J., Inorg. Chem., 6, 1199 (1967).
3. Hawthorne, M. F., et al., J. Am. Chem. Soc., 87, 3987 (1965).
4. Berry, T. E. and M. F. Hawthorne, J. Am. Chem. Soc., 88, 4513 (1966).
5. Hawthorne, M. F., et al., J. Am. Chem. Soc., 87, 1818 (1965).
6. Hawthorne, M. F., et al., J. Am. Chem. Soc., 87, 2496 (1965).
7. Zalkin, A., D. H. Templeton, et al., J. Am. Chem. Soc., 87, 3989 (1965).
8. Hoffmann, R. and W. N. Lipscomb, J. Chem. Phys., 36, 3489 (1962).
9. Scott, D. R. and R. S. Becker, J. Chem. Phys., 35, 516 (1961).
10. Armstrong, A. T., F. Smith and S. P. McGlynn, J. Chem. Phys.
11. This research report.
12. C. K. Jorgensen, Mol. Phys., 2, 309 (1959).
13. Fischer, E. O. and H. P. Fritz, Adv. Inorg. Chem. and Rad., 1, 1959, p. 55.
14. Orgel, L. E., An Intro. to Trans. Metal Chem., 2nd edition, 1966, p. 157.
15. Carrington, A. and A. D. McLachlan, Intro. to Mag. Resonance, 1967, p. 155.

Proposition III

A polarization study of the visible and Soret bands of porphyrins and metalloporphyrins employing liquid crystal technique is proposed.

Porphyrins and metalloporphyrins constitute a very important class of molecules because of their role in photosynthesis, biological redox processes and oxygen transport. Porphyrins are derived from the parent porphin and form chelate complexes with various metals (see below).

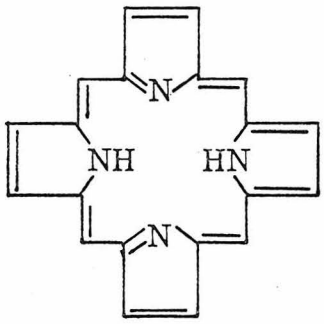

a, porphin free base

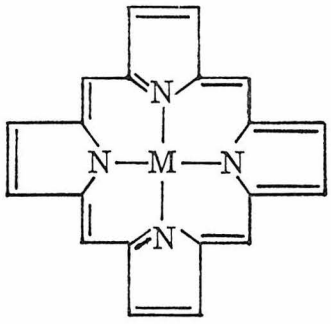

b, metalloporphyrin

Both of these systems have high molecular symmetry (D_{2h} for a, D_{4h} for b) and are amenable to theoretical treatment. Extensive theoretical work has been reported by Platt[1, 2] and more recently by Gouterman and his coworkers.[3-8] Gouterman and Platt both agree that the lowest empty orbital is e_g and two highest filled orbitals are a_{1u} and a_{2u}. There is strong configuration interaction between these

two filled orbitals. The electronic absorption spectra of porphyrins and metalloporphyrins are explicable in terms of this molecular orbital ordering. Typical electronic spectra of porphyrins (D_{2h} symmetry) show four visible bands (Q bands) and a stronger near-ultraviolet band (B band). The visible bands were assigned as $a_{2u} \rightarrow e_g$ transition and the near-ultraviolet Soret band is ascribed as a $a_{1u} \rightarrow e_g$ transition. The four visible bands were classified as Qx(0 ← 0), Qx(1 ← 0), Qy(0 ← 0), Qy(1 ← 0). In metalloporphyrins the x, y components become degenerate because of their higher symmetry (D_{4h}) and only two visible bands (α, β) are observed. According to the theories developed by Platt and Gouterman, the behavior of the visible bands should be nearly identical with that of the Soret band because both transitions (a_{2u}, $a_{1u} \rightarrow e_g$) are $\pi \rightarrow \pi^*$ transitions and should be polarized in the molecular plane. These workers also concluded from molecular orbital calculations and observed spectral patterns that the central metals interact only weakly with the porphyrin rings. However, recently the above band assignment was strongly questioned by Corwin and his coworkers.[9] These authors experimentally observed the fact that in metal mesoporphyrins with additional ligands the band shift of Q and B transitions is not identical and that fluorosulfonic acid destroys the usual four banded spectrum of porphyrin free bases without changing the Soret band. These authors proposed a new assignment of the visible bands as $n \rightarrow \pi^*$ or $\ell \rightarrow \pi^*$ transition.

To establish the band assignments of porphyrin and metalloporphyrin spectra, a band polarization study is

probably the most promising tool, since in these particular systems the polarizations of $n \rightarrow \pi^*$ and $\pi \rightarrow \pi^*$ transitions are theoretically perpendicular to each other and easily distinguishable. However, only a few papers[10-12] reported band polarization measurements of porphyrins and metalloporphyrins. In early reports[10,11] they could measure only relative polarizations of the visible bands using fluorescence polarization spectroscopy, and so no absolute assignment could be given. For single crystal polarization measurement of TPP Anex and Umans[12] employed reflection spectroscopy because of the high molar extinction coefficients ($> 10^4$) of the visible bands. No direct measurement of absorption polarization of porphyrin and metalloporphyrin bands has been yet reported. Furthermore, the polarization data obtained in single crystal environment are not always the same as those for an isolated single molecule. For instance, a considerable spectral difference has been noticed between the liquid crystal and single crystal spectra of anthracene and napthacene.[21] It is advantageous to deal with an isolated molecule.

Liquid crystals would probably be the ideal media to accomplish this goal. Liquid crystals were popularly used in magnetic resonance experiments,[13-15] but in recent years, it was proved that they could be used for both infrared and visible-ultraviolet spectroscopy.[16-18] A liquid crystal is an oriented liquid matrix in which their rodlike molecules are aligned in one direction. Liquid crystals frequently used as nematic medium are butyl p-(p-ethoxyphenoxycarbonyl)phenyl carbonate (BPC) and 2,4-nonadienoic acid (NDA) (see below).

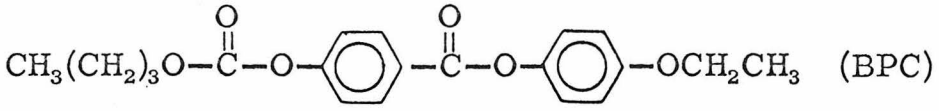

(BPC)

$CH_3(CH_2)_4 \cdot CH{=}CH{-}CH{=}CH{-}CO_2H$ (NDA)

It is generally known from liquid crystal nmr studies[19] that the solute molecules of interest are aligned with their long molecular axis parallel to the long axis of the liquid crystal molecules. Further confirmation on the molecular orientation can be made by measuring some known polarizations of some infrared bands in the same liquid crystal. From the above point of view, porphyrins and metalloporphyrins are recognized to be a very suitable system for liquid crystal spectroscopy.

It has been shown[17] that the measured polarization data ($\epsilon_{\parallel}$ and $\epsilon_{\perp}$) are related to the extinction coefficient components, ϵ_x, ϵ_y, ϵ_z, in the following way

$$\epsilon_{\parallel} - \epsilon_{\perp} = S_{xx}\epsilon_x + S_{yy}\epsilon_y + S_{zz}\epsilon_z$$

where $\epsilon_{\parallel}$ and $\epsilon_{\perp}$ are extinction coefficients measured with the electric vector of light parallel and perpendicular, respectively, to the direction of alignment of the long axis of the liquid crystals, and S_{ii} are parameters describing the orientation of the solute in the liquid crystal and are given as

$$S_{ii} = \left\langle \frac{3\cos\theta_i - 1}{2} \right\rangle_{\text{average}}$$

where θ_i is the angle of the ith molecular axis with respect to the long axis of the liquid crystal.

Now let us consider a limiting case of simple metalloporphyrin system according to the above formula. It has been concluded from nmr studies, as previously pointed out, that the planar molecules orient their long axis parallel to the long axis of the liquid crystal. The metalloporphyrin molecules (D_{4h}) will align their molecular plane parallel to the alignment of the liquid crystal, but x, y molecular axes of the metalloporphyrins are not distinguishable. Therefore, the following values are obtained for the orientation parameters; $S_{xx} = S_{yy} = \frac{1}{4}$, $S_{zz} = -\frac{1}{2}$. Hence,

$$\epsilon_{\parallel} - \epsilon_{\perp} = \tfrac{1}{2}\epsilon_x - \tfrac{1}{2}\epsilon_z.$$

Therefore, for any particular band of the metalloporphyrins the difference of the measured extinction coefficients, $\epsilon_{\parallel}$ and $\epsilon_{\perp}$ will yield very valuable information on whether the transition is polarized in the plane or perpendicular to it. For instance, if the band of interest is a $\pi \rightarrow \pi^*$ transition which is plane-polarized, then the following will be the result.

$$\epsilon_{\parallel} - \epsilon_{\perp} = \tfrac{1}{2}\epsilon_x \text{ (positive).}$$

On the other hand, if the transition is $n \rightarrow \pi^*$, then

$$\epsilon_{\parallel} - \epsilon_{\perp} = -\tfrac{1}{2}\epsilon_z \text{ (negative).}$$

In case of porphyrins whose symmetry is D_{2h} the orientation of x, y molecular axes with respect to the liquid crystal molecular axis seems not clear. However, diprotonation (by adding a proper acid) leads to the same symmetry as the metalloporphyrins.

The application of liquid crystal spectroscopy may be extended to a more complicated metalloporphyrins with additional ligands. Particularly, the interesting system may be six coordinate manganese porphyrins which have been recently reported by Boucher.[20] The molecular structure of manganese protoporphyrin IX dimethyl ester complexes of the halide ions was found to have a distorted octahedral environment around the manganese ion. These manganese porphyrins show a considerably different spectrum from the usual metalloporphyrin spectra. Some additional bands at low energy ($\sim$12.5 and $\sim$14.5 kk) with $\epsilon \sim 10^3$ and at high energy ($\sim$27.0 kk) with $\epsilon \sim 10^5$ were observed besides the characteristic B and Q (α, β) bands of the usual metalloporphyrins. A strong metal-porphyrin interaction seems involved. Polarization study using liquid crystals will also aid assignment for the additional bands.

References

1. J. R. Platt, Radiation Biology, Vol. III, A. Hollaender Ed., McGraw-Hill Book Co., Inc., New York, N. Y., 1956.
2. H. C. Longuet-Higgins, C. W. Rector and J. R. Platt, J. Chem. Phys., 18, 1174 (1950).
3. M. Gouterman, J. Chem. Phys., 30, 1139 (1959).
4. M. Gouterman, J. Mol. Spectry., 6, 138 (1961).
5. M. Gouterman, G. H. Wagniere and L. C. Snyder, ibid., 11, 108 (1963).
6. M. Zerner and M. Gouterman, ibid., 16, 415 (1965).
7. M. Gouterman, Theoret. Chim. Acta, 4, 44 (1966).
8. M. Zerner, M. Gouterman and H. Kobayashi, ibid., 6, 363 (1966).
9. A. H. Corwin, A. B. Ehivvis, R. W. Poor, D. G. Whitten and E. W. Baker, J. Am. Chem. Soc., 90, 6577 (1968).
10. M. Gouterman and L. Stryer, J. Chem. Phys., 37, 2260 (1962).
11. G. P. Gurinovich, A. N. Sevchenko and K. N. Solov'ev, Cryst. Spectry. (USSR), 10, 396 (1961).
12. B. G. Anex and R. S. Ulmans, J. Am. Chem. Soc., 86, 5026 (1964).
13. A. Sanpe, Angew. Chem. Intern. Ed., 7, 97 (1968).
14. G. P. Ceaser, C. S. Yannoni and B. Dailey, J. Chem. Phys., 50, 373 (1969).
15. S. Meiboom and L. C. Snyder, J. Am. Chem. Soc., 90, 2183 (1968) and references therein.
16. G. P. Ceasar and H. B. Gray, J. Am. Chem. Soc., 91, 191 (1969).

17. G. P. Ceasar and H. B. Gray, ibid., 91, 191 (1969).

18. E. Sackmann, J. Am. Chem. Soc., 90, 3569 (1968).

19. For a review see A. D. Buckingham and K. A. McLauchlan, "Progress in Nuclear Magnetic Resonance Spectroscopy," Vol. 2, Pergamon Press, Oxford, 1967.

20. L. J. Boucher, J. Am. Chem. Soc., 90, 6640 (1968).

21. R. A. Levenson, Thesis, Columbia University, 1970.

Proposition IV

Low temperature electronic absorption spectral measurements of hexafluoroiridate (III) and (IV) are proposed.

Crystal field theory[1-8] has been applied successfully to the interpretation of the observed absorption spectra of hexahalometalate complexes with partly filled 3d-shells. Jørgensen[9-11] demonstrated that in the low-spin d^6 systems of heavier transition metal complexes (4d and 5d) with octahedral symmetry, crystal field theory also predicted the observed bands with reasonable accuracy. However, complications arise in band assignments for the d^5 hexahalometalate complexes of the heavier transition metals and a further study is necessary. In this proposition hexafluoroiridate (III) and (IV) complexes were selected as a model system for a low temperature experiment.

This very interesting experiment has not been reported yet. A comprehensive series of the hexachloro, bromo, and iodo complexes of VIII group transition metals covering Ru, Rh, Pd, Os, Ir, and Pt has been studied collectively by Jørgensen,[11] but the series does not include the hexafluoro complexes which are very important. The reason for this omission is supposed to be that the fluoro compounds are generally difficult to handle and not easily obtainable. Most of the known hexafluoro complexes[12,13] of the high oxidation states of metals are unstable, sensitive to moisture, and hydrolyzed to oxides in water. Nevertheless, potassium hexafluoro iridate (IV)

has been prepared by Schlesinger and Tarpley.[14] Iridium was reacted with a double salt, $3KF \cdot HF \cdot PbF_4$ by fusion in a nickel crucible at high temperature. The K_2IrF_6 formed is moderately stable in water, giving a red-color and not much difficulty is expected in carrying out measurements. It should not be too difficult to make IrF_6^{---} from IrF_6^{--}.

It is expected that the Laporte forbidden weak bands appearing in the low frequency range ($< 20,000$ cm^{-1}) may have vibrational structure at low temperature and the vibrational analysis may add confirmative evidence for the assignment of the ligand field bands. It may be instructive to briefly look over the experimental results studied by Jørgensen.[10,11] In the low spin d^6 complexes, there appear four distinct weak bands, Laporte forbidden, in the range between 15000 cm^{-1} and 30000 cm^{-1}. For example, the spectral results for $IrCl_6^{---}$ spectrum are given in the following table.

Bands	ν (cm^{-1})	ϵ max	f	δ (half width) (cm^{-1})
(a)	16300	7.5	0.00007	1200
(b)	17900	10	0.00011	900
(c)	24100	76	0.00125	1800
(d)	28100	64	0.00120	-

Now applying crystal field theory to this regular octahedral symmetry, the following four transitions are predicted:

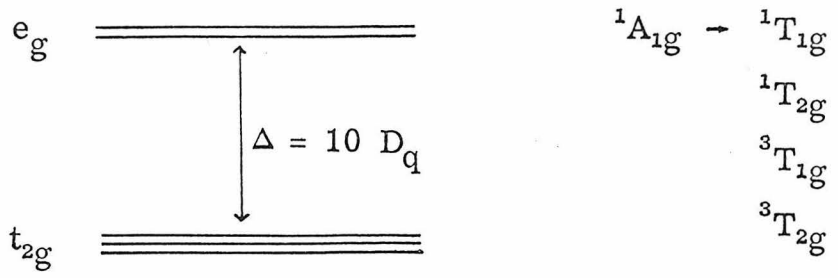

Of the four transitions, the two spin-forbidden ones clearly belong to bands (a) and (b), and the two spin-allowed transitions to (c) and (d). However, it is not yet certain which is $^1A_{1g} \rightarrow {}^1T_{1g}$ or $^1A_{1g} \rightarrow {}^1T_{2g}$. Now, as proposed here, analysis of the vibrational structure which is expected to be visible at low temperature and comparison of the low temperature spectra of the two model complexes, IrF_6^{--} and IrF_6^{---}, might result in a definitive assignment of these transitions. There is some evidence supporting this possibility. The vibrational structure of the ligand field bands of the hexafluorides of the heavy transition metals, including iridium hexafluoride, was observed in the vapor state by Moffitt, et al.[15] It was also shown by Goodman, et al.[16] that the spectra of hexafluorides at low temperature give vibrational fine structure. Thus, the hexafluoro iridium (IV) and (III) ions are probably the most suitable case for this study, because many studies have been made on the molecular vibrations of this compound.[17,18] It should be easy to identify the vibrational structure in this case, since the difference between the stretching and bending vibrational frequencies is considerably large (0.3 ~ 0.4 kK), as compared with the other halides such as $ReCl_6^{3-}$, and $OsCl_6^{2-}$ (~ 0.15 kK).

The term "charge transfer" is not consistent with the crystal field description. The words "electron transfer" are probably better, but the former will be used here. It is certain, as pointed out by Jørgensen,[19] that in all of these hexafluoro complexes the charge transfer is the type L → M. In the low spin d^6 complexes, except for the weak bands discussed above, there are one or two very strong bands ($\epsilon \gtrsim 20000$) in the high frequency range (3-50000 cm^{-1}) which can be assigned with certainty as $\pi \rightarrow e_g$ or $\sigma \rightarrow e_g$ according to the crystal field model, since the lower t_{2g} level is filled completely with six electrons. However, a complicated situation arises in the d^5 cases. The absorption spectra of hexachloro complexes of d^5 do not have the weak bands as is seen in d^6 complexes, and instead there appear four bands, the number, shape and band width of which are similar to those of the ligand field bands, but the absorption of which are larger (ϵ = 5000-8000). All these bands were considered to be other charge transfer bands. Thus, ligand field bands were not considered in the d^5 system. This looks improper. As was shown in the spectra,[11] the first band appearing in the lowest frequency range is very weak and is comparable to the strength of an intense ligand field band. The band width of this band (δ = 1-1.5 kK) is also comparable to that of ligand field bands. Therefore, it seems very hard to explain the nature of these bands. In addition to these, one or two very strong bands similar to the ones in the d^6 case followed immediately, which certainly have the same origin. Possible explanations are the following: We have four possible types of charge transfers within the crystal field formalism:

(i) $\pi \rightarrow e_g$, (ii) $\pi \rightarrow t_{2g}$, (iii) $\sigma \rightarrow e_g$, (iv) $\sigma \rightarrow t_{2g}$.

Since the ligand σ-orbital energy is nearly the same as or lower than the π-orbital, it is seen that (i) and (iii) are the highest energy transitions which were assigned as the highest frequency bands, as above. It was pointed out[19] that from symmetry considerations of the σ-ligand orbitals, the transition (iv) is not probable. As a result, all four narrow bands with intermediate intensities were assigned to transition (ii).

It may be regarded that the ligand field bands are hidden by these strong bands. It is generally known that fluoride complexes rarely exhibit L → M charge transfer bands because of the high electronegativity of fluorine. Therefore, the low temperature spectral measurements of IrF_6^{--} and IrF_6^{---} will clarify the problem involved in the assignment of d-d transitions of the general hexahalometalate complexes.

References

1. Finkelstein, R. and J. H. Van Vleck, J. Chem. Phys., 8, 790 (1940).
2. Abragam, A. and M. H. Pryce, Proc. Roy. Soc. London, 206A, 173 (1951).
3. Ballhausen, C. J., Kgl. Danske Videnskab. Selskab. Mat-fyz Medd., 29, No. 4 (1954); 29, No. 8 (1955).
4. Jørgensen, C. K., Acta. Chem. Scand., 8, 1502 (1954); 9, 116 (1955).
5. Owen, J., Proc. Roy. Soc. London, 227A, 183 (1955).
6. Jørgensen, C. K. and J. Bjerrum, Acta. Chem. Scand., 9, 180 (1955).
7. Orgel, L. E., J. Chem. Phys., 23, 1004, 1819 (1955).
8. Basolo, F., C. J. Ballhausen and J. Bjerrum, Acta. Chem. Scand., 9, 810 (1955).
9. Jørgensen, C. K., Acta. Chem. Scand., 10, 500 (1956).
10. Jørgensen, C. K., Acta. Chem. Scand., 10, 518 (1956).
11. Jørgensen, C. K., Mol. Phys., 2, 309 (1959).
12. Cotton, W., Adv. Inorg. Chem., 2nd edition, 1962, p. 835.
13. Braner, G., Handbook of Prep. Inorg. Chem., 2nd edition, 1963, pp. 264-269.
14. Schlesinger, H. I. and M. W. Tarpley, J. Am. Chem. Soc., 46, 276 (1924).
15. Moffitt, W., G. L. Goodman, M. Fred, B. Weinstock, Mol. Phys. 2, 109 (1959).

16. Weinstock, B. F. Edgar, J. Westrum and G. L. Goodman, Proc. Intern. Conf. Low Temp. Phys., 8th, London, 1962, p. 405.

17. Heath, D. F. and J. W. Linnett, Trans. Far. Soc., 45, 264 (1949).

18. Nagarajan, G., Bull. Soc. Chim. Belg., 72, 276-285 (1963).

19. Jørgensen, C. K., Absorp. Spect. Chem. Bond Compl., 1962 p. 146.

Preposition V

A proton contact shift study of the oxo-bridged Fe (III) chelates $[Fe_2(phen)_4O]^{4+}$ and $[Fe_2(bipy)_4O]^{4+}$, as model systems for dimeric oxo-bridged hematins, is proposed. Specifically, it is proposed to apply the results of such a study in interpreting the proton NMR spectra of a simple form of dimeric hematin derived from tetraphenylporphine (TPP).

In paramagnetic transition metal complexes the unpaired electrons on the transition metal ions interact strongly with the nuclear spins (the protons in this case) of the ligands. This hyperfine interaction sometimes results in broadening the ligand's NMR peaks to such a degree that no NMR spectrum is observable. The condition for observing nuclear magnetic resonances in paramagnetic compounds of this type is given[1] by

$$\frac{1}{T_1} \gg A_N$$

where T_1 is the electron-spin relaxation time and A_N is the appropriate hyperfine coupling constant. Fortunately, many transition metal complexes exhibit T_1, short enough to allow the observations of NMR spectra.

Isotropic hyperfine interactions usually lead to shifts much larger than the normal chemical shifts and yield valuable information on the geometry and metal-ligand bonding of the complexes. These large

NMR shifts are attributed to either Fermi contact interaction or pseudo-contact interaction, or a combination of both. The Fermi contact contribution is given by[2]

$$\frac{\Delta H_i}{H} = \frac{\Delta \nu_i}{\nu} = -A_i \frac{\gamma_e}{\gamma_n} \frac{g\beta S(S+1)}{6S' kT}$$

and the pseudo-contact contribution (for a solid) by

$$\frac{\Delta H_i}{H} = \frac{\Delta \nu_i}{\nu} = -(3\cos^2\theta - 1)(g_{\parallel} - g_{\perp})(g_{\parallel} + 2g_{\perp}) \frac{\beta^2 H_o S(S+1)}{27 kT d^3} .$$

In these equations ΔH_i and $\Delta \nu_i$ are the differences in resonance field and frequency, respectively, of the nucleus i at applied field H or frequency ν, respectively; S is the total electron spin and S′ is the total spin of those unpaired electrons involved in delocalization; d is the distance from the metal atom to the nucleus; and θ is the angle between this distance vector and the principal magnetic axis of the molecule. The other symbols have their usual meaning. As is seen in the above equations, the pseudo-contact interaction arises from the anisotropy of the g-values. Pseudo-contact contributions can be calculated if the principal g-values and molecular geometry are known. Thus, the pseudo-contact shift can be subtracted from the observed contact shift leaving the Fermi contact shift. The Fermi contact shift can be used to characterize the orbital in which the unpaired electron resides.

Proton contact shifts have been observed in many non-biological paramagnetic transition metal complexes[3, 4] and in cytochromes-c, hemoglobins, myoglobins[5, 7] and quite recently ferredoxin,[8] and have

been of great value in elucidating the electronic and geometrical structure of these systems. In the biological systems which possess many magnetically distinct hydrogens in proximity to the metal site the uncertainty associated with assignment of specific resonance considerably clouds the interpretation of metal ligand bonding. In addition, as was pointed out by DeSimone and Drago,[4] much of the previous quantitative work even on relatively simple inorganic systems has been hampered by an incorrect evaluation of the pseudo-contact contribution, and the interpretation of the observed shifts in terms of spin-density delocalization is likely to be misleading.

A recent report on a high spin Fe (III) binuclear oxo-bridged complex[9] indicates the possibility of a contact shift study on some oxo-bridged biochemical systems of high-spin Fe (III), particularly, hematin which is known to undergo dimerization and polymerization in solution.[10]

It is proposed to study the proton contact shifts of oxo-bridged dimeric hematins derived from tetraphenylporphine (TPP), prefacing such a study by thorough investigations of the following good model systems: $[Fe_2(phen)_4O](NO_3)_4 \cdot 3H_2O$ and $[Fe_2(bipy)_4O](SO_4)_2\text{-}3.5\ H_2O$.[11] These two oxo-bridged Fe (III) chelates are magnetically very similar to $[Fe_2(phen)_4OCl_2]Cl_2$[12, 13] which has been found to exhibit distinct NMR resonance signals for all four protons.[9] The Fe (III) ions in $[Fe_2(phen)_4O]^{4+}$ and $[Fe_2(bipy)_4O]^{4+}$ have been shown[11, 14] to be in sextet ($S = \frac{5}{2}$) spin states by magnetic, Mössbauer and spectroscopic studies. Similar results hold for $[Fe(phen)_4OCl_2]Cl_2$. These three inorganic oxo-bridged complexes possess anomalous room temperature magnetic moments[11, 14] (1.83 BM for $[Fe_2(Phen)_4OCl_2]Cl_2$, 1.74 BM

for $[Fe_2(phen)_4O](NO_2)_4$, 1.86 BM for $[Fe_2(bipy)_4O](SO_4)_2$). Therefore, the two model complexes selected should be amenable to NMR study. However, unlike the octahedral ion environment in

$$[Fe(phen)_2 \underset{Cl}{Fe} - O - \underset{Cl}{Fe}(phen)_2]Cl_2$$

which probably has an isotropic g tensor, pseudo-contact interactions may be significant in the selected model systems, since the latter probably have distorted square-pyramidal symmetry around the Fe (III) atoms. It will be necessary

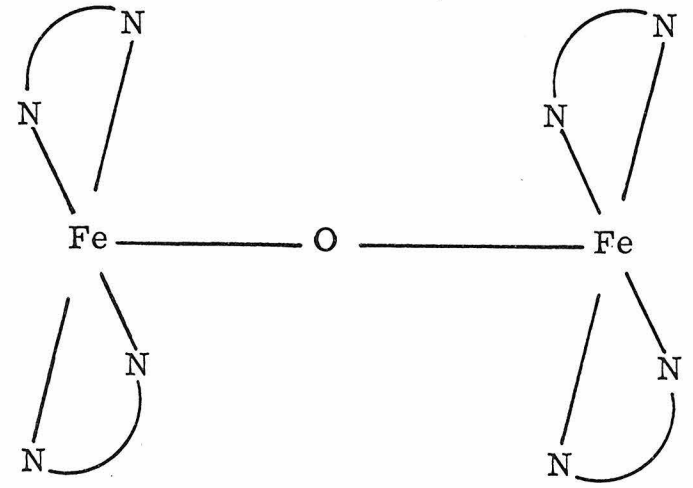

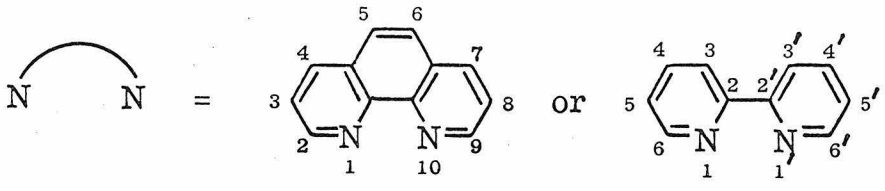

in these complexes to calculate the pseudo-contact contribution from the crystal structure and g-tensors. Unfortunately, the crystal structure and g-tensors for these complexes are presently not available, but both model compounds have been isolated in the crystalline state and no difficulties are anticipated in determining these data. Theoretically, then in these model systems the pseudo-contact contribution is calculable resulting in an evaluation of the Fermi-contact shifts for the various protons.

The Fermi contact contribution in the model system is expected to parallel the observed NMR isotropic shifts[9] of

$$[\,(phen)_2\,\underset{Cl}{Fe} - O - \underset{Cl}{Fe}\,(phen)_2\,]\,Cl_2$$ which are attributed only

to Fermi-contact interaction. The isotropic shifts observed for this high spin ($S = \frac{5}{2}$) oxo-bridged case are very much lower than those of the monomeric low-spin octahedral compound, $Fe(phen)_3(PF_6)_3$[4] as is shown in the following table.

	$\Delta\nu_{2,9}$	$\Delta\nu_{3,8}$	$\Delta\nu_{4,7}$	$\Delta\nu_{5,6}$
$[Fe(phen)_3]\ (PF_6)_3$	+1781	+444	+572	+377
$[Fe_2(phen)_4OCl_2]\ Cl_2$	-1320	-525	+21	-180

It has been shown that in the low-spin monomer the π-delocalization mechanism is dominant in the Fermi contact contribution and in the high-spin oxo-bridged dimer the σ mechanism is dominant. It seems likely that the unpaired spin density in the dimer is probably localized on Fe — O — Fe unit. It may be necessary, however, to see the changes of proton isotropic

shifts, resultant from methyl group substitution on the rings in the model systems. Moving the proton from the ring to a methyl group gives an estimate of the contribution from the π-delocalization mechanism. Thus, the π-unpaired spin density on the carbon atom polarizes the hydrogen is electron of the directly-bonded hydrogen and leads to a hyperfine interaction, $AI \cdot S$, where the hyperfine coupling constant for the hydrogen, A_H, is given by[15]

$$A_H = Q \cdot \rho_C$$

In this case, Q is a negative constand and ρ_C is the spin density on the carbon. When the hydrogen is replaced in C— H fragment by — CH_3 group, Q_{CH_3} becomes positive, since a hyperconjugative effect leads to direct transfer of positive spin to the methyl hydrogens. Therefore, the change of the hyperfine coupling constant A_H to A_{CH_3} gives a valuable criteria for checking for the π-delocalization mechanism. After the pseudo-contact contribution and the π-delocalization mechanism are thoroughly studied in the model systems NMR studies of the hematin systems can be initiated on these foundations.

It is well known that hematins dimerize and polymerize in solution.[10] Magnetic studies by Rawlinson and Scutt[16] and Blauer and Ehrenberg[17] indicated that the effective magnetic moments of hematins are variable from 5.8 BM to 2.4 BM depending on the nature of solution. There are also electrochemical[18] and kinetic data[19] on the dimerization and polymerization of hematins. The behavior of hematins in solution is probably amenable to NMR study since the hematin dimers are regarded to be

oxo-bridged complexes similar to the model systems. The most interesting system of these is a hematin derived from tetraphenylporphine (TPP) studied by Cohen.[20] The author identified an oxo-bridged dimer in methylene chloride and measured the magnetic moment of this dimeric hematin (1.74 BM per iron). The low magnetic moment is very close to those of the model system which exhibit a strong antiferromagnetic behavior ($J \simeq -100\ cm^{-1}$).[11,14]

The hematin derived from TPP should be a biochemical system suitable for NMR study. There are four distinct hydrogens but only one would probably show contact shift, since the other three on the phenyl group are probably too remote to sense the unpaired spin which is probably in a predominantly metal orbital. Furthermore, the pseudo-contact contribution in this dimer is expected to be almost the same as in the model systems, since the molecular symmetry would be the same in both model and hematin dimers. In solution the free rotation along the axis Fe — O — Fe and elongation of this axis would be permitted, but such motions would not drastically change the magnetic anisotropy. Therefore, the pseudo-contact contribution calculated for the solid molecule would be reasonable. In summary, a study of the isotropic proton contact shifts coupled with methyl group substitutions for the protons will be useful in understanding the metal ligand and Fe — O — Fe bonding. The results of the contact shift study of this dimer may be further applied in a study of the behavior and structure of other types of hematins.

References

1. H. M. McConnell and D. B. Chesnut, J. Chem. Phys., 28, 107 (1958).
2. D. R. Eaton, J. Amer. Chem. Soc., 87, 3097 (1965).
3. D. R. Eaton and W. D. Phillips, Adv. Tn. Mag. Res., 1, 103, (1965), and references therein.
4. R. E. DeSimone and R. S. Drago, J. Amer. Chem. Soc., 92, 2343 (1970), and references therein.
5. R. J. Kurland, D. G. Davis, and C. Ho., J. Amer. Chem. Soc., 90, 2700 (1968).
6. K. Wüthrich, R. G. Shulman and J. Peisuch, Proc. Natl. Acad. Sci., (U.S.), 60, 373 (1968).
7. R. G. Shulman, S. Ogawa, K. Wüthrich, J. Yamane, J. Peisach, and W. E. Blumberg, Science, 165, 251 (1969).
8. M. Poe, W. D. Phillips, C. C. McDonald and W. Lorenberg, private communication.
9. M. Wicholas, J. Amer. Chem. Soc., 92, 4141 (1970).
10. J. E. Falk, "Porphyrins and Metalloporphyrins," Elsevier Publishing Co., Amsterdam, 1964, p. 45, and references therein.
11. W. M. Reiff, W. A. Baker, Jr., and N. E. Erickson, J. Amer. Chem. Soc., 90, 4794 (1968).
12. J. Lewis, F. E. Mabbs, and A. Richards, J. Chem. Soc., A, 1014 (1967).
13. R. R. Berrett, B. W. Fitzsimmons and A. A. Owusn, J. Chem. Soc., A, 1575, (1968).

14. W. M. Reiff, G. J. Long, and W. A. Baker, Jr., J. Amer. Chem. Soc., 90, 4794 (1968).

15. H. A. D. Hill, and P. Day,"Physical Methods in Adv. Inorg. Chem." Interscience Publishers, New York, N. Y. 1968.

16. W. A. Rawlinson and P. B. Scutt, Aus. J. Sci. Res., 50A, 173, (1952).

17. G. Blauer and A. Ehrenberg, BBA, 112, 496 (1966).

18. T. M. Bednarski and J. Jordan, J. Amer. Chem. Soc., 89, 1552, (1967).

19. Y. Inada and K. Shibata, BBRC, 9, 323, (1962).

20. I. A. Cohen, J. Amer. Chem. Soc., 91, 1980 (1969).